A Pathway to Artificial Metalloenzymes

Dissertation by

Johannes Patrick Nikolaus Fischer

In Partial Fulfillment of the Requirements

For the Degree of

Doctor of Philosophy

King Abdullah University of Science and Technology

Thuwal, Kingdom of Saudi Arabia

&

Technische Universität München

Munich, Germany

EXAMINATION COMMITTEE APPROVALS FORM

The dissertation of Johannes Patrick Nikolaus Fischer is reviewed and approved by the examination committee:

Jörg Eppinger
Assistant Professor
Chemical Science
King Abdullah University of Science and Technology
Committee Chairperson

Michael Groll
Full Professor
Biochemistry
Technical University Munich
External Committee Member

Stefan Arold
Associate Professor
Mechanical Engineering
King Abdullah University of Science and Technology
Committee Member

Sami Hamdan
Associate Professor
Mechanical Engineering
King Abdullah University of Science and Technology
Committee Member

Uwe Bunz
Full Professor
Organic Chemistry
University of Heidelberg
External Committee Member

Maach et joot, ävver nit zo off

A PATHWAY TO ARTIFICIAL METALLOENZYMES

LIST OF ABBREVIATIONS

Abs	Absorption
ArM/s	Artificial Metalloenzyme/s
ACN	Acetonitrile
CD	Circular dichroism
DMSO	Dimethyl sulfoxide
ee	Enantiomeric excess
Em	Emission
ESI	Electrospray ionization
FA	Formic acid
FP	Fluorescent Protein
FRET	Förster Resonance Energy Transfer
HEPES	4-(2-hydroxyethyl)-1-piperazineethanesulfonic acid
IPTG	Isopropyl-β-D-1-thiogalactopyranoside
LB	Luria Broth (Lysogeny Broth)
MES	2-(N-morpholino)-ethanesulfonic acid
M	Moles per Liter
mM	Millimoles per Liter
μM	Micromoles per Liter
mTFP	monomeric teal Fluorescent Protein
mTFPmb	monomeric teal Fluorescent Protein Metal Binder
NHS-Ester	N-Hydroxysuccinimide-Ester
PDB	Protein Database
PEG	Polyethylene glycol
RMSD	Root Mean Square Deviations
TCEP	Phosphanetriyltripropanoic acid
tmFRET	Transition Metal FRET
TOF	Time of flight
TRIS	2-Amino-2-hydroxymethyl-propane-1,3-diol

LIST OF FIGURES

LIST OF TABLES

ABSTRACT

The advancement of catalytic systems and the application thereof has proven to be the key to overcome traditional limitations of industrial-scale synthetic processes[1]. Converging organometallic and biocatalytic principles lead to the development of Artificial Metalloenzymes (ArMs) that comprise a synthetic metal catalyst embedded in a protein scaffold, thereby combining the reactivity of the former with the versatility of the latter[2-6]. This synergistic approach introduces rationally designed building blocks for the catalytic site and the host protein to assemble enzyme-like structures that follow regio-, chemo-, enantio- and substrate-selective principles[7-10]. Yet, the identification of suitable protein scaffolds has thus far been challenging[4].

Herein we report a rationally optimized fluorescent protein host, mTFP*, that was engineered to have no intrinsic metal binding capability and, owing to its robust nature, can act as scaffold for the design of novel ArMs. We demonstrate the potential of site-specific modifications within the protein host, use protein X-Ray analysis to validate the respective scaffolds and show how artificial mutant binding sites can be introduced. Transition metal Förster Resonance Energy transfer (tmFRET) methodologies help to evaluate micromolar dissociation constants and reveal structural rearrangements upon coordination of the metal centers. In conjunction with molecular insights from X-Ray crystallographic structure determination, dynamics of the binding pocket can be inferred. The versatile subset of different binding motifs paired with transition metal catalysts create artificial metalloenzymes that provide reactivities which otherwise do not exist in nature. As a proof of concept, Diels-Alder cycloadditions highlight the potential of the present mTFP* based catalysts by stereoselectively converting azachalcone and cyclopentadiene substrates. Screens indicate an enantiomeric excess of up to 60% and provide insights into the electronic and geometric constitution of the first coordination spheres binding the catalysts.

We further apply two general principles to optimize selective conversions of the generated ArMs. 1) Utilizing site-specific mutagenesis, increased hydrophobicity is introduced to the second

coordination sphere. 2) *In-vitro* post-expressional modification utilizing N-hydroxysuccinimide esters is anticipated to introduce a sterically more demanding second coordination sphere that influences substrate entry by favoring a particular stereoisomer. The latter approach however also enhances the host proteins robustness under processing conditions.

The presented study investigates a novel approach to create artificial metalloenzymes based on non-enzymatic precursor proteins. It illustrates means of modification and functionalization. Further guidance to overcome the general problem of insufficient stereoselectivity and stability is also presented. In view of the insights gained we see the importance of further mutagenic studies, i.e. through means of guided evolution, to extend stereoselectivities. *In*-vivo applications of artificial metalloenzymes could thus be used to pursue metabolomic engineering.

A. INTRODUCTION

1. PREAMBLE

Understanding all catalytic kingdoms and the advancements thereof has proven to be the key to overcome traditional limitations that industrial-scale synthetic processes suffered from[1]. Despite this development and the insights to countless reactions, still most metal catalysts are lacking conversions with demanding scopes in either selectivity or/and reactivity and are therefore hard to integrate within larger scale applications without the loss of either catalyst or capital[3]. At times the general inefficiency seems to be outperformed with ease by nature's biocatalytic portfolio. Engineered mutants thereof have found their way to economically significant productions[1,11]. Increasing insights to mode of actions and advances in bioinformatics have pushed de novo designs and enhanced mutants to new boundaries[7,12].

Generally speaking, enzymes are believed to employ a great deal of properties that other catalysts clearly miss. Namely they are cheap to produce, sustainable and biocompatible (environmentally benign). They utilize a narrow substrate scope at a high efficiency and require less energy whilst producing fewer by-products at a smaller number of synthetic reaction steps[7,13,14]. They appear powerful with the respect to the quality of products they are able to synthesize, however weak as they lack the multitude of reactions that non-biological catalysts such as transition metal complexes clearly incorporate. This promiscuity of transition-metals draws much attention from all synthetic industries as respective biological homologues fail to display sufficient activities with many reagents that inorganic catalysts convert at high rates. A general trend for more functionality in pharmaceuticals or other synthetic products, that is foreign to nature, accounts for this. Evolution has granted means of modification and production to substrates that show bioavailability in aqueous media. Thus genetically engineered and optimized mutants encounter

troubles to catalyse all synthetically important transformations that can be performed with transition-metal catalysts, in organic solvents or rarely in aqueous buffer[7,15].

Consequently the convergence of either catalytic principle develops the idea of Artificial Metalloenzymes (ArMs) that would comprise the synthetic metal catalyst embedded into a biological scaffold[2-4]. Hence combining the reactivity of the former with the versatility of the latter[3]. Following this synergistic approach targets to introduce rationally designed functionalities to provide not only building blocks for the catalysis of asymmetric reactions, but also enzyme-like structures that follow regio-, chemo-, enantio- and substrate-selective principles[7-10]. To accomplish this, the identification of suitable scaffolds, i.e. a protein hosts, reveals to be challenging[4]. Several reports demonstrate potential candidates for ArMs and present a range of applications they could be utilized in[3,7,15,16]. Prominent candidates however, are rare.
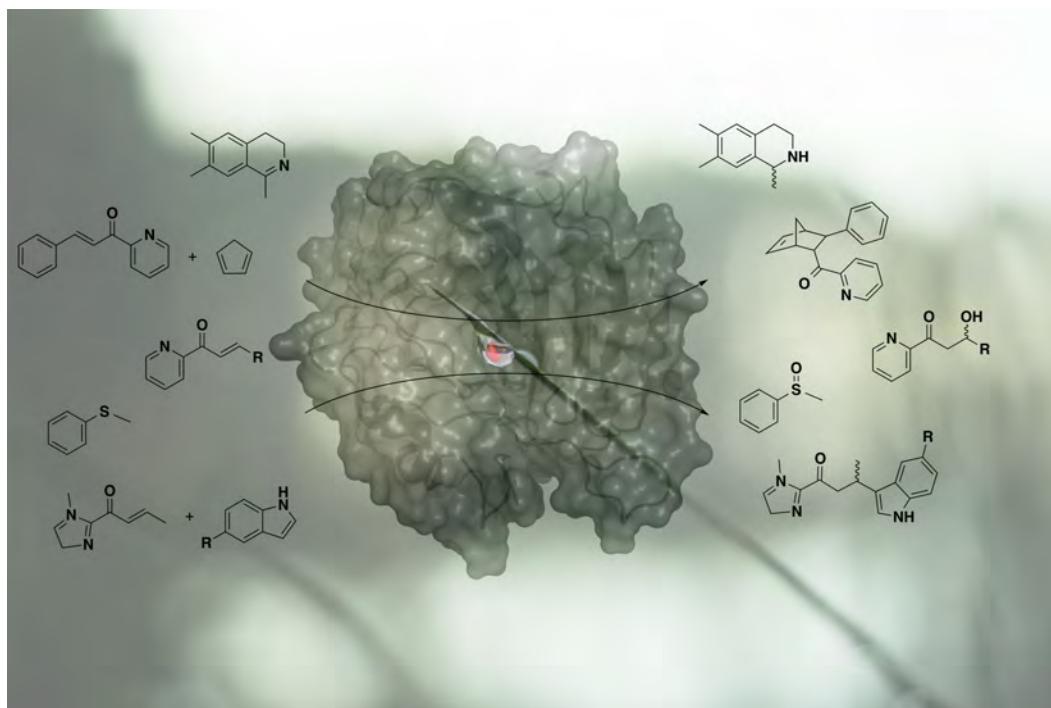
Figure 1 Catalytic Portfolio of Artificial Metalloenzymes

2. INTRODUCTION TO CATALYSIS

The discovery of catalytic principles dates back to observations made by the Swedish Chemist Berzelius in 1836. Although catalysis itself, i.e. the conversion of sugars to alcohol or subsequently to acetic acid, was known and applied for much longer, it remained unknown that besides the conversion of substrates to products certain substances, accidently added to or being present in the mixture were essentially enhancing the process[17]. Only in 1894, Wilhelm Ostwald first attempted to argue a general definition of catalysis (from Greek *katalusis*: dissolution) and described a phenomenon by which a substance, called a catalyst, positively influences a reaction profile without undergoing any permanent change. He stated that catalysts would enhance the rates of chemical reactions by providing an alternative reaction mechanism, involving various transition states, thus decreasing the activation energy ($\Delta G^{\ddagger}_{cat} < \Delta G^{\ddagger}_{no-cat}$) , however not affecting the overall thermodynamic equilibrium ($\Delta G_{Reaction}$) (Figure 2)[18].
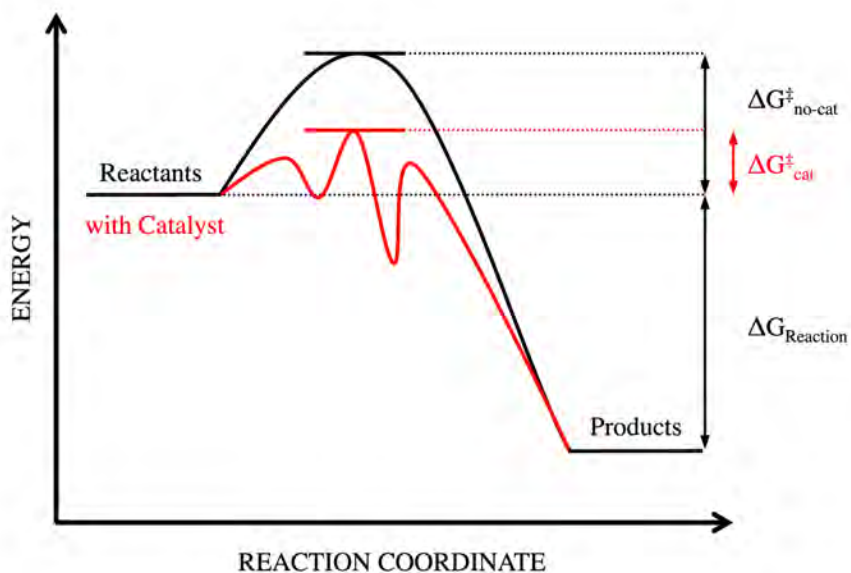
Figure 2 Catalysis: Providing an alternative reaction mechanism

In recognition of his work in catalysis, Wilhelm Ostwald received the Nobel Price in Chemistry in 1909[17]. At the time of these ground-breaking insights industrial catalysis sparked only to gain enormous attention merely a few years later. The inexpensive production of ammonia utilizing the Haber-Bosch process not only substantiated the industrial revolution in Europe, but also introduced the new era of catalysis that lasts until today. The importance of catalysis for mankind was further endorsed by the amount of attention the field received throughout the twentieth century. Innovative approaches have lead to the development of effective catalysts that contribute essentially in the production and functionalization of numerous materials[19]. More than ever catalysis has evolved to impact industries on a global scale, being apparent in all major domains such as health, nutrition and energy[20]. Considering this omnipresence the field evolved drastically and a great range of catalytically active systems, including heterogeneous and homogenous catalysts, have been developed and optimized for industrial scale applications[21]. Recent Nobel Prizes further acknowledge the persistent importance of the field and uplift the remarkable improvements that have been: William S. Knowles, Ryoji Noyori and K. Barry Sharpless on metal catalysed transformations (2001), Yves Chauvin, Robert H. Grubbs and Richard R. Schrock for the development of the metathesis reactions (2005), Gerhard Ertl for his studies of chemical processes on solid surfaces (2007) and Richard F. Heck, Ei-ichi Negishi and Akira Suzuki for palladium-catalysed cross coupling reactions (2010)[22-30].

2.1. Catalysts Performance

Catalysts come in a multitude of forms, varying from atoms and molecules to large structures like enzymes. Bearing the popularity of the field, but also taking industrial application into account, evaluating the quality and performance of a catalyst remains of great importance. Generally this may be accomplished by analyzing activity and specificity towards substrates and products of a catalyst in a given reaction. The activity of a catalyst is defined by the amount of product produced per equivalent of a catalyst in a particular amount of time. Herein several key parameters such as temperature, pH or solvent content are of vast importance and influence aforementioned activity greatly[31]. Specificity refers to the bias of a catalyst to convert substrates, or to form products of a specific stereotype. Within the concept of artificial metalloenzymes and the context biocatalysis that largely deals with the performance of enzymes and the chiral biological world, the definition is amended by the dependency of conversion to unit mass of enzyme present – thus Michaelis Menten kinetics.

$$E \quad + \quad S \quad \underset{k_{-1}}{\overset{k_1}{\rightleftharpoons}} \quad ES \quad \xrightarrow{k_2} \quad E \quad + \quad P$$

Figure 3 Enzymes Kinetics

Herein, the enzyme (E) and the substrate (S) associate in a rapid and reversible step to form a complex (ES). This complex then undergoes chemical conversion, usually a kinetically much slower process, into the desired product (P) and the recoverable enzyme (E). Hence the overall rate-determining step is product formation rather than substrate binding ($k_2 \gg k_1$)[32,33]. Michaelis-Menten kinetics therefore describes the overall dissociation of product from the complex as the catalytic rate constant, k_{cat}, that depends on Enzyme and Substrate concentration (*[E], [S]*).

$$v = k_{cat}[E] \frac{[S]}{K_M + [S]}$$

Experimentally the dissociation constant K_M as well as the rate constant k_{cat}, can be determined. The ideal case for an enzyme shows high specificity and enhanced activity towards specific substrates. However limited are the insights from Michaelis-Menten kinetics towards a chiral bias – a feature of utmost importance in the context of artificial metalloenzymes.

2.2. Stereoselectivity

A molecule is chiral when its mirror image cannot be superposed to the original molecule. With this regard, stereoselectivity is an intrinsic property of matter and implies the existence of constitutionally identical compounds that don't share an identical steric configuration. A simplistic example is R, S configured lactic acid. Constitutionally both molecules are alike, however their mirror image cannot be superposed with means of translation or rotation (Figure 4).
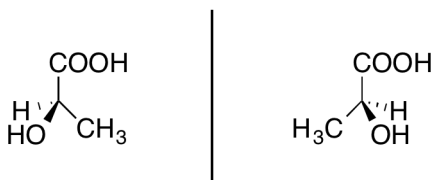
Figure 4 Stereoselectivity: (R)-, (S)-Lactic Acid

Effectively the basic compounds of life, amino acids, carbohydrates, fatty or nucleic acids are molecules that each share a unique stereo configuration. Thus everything they constitute comprises unique features with respect to the smallest component. This intriguing and widespread property of nature is best shown in proteins. All amino acids, but glycine are chiral and almost exclusively provided and found in nature in the L-configuration[34]. Proteins are therefore chiral polymers that can show different responses and thus biological effects towards different enantiomers. Thalidomide, a powerful sedative used in the 60s to treat morning sickness in pregnant women is probably the best-known example. Whereas the R-configuration shows the desired effects, the S-configuration accounted for severe birth defects owing its teratogenic properties (Figure 5)[35,36].

(R)-Thalidomide   (S)-Thalidomide
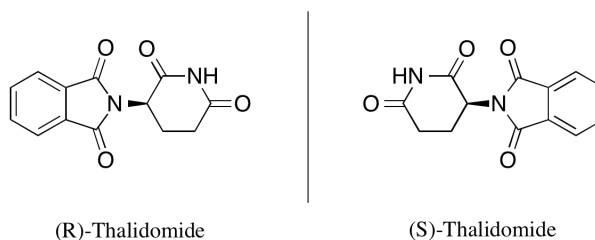
Figure 5 Stereoselectivity: (R)-, (S)-Thalidomide

Especially since then stereoselective means have taken an important role, especially in pharmaceutical industry or fine chemistry. Three main routes exist for the preparation of enantiomerically pure compounds: enantiomer separation, transformation of a chiral precursor from a chiral pool and performing enantioselective reactions, either stoichiometric or quantitative. In economic terms however only total control of any catalytic reaction is feasible to enable production of desired enantiomers. Means of separation or production of chiral precursor pools account for chemical waste and therefore the loss of capital[37]. Research regarding direct enantioselective conversion has therefore received much attention in the last decades and yielded into great advancements in synthetic methodologies[38]. Quantifying these, the enantiomeric excess, which refers to the bias of one enantiomer in a mixture, needs to be addressed. This can be accomplished using means of spectroscopy (NMR) or chromatography (HPLC) and is defined as follows:

$$ee = \left(\frac{|([R] - [S])|}{([R] + [S])} \right) \times 100$$

Research on stereoselective catalysis focuses on all domains: heterogeneous, homogenous and enzymatic catalysis. Despite the efforts and advances of synthetic, heterogeneous methodologies, biological applications and moreover the integration of designed enantioselective catalysts has emerged as an alternative tool for the synthesis of enantiopure compounds. Finally it remains very difficult to predict outcomes of catalytic reactions referring to the marginal energetic differences of transition states[39,40]. Hence ways to screen and optimize different catalysts are of key importance – owing to what known from nature, means of evolution seem more applicable to biocatalysts!
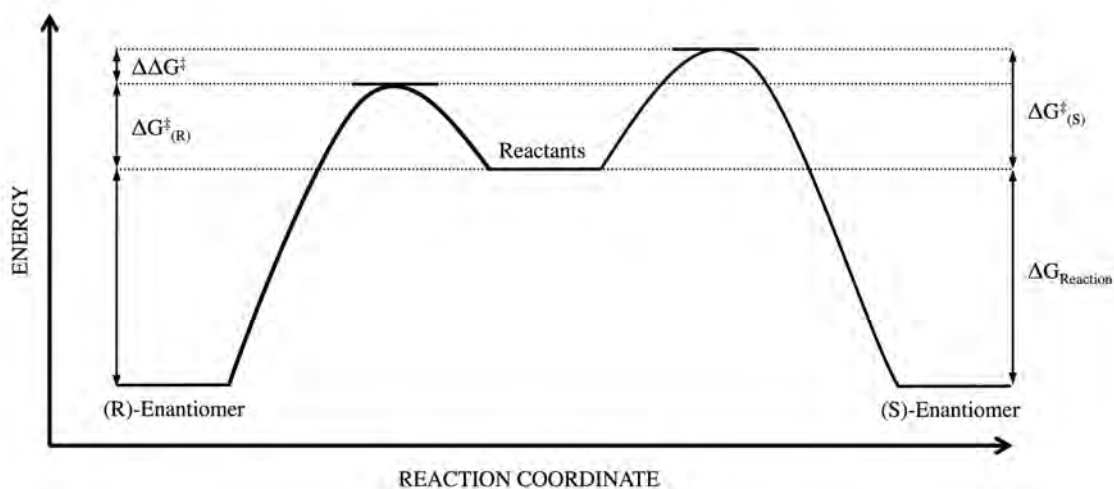
Figure 6 Reaction Energetics: Marginal difference of activation energies ($\Delta\Delta G^{\ddagger}$) complicates enantiomer predictions

2.3. Diels-Alder Catalysis

Diels-Alder reactions belong to the most useful cycloadditions reactions that are known in synthetic chemistry. Herein the concerted conjugation of a diene and dienophile constructs a wide variety of simple to complex chiral molecules on the basis of cyclohexene[41-43]. Generations of experimental and theoretical chemists have contributed to a deep understanding of the reaction mechanisms involved. The formation of cyclohexene requires a butadiene and an ethylene and is usually considered an energy intensive process, as it requires the adjustment of the lowest unoccupied orbital (LUMO) from ethylene to the highest occupied orbital (HOMO) of butadiene. Finding means of minimizing this gap leads to drastic rate acceleration.
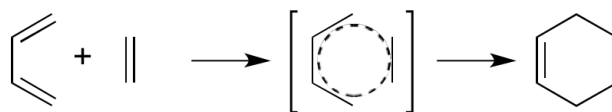
Figure 7 Diels-Alder Reactions: 4+2 Cycloaddition of butadiene and ethylene

Generally modifications of the dienophiles throughout electron withdrawing substituents, like carbonyl or nitro groups, cause for a lowering of the LUMO and thus account for enhanced reactivity. Moreover if a Lewis Acid, an electron accepting species is closely oriented dramatic rate enhancements can be achieved[44]. These early observations set the developing stage for catalysts that could induce asymmetry in this cycloaddition reaction. To date numerous examples of transition metals and organocatalysts have been exploited for their influences on enantioselective C-C bond formations[45-48]. Hence from a purely synthetic perspective the long-standing problem of catalytic asymmetry in Diels-Alder is solved. Regardless of these advancements catalytic versions of Diels-Alder reactions in Nature still provide a conundrum. Several cases are known in which a chiral product in biology results from Diels-Alder reactions, although it is not known whether these originate from putative Diels-Alderases that perform the

conducted actions of an enzyme[41,49-51]. The amount of evidence presented and argued strongly suggests that nature scrutinizes mechanistics of this kind, however it also accounts for the vision not only to mimic, but to guide means to create novel, bio-compatible Diels-Alderases.

2.4. Enzymes and Homogenous catalysis

Enzymes are functional proteins that nature uses as catalysts. Their structure, which results in a shape specific active site, provides means to transform a specific substrate. Functionality follows form and the optimum configuration for a reaction allows incredibly efficient and specific, concerted reactions[31]. A classical yet powerful example is catalase that decomposes hydrogen peroxide into water and oxygen at an incredibly high rate of up to 10^7 molecules per second[52]:

$$2\,H_2O_2 \xrightarrow{\text{Catalase}} H_2O \;+\; O_2$$

Figure 8 Catalase Reaction

Homogenous catalysts are similar as they function in the same phase as the reactants. This however does not necessarily imply a liquid one. Classical examples that are applied in industry refer to all kinds of conversions to produce chemicals like acetic acid[53]. Herein complexes of Ruthenium account for the efficient conversion of methanol in a process called carbonylation:

$$CH_3OH \;+\; CO \xrightarrow{\text{Rh}} CH_3COOH$$

Figure 9 Carbonylation of Methanol to Acetic Acid

Owing that almost half of all proteins known to date are metalloproteins and thus comprise a metal, provides a great possibility that was so far limited by the metabolic need of nature[54,55]. The merger of homogenous and enzyme catalysis is believed to provide scopes that hold great promise to address existing challenges in medicine, biotechnology and fine chemistry. With respect to enzymes, the exquisite scaffolds summon their potency with tailored first and second coordination spheres and empower enormous rate accelerations, high substrate selectivities, yet

selective transformations of multifunctional substrates. Homogenous catalysts however provide a first coordination sphere and therefore generate their influences through the electronic and geometric structure. The influences of solvents and counter ions, which often have a crucial role, are however left behind. Anticipating synergies of principle homogenous catalysis and enzymes creates a promising area of research referring to the number of tools available to develop and advance sustainable technologies. Traditional mysteries of prediction could be outperformed by means of evolution. Thus both academic and industrial community agree on the potency of this combination to outperform the modest advances of traditional transition metal, heterogeneous, catalysis[56]. Applications thereof already include pharmaceuticals, probes for imaging, contrast agents and biosensors[57-61].

3. ARTIFICIAL METALLOENZYMES

3.1. Introductory

The concept of Artificial Metalloenzymes was first introduced and applied by Wilson and Whitesides in 1978 in their pioneering work on asymmetric hydrogenation catalysts[62]. Herein Rhodium conjugated biotin moieties were paired with well-characterized avidin tetramers and evaluated for catalytic activity and selectivity. While initially considered a curiosity, their work and success showed that the mere combination of two well known catalytic kingdoms could lead to a whole new class of bioinorganic catalysts – a vibrant field of research in the last decades[63].

3.2. Concept and Strategies

Generally speaking Artificial Metalloenzymes are hybrid catalysts created by the inclusion of a non-natural metal cofactor into a scaffold of choice. Largely speaking these scaffolds could be of any nature thus Proteins, Nucleic Acids and so on, however require to serve the purpose described below. In the context of this Dissertation Proteins are of solitary interest to the description of Artificial Metalloenzymes. Herein a transition metal catalyst bound to a hosting ligand, generally described as the first coordination sphere is paired with the environment of a protein, referred as the second coordination sphere (Figure 10). Upon ideal pairing of metal with first and second sphere, the combination may mimic functionalities that otherwise do not exist in nature. Generally speaking functionality is introduced throughout the metal catalyst itself, however the environmental limitation established by the protein scaffold not limits the possible conformations, but also conducts substrate orientation and thereby initiates enzyme-like selectivity. Essentially supramolecular interactions between the substrate of choice and the amino-acid environment provided by the protein cause a direct delivery to the active site and

stabilize transition states. Thus an ideal pairing may result in high selectivity and rate acceleration in the reaction of interest.
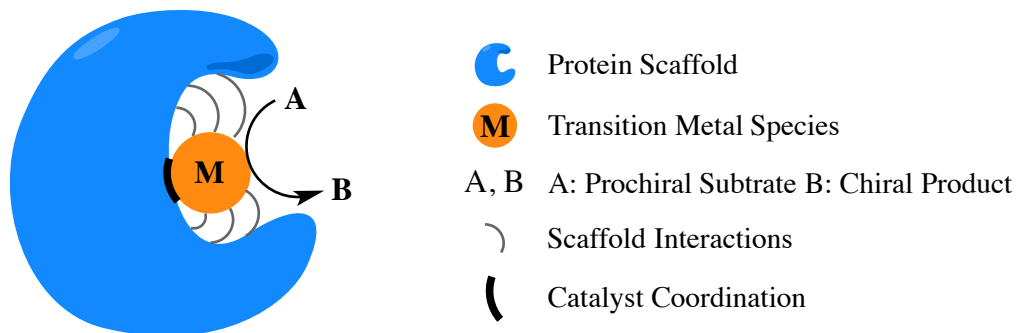
Figure 10 Artificial Metalloenzymes: Concept

Three major strategies are commonly employed to create Artificial Metalloenzymes. To facilitate a catalytically active species with first coordination sphere and with a specificity determining second coordination sphere, yet a chiral environment, namely supramolecular-, covalent- and dative anchoring provide means of bioconjugation that suffice the purpose.

3.2.1. Supramolecular Anchoring

Supramolecular anchoring is a non-covalent approach based on the high affinity between a protein host and a small molecule that satisfies the purpose of coordinating a metal species vigorously (Figure 11). Since both parts can be established separately, the key advantage relies with the ease of introducing chemical modifications to the metal anchoring guest molecule or mutations to the hosting scaffold. Since the establishment of the field ArMs based on supramolecular anchoring strategies have outperformed others and are currently leading the field in terms functionality[14,63]. Prominent examples, reaching stereoselectivities of 90% and beyond, are the on-going advancements of the biotin-(strept-)avidin system. The originator to the field has shown interesting properties in a variety of late transition metal catalyzed chemical reactions[64-68]. The popularity of this approach involves the judicious positioning of the catalyst using a well-described protein environment and artificially established derivatives of biotin. Owing to the restriction of the second coordination sphere and the limited whole cell applicability, recent explorations also focus on the de-novo design using protein scaffolds that do not solely depend on one specific linker molecule, but that show general affinities to planar coordination complexes[69].
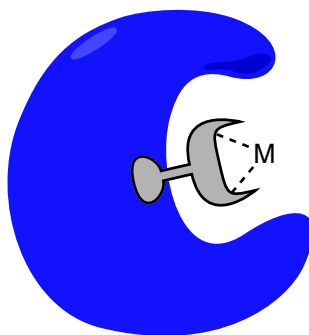
Figure 11 Artificial Metalloenzymes: Supramolecular Anchoring

3.2.2. Covalent Anchoring

Within Covalent Anchoring the scaffold of choice is coupled to an organometallic moiety in order to achieve the hybrid catalyst. As innovators of this approach Kaiser and Lawrence performed alterations at specific residues in 1984. Largely scrutinizing thiol reactivities of cysteines close to the active site created a semisynthetic enzyme with different catalytic activities compared to its predecessor[70]. Ever since covalent modifications of a multitude of scaffolds, including albumins, proteases or lipases and many more, and the combination with a similar multitude of ligands has lead to potent ArMs[7,15,71,72]. Moreover with respect to the precision attachment of moieties, implying a regio- and site-selective anchoring of the catalyst, insights into reaction mechanisms and the involvement of the scaffold have been highlighted. Another approach to covalent anchoring utilizes the incorporation of artificial ligands on a ribosomal level; unnatural amino acid. Using the expanded genetic code methodology introduced by Peter Schultz, many reported the establishment of metalloproteins or artificial metalloenzymes containing non-canonical amino acids with metal binding or functionalization capabilities[73-77]. Overall, prominent examples remain the Lactococcal multidrug resistance Regulator-based (LmrR) artificial metalloenzymes by Roelfes et al. containing 2,2'-bipyridin-5-alanine or 8-hydroxyquinolin-alanine or the thermostable synthase subunit of imidazole glycerol phosphate synthase tHisF from *Thermotoga maritima* conjugated with a libaray of Thiol reactive probes by Reetz et al.[15,78].
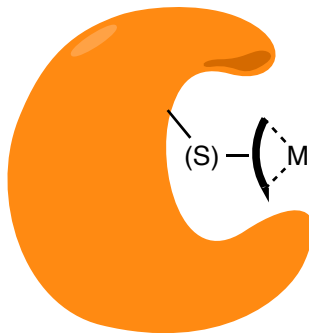
Figure 12 Artificial Metalloenzymes: Covalent Anchoring

3.2.3. Dative Anchoring

The dative anchoring approach built on direct interactions of the catalytic transition metal with the surface or other functionalities presented by the biomolecular scaffold. Precisely the catalytically active organometallic hybrid is established by coordinating transition metals in a defined cavity or environment. In this way a potent center of interest can be introduced targeting a particular reaction. Kaiser et al. were the first to adopt these principles by replacing Zn^{+2} with Cu^{2+} in the active center of Carboxypeptidase A (CPA). In 1976 the resulting artificial metalloenzyme selectively oxidized ascorbic acid and symbolized a landmark in the field. Generally speaking within dative anchoring the paradigm of replacing existing metal centers is still most predominant. The groups of Kazlauskas and Soumillion both described the replacement of the core Zn^{+2} of a carbonic anhydrase with Mn^{+2} establishing functionalities towards asymmetric epoxidation[79,80]. Nevertheless adopting natural amino acid patterns that successfully coordinate metal centers has been of great interest, too. Since metals are present in nearly half of the characterized proteome, challenging transformations could eventually be performed by trimmed and optimized proteins or mutants of their coordinative site[54]. Hence in recent years the broad functional scope of protein-bound metals found in naturally evolved catalysts has inspired different approaches to create artificial metalloenzymes. The group of Manfred Reetz reported the creation of an artificial copper-binding site in the aforementioned synthase from *Thermotoga maritime* (tHisF) as they introduced the recurring and versatile two-histidine one-carboxylate motif[81-85]. The respective metalloenzyme converted stereoselectively in Diels-Alder reactions however exemplified also the challenges of this novel approach. Ward and co-workers argued a systematic approach to identify potent motifs from x-ray structures available to date. They anticipated to convert the identified structures to functional artificial metalloenzymes. However the conundrum of the mere presence of any envisioned motif, but lacking functionality in the first

place, or the simple absence of coordinated transition metals further supported the view on this approach. Since then ArMs scrutinizing means of design or motif identification are scarce[86,87].
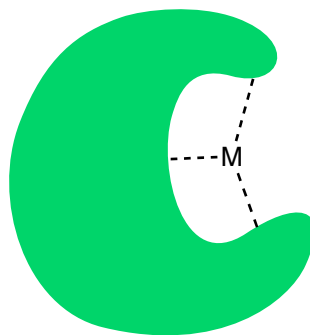
Figure 13 Artificial Metalloenzymes: Dative Anchoring

3.3. Limitation

A variety of methods to generate metal binding sites were developed and since the initial pioneering work, multiple examples of artificial catalysts greatly advanced the field[7,8,14,15,72]. Some systems achieved impressive stereoselectivity or demonstrate the power of co-activation through the second coordination sphere. Nevertheless, despite the rush for new reactivities and advanced selectivities, or the sole enhancement of turnover numbers prominent candidates are rare.

Still a considerable drawback is the general establishment of ArMs as well as the optimization and redesign. Reetz and Co-Workers elegantly describe Darwinian principles to overcome some of the attached issues[2,4]. However owing to complexity of forming ArMs the number of tools to advance them is again further limited[85]. Generally speaking the generation, which is based on artificial cofactors or natural amino acid incorporation, is too cumbersome, while solubility and/or stability towards temperature, pH and organic solvents are insufficient. Moreover due to the nature of amino acids and the composition of proteins, multiple sites for metal binding are present in almost every entity existing. Hence selective creation of catalysts with a defined transition metal center is problematic. Also, real-world applications in organic synthesis, material sciences or most importantly whole cell biocatalysis towards novel biochemical pathways so far suffer from practical drawbacks. Limited turnover numbers and expensive co-factors are an apparent problem. Also the low *in-vivo* applicability of approaches like supramolecular or covalent co-factor anchoring considerably limits advances – especially owing the fact that most artificial metalloenzymes come from those.

Hence tuning and rationalizing the work on artificial metalloenzymes literature agrees on systematic prerequisites to success: 1. A potent expression system needs to be available. 2. The scaffold of choice should be of a robust nature to withstand catalytic processes. 3. Purification principles of the scaffold should be simple and possible allow recycling. 4. Bioconjugation of inorganic catalysts need to be quantitative at mild conditions and easy to perform[1,41].

B. OBJECTIVES AND PRECONSIDERATIONS

Since Artificial Metalloenzymes represent a young area of research, the presented dissertation project is firstly, to generate a fundamental understanding regarding strategies that can evolve optimized host proteins for the purpose of artificial metalloenzymes; secondly to develop and evaluate designed metalloproteins on the basis of covalent and dative modifications that could be utilized in catalysis, thirdly to scrutinize their distinctive features converting them into active species that show conversion in the sense of a catalyst; fourthly to evaluate the electronic and geometric influences of the metal binding motif gaining insights regarding their interplay; fifthly to provide an understanding how the second coordination sphere influences catalysis and sixthly to show ways to enhance the developed catalysts to the highest extend possible by screening for conditions and providing means of optimization. Herein the anticipated parallel approach integrates currently established pathways; namely dative and covalent anchoring of transition metal complexes prove our endeavors from different angles and provide general design principles that allow the establishment of Artificial Metalloenzymes.

The initial target lies within the identification of a suitable, yet robust host protein that allows the incorporation of artificial metal centers and survives hostile catalytic conditions (1). Further an in
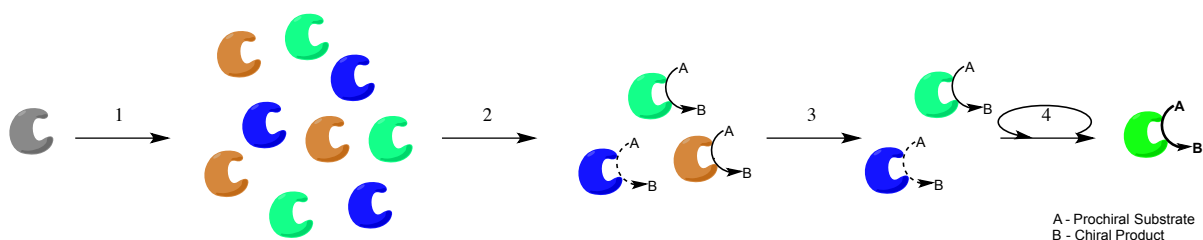
Figure 14 Schematic Outline to Artificial Metalloenzymes: 1) Identification 2) Characterization and Functionalization 3) Testing 4) Optimization

depth understanding of the biochemical and molecular integrity needs to be acquired (2). Herein the conditions have to be estimated that the protein host is able to withstand, thus allowing successful catalysis at a later stage. Moreover conclusions are to be made how to monitor and govern principle interactions of non-biogenic transition metals with a determined or designed first coordination sphere in the protein of interest. To standardize and quantify respective artificial metalloenzymes, a lean assay is to be developed (3). Results are then adopted to optimize the triad of host (ligand), metal center and reaction conditions in an iterative manner (4). Following this pathway should result in a novel and potent artificial metalloenzyme family that converts stereoselectively in Lewis Acid catalyzed reactions.

C. RESULTS AND DISCUSSION

1. SELECTION AND OPTIMIZATION OF A NOVEL METALLOPROTEIN

1.1. Host Protein Selection

Demonstrating a rationally designed host requires the prior consideration of a suitable biomolecular scaffold, the mode of attaching the catalyst to it and lastly the transition metal that is to perform the catalysis[63]. These key parameters largely define the versatility of the rising artificial metalloenzyme. With targeting diverse functionalities potential hosts for ArMs require a vastly durable nature, yet a decent pH, temperature and solvent tolerance[3,7,63,88]. We envisioned to utilize Fluorescent Proteins (FPs) for this purpose, as their robust nature had been described elsewhere[89]. Consequently after screening and evaluating a small selection (data not shown) we employed a monomeric, brightly fluorescent and very durable mutant of cyan FP, mTFP1 (PDB: 2HQK) as host[90].

~ 4 nm

~ 3 nm
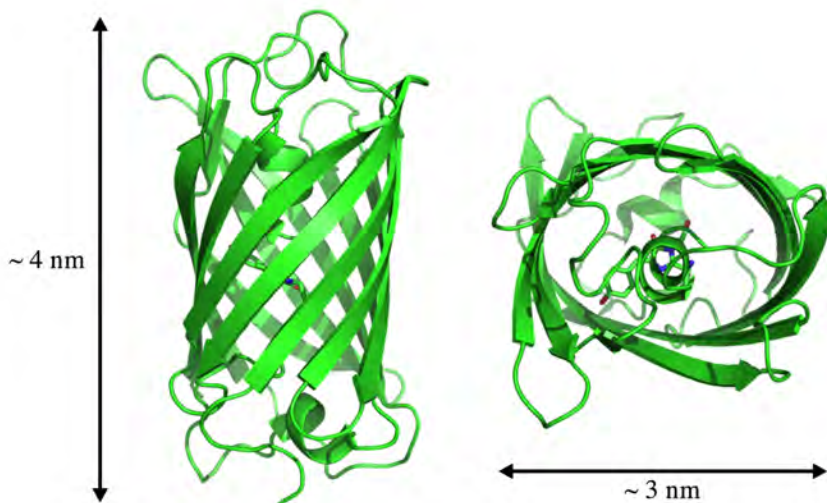
Figure 15 Crystal Structure: mTFP1 (PDB: 2HQK) shows protein dimensions of 4 x 3nm

1.2. Engineering of mTFP* as a novel Host

(the work of this Section has been accomplished in collaboration with Abdul Rajjak)

Exploiting the scaffold (PDB: 2HQK), and pursuing with an *in silico* design we obliged more rules that our host was to follow. At first, combining inorganic catalytic motifs with protein scaffolds to accomplish bioorthogonal hybrid enzymes required a combinatorial approach towards the first and second coordination sphere. Whereas in traditional transition metal catalysis activity and selectivity are almost exclusively controlled by the first coordination sphere, that is provided by the chelating ligand, enzymes utilize their protein scaffold, the second coordination sphere to introduce a chiral, yet defined environment[6,63]. Adopting these principles to ArMs therefore involves expressing a protein scaffold with a well-defined cavity that hosts both ligand and the catalytically active metal species. At second, ArMs target to exploit the reactivity of a transition metal complex within mentioned chiral environment that favors the enantiomer of interest. Therefore ambiguous binding of metals to the scaffold is not wished for. Since experimental studies have found that surface exposed cysteine, histidine and methionine residues might interfere with selective coupling reactions, by coordinating the metal catalysts, we evaluated the crystal structure of mTFP1 (PDB: 2HQK).

In silico, residues H30, M118, H128, H177, H178 and H209 from the gene of mTFP1 (GenBank: DQ676819) were analyzed for their conservation among homologues using ConSurf Algorithm[91]. These exposed amino acids were then screened for vital hydrogen bonding and the relative free energy of folding was predicted using FoldX (Version 3.0)[92,93]. To maintain a good solubility, we only considered the seven amino acids (R, K, E, D, Q, N, Y) with a hydrophobicity index lower than that of histidine on the on empirical hydrophobicity scale of Janin, as well as the usually unproblematic alanine mutation[94]. For position M118 additionally the two similarly sized amino acids L and I were included. The FoldX algorithm gave the highest stabilization energies for Y

introduction at the H positions 30, 128, 117, 178 and 209 and for the mutation M118L. According to these predictions, the amino acids with a very similar hydrophobicity index (H: -0.2, Y: -0.4; M: 0.4, L: 0.5) would give the best folding energy. Additional stabilizing mutations were predicted for positions H128 (E, Q, K, R), H177 (K, R) and H178 (K). Subsequently, we generated an *in silico* library of 30 mutants, which include all possible combinations of the predicted stabilizing point mutations and used again a FoldX prediction to rank the library members according to the predicted free folding energy changes. Finally we submitted homology models of the four top scoring mutants (predicted stabilization energies of 4.0 - 4.9 kcal/mol compared to *wilde-type* mTFP1) to molecular dynamics simulation at 298 K and 343 K. All mutant model folds remained stable and comparison of the root mean square deviations (RMSD) of atomic positions and B-factors with the calculated trajectory of the *wilde-type* mTFP1 did not reveal any significantly increased thermal movement (Figure 16).
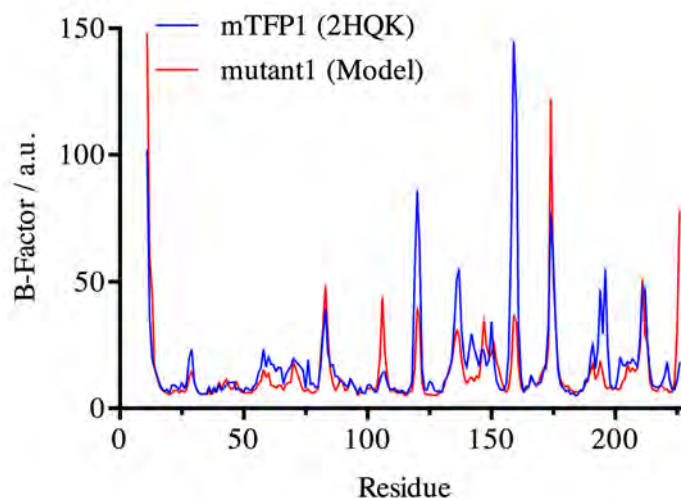
Figure 16 Molecular Dynamics Simulation: 2HQK versus mutant1

We proceeded with expression studies of the simplest version mutant1 that comprised the following mutations referring to mTFP1 (GenBank: DQ676819): H30Y, M118L, H128Y, H177Y, H178Y and H209Y
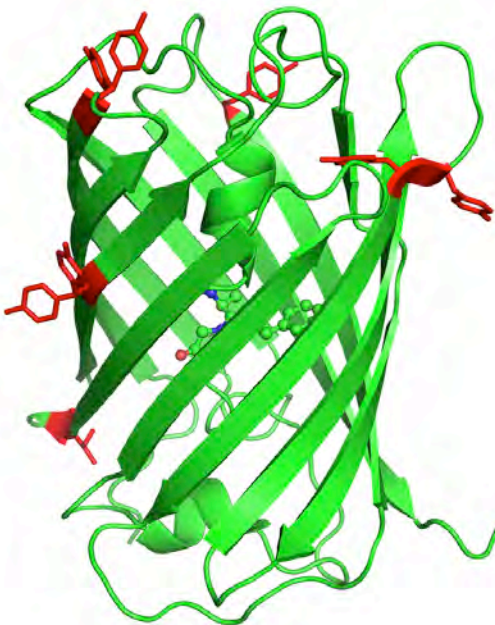
Figure 17 Crystal Structure: mTFP1 (PDB: 2HQK), red residues indicate mutations respective to mutant1

1.3. Molecular Biology

Experimental molecular biology work towards the establishment and characterization of our model protein started with the acquisition of the gene of fluorescent protein mTFP1, as described in literature[90]. Comparing the crystal structure of mTFP1 (PDB: 2HQK) with the sequence of our mutant, two N- and C-terminal linker domains became apparent (Figure S 2). Due to their variability Campbell et al., the originators of mTFP1, had already disregarded several residues in their design of 2HQK (10 C-terminally, 5 N-terminally; Figure S 4), however in our approach we proceeded with the removal of two additional, C-terminally located, amino acids as the crystal structure revealed great flexibility within this domain. Thus the design of our primers shortened the construct of mTFP1 in the course of insertion into our established host vector and formed pET303/SUMO_mTFP1.1 (Figure 18). A pET303/CT-His vector that comprised a N-terminally introduced His6-SUMO coding sequence, Smt3, from *Saccharomyces cerevisiae*. It should be noted at this point that due to the introduction of a SUMO-Tag our construct would comprise an additional, N-terminally located serine residue that remained on the protein after digestion with SUMO-Protease, Ulp1, from *Sacharomyces cerevisiae*.
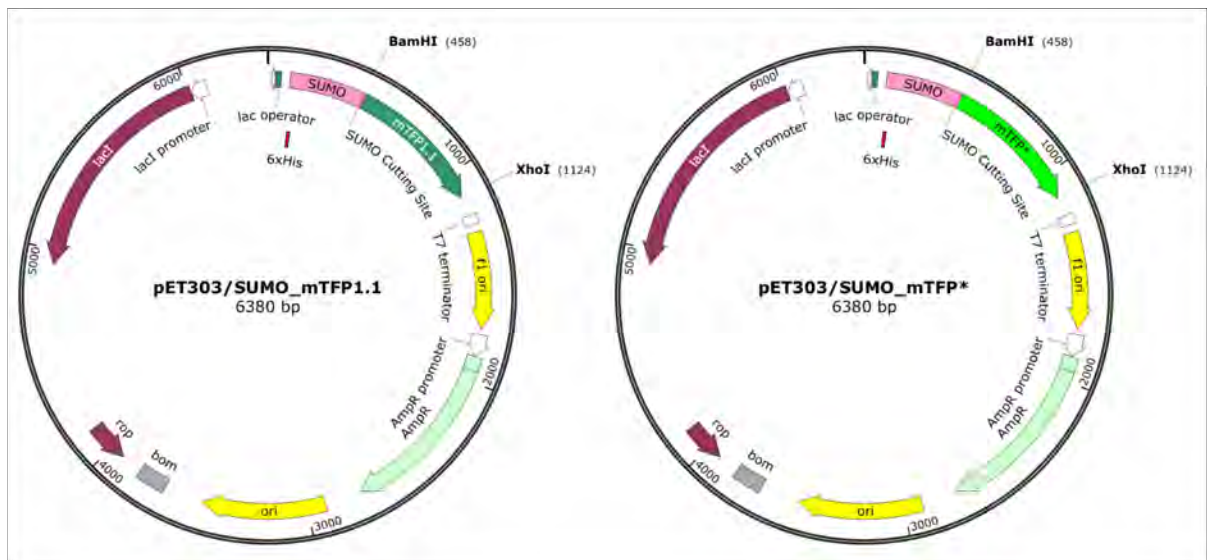
Figure 18 pET303/SUMO_mTFP1.1, mTFP*

Subsequently all identified positions (Table S 1) were mutated in a step-by-step manner, expressed under standard conditions and evaluated via fluorescence and circular dichroism to assure little perturbation of the resulting mutants. The confirmed final construct pET303/SUMO_mTFP* (Figure S 3) was then used to optimize expression levels in BL21 (DE3) Gold cells. In the course we identified an induction with 1 mM IPTG at OD_{600}=0.6 and a following 48 hours expression at 20 °C could yield in up to 300 mg/L. We proceeded with large-scale cultures to obtain quantitative amounts of protein. After harvest and according to the outline in the experimental section, His6-SUMO_mTFP* was purified from the crude extract via initial affinity chromatography, digested with SUMO protease and further heat treated to precipitate impurities that were present even after additional chromatography. Pure samples of mTFP* (as judged by SDS-PAGE, Figure S 5) were then characterized more vigorously.

1.4. Characterization of mTFP*

1.4.1. Introductory Remarks

Initial biochemical characterization revealed very distinctive properties of mTFP*, thus allowed a good estimation of its capabilities to act as scaffold for ArMs. We envisioned to scrutinize a subset of methodologies to gain a good understanding towards our designed host protein. Namely means of mass- and light-spectroscopy as well as crystallography were believed to suffice the purpose to assess all required properties. Starting of initial samples of pure mTFP* were analyzed via ESI-TOF mass spectrometry and we observed the expected mass, 25154 Da (25174 Da, as calculated with Protparam[95], ignoring the maturation step mentioned outlined below) to have almost 100% abundance (Figure 19, Figure S 5).
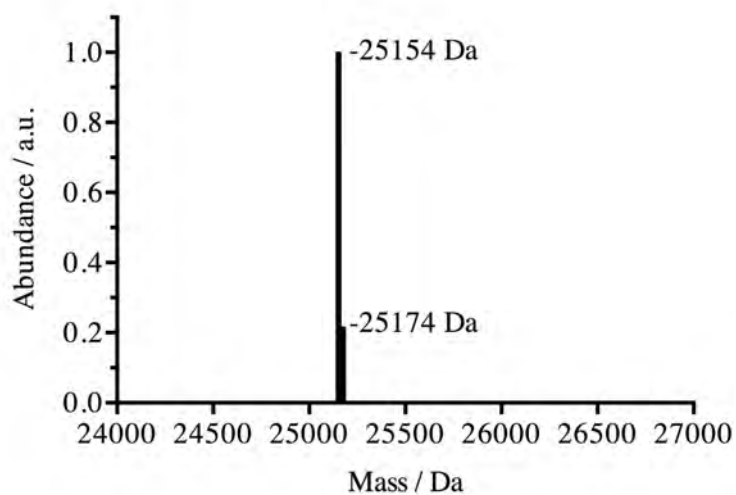
Figure 19 ESI-TOF: mTFP* 25154 and 25174 Da indicating mature and unmaturated protein

1.4.2. Spectral Properties

Further the spectral properties were assessed. The chromophore of mTFP* (A62-Y63-G64), that forms in the course of a cyclisation and gains its fluorescence after a subsequent maturation, demonstrated an absorbance maximum at 468 nm as well as a sharp fluorescent emission peaking at 495 nm and therefore deviated from previously reported values 462 and 492 nm (Figure 20)[90,96].
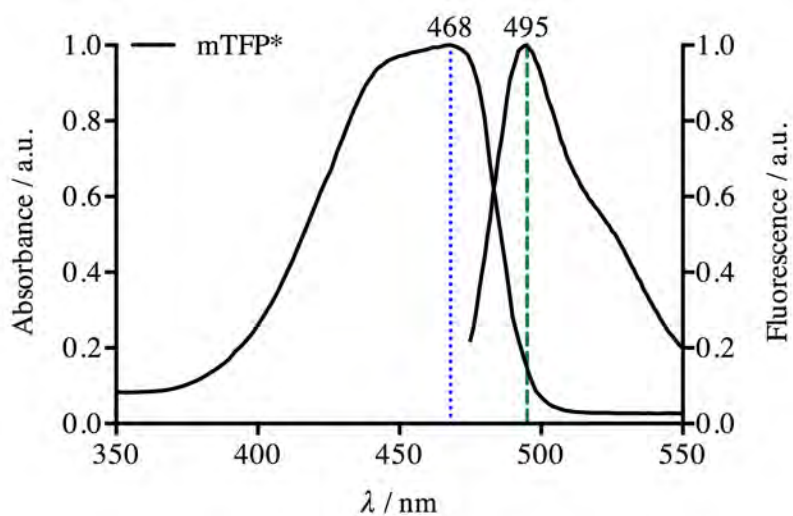
Figure 20 Absorbance and Fluorescence: mTFP* (Absorbance: 468 nm, Emission: 495 nm)

Within most ESI-TOF measurements (APPENDIX/Mass Spectrometry data) this maturation step could be followed upon, as the protein mass decreased by 20 Da (Figure 19) due to the occurring condensation of water and subsequent deprotonation (Figure 21). Especially before and after heat purifications the relative ratio of maturated to unmaturated FP increased. Nevertheless, both absorbance and fluorescence are specific to determine the concentrations of mTFP* in solution. Thus via standardized fluorescence and absorbance measurements maturated scaffold concentrations could be determined under processing conditions and therefore act as intrinsic probe, monitoring a potential catalyst (Figure S 12).
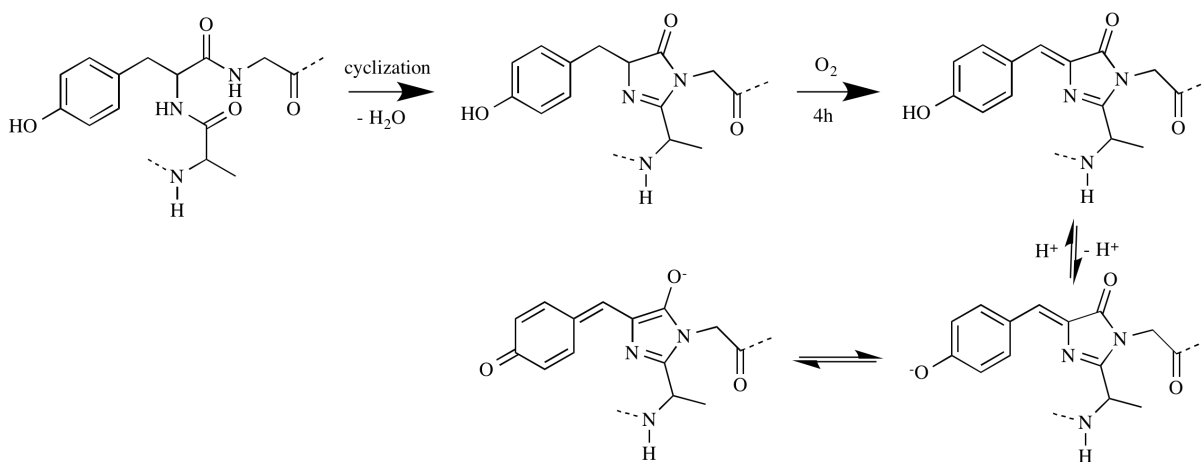
Figure 21 Chromophore Formation: Amino Acid Triplet (A62-Y63-G64) undergoes cyclisation.

1.4.3. Thermal Stability

Further the inalienable stability of mTFP* was evaluated by looking into circular dichroism (CD) and fluorescence measurements. Herein we identified a distinctive decrease in the ellipticity at 205 nm or a sudden decrease in fluorescence once the structural integrity was compromised and unfolding occurred (Figure 22, Figure 25).
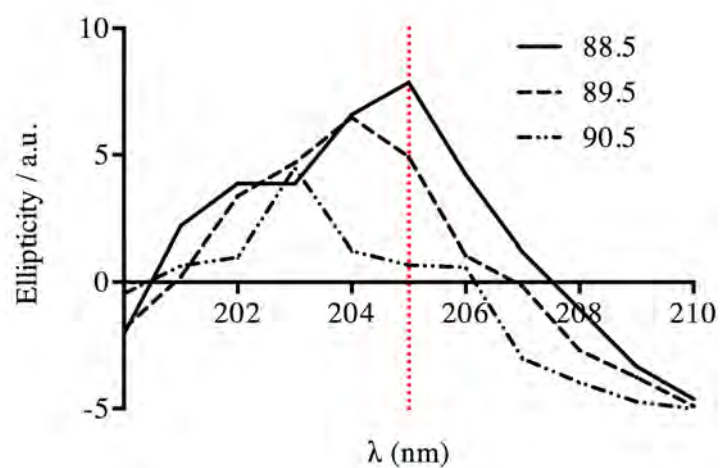
Figure 22 Circular Dichroism Scan: mTFP*; signal reduction upon unfolding

Despite the number of mutations that were introduced, it appeared that mTFP* and respective mutants (in 50 mM Tris/HCl, pH 7.4) obeyed the required robustness, yet a durable nature. In the course of thermal stability testings, samples could be heated up to 88 °C, as we observed only little perturbation from CD beforehand (Figure 23).
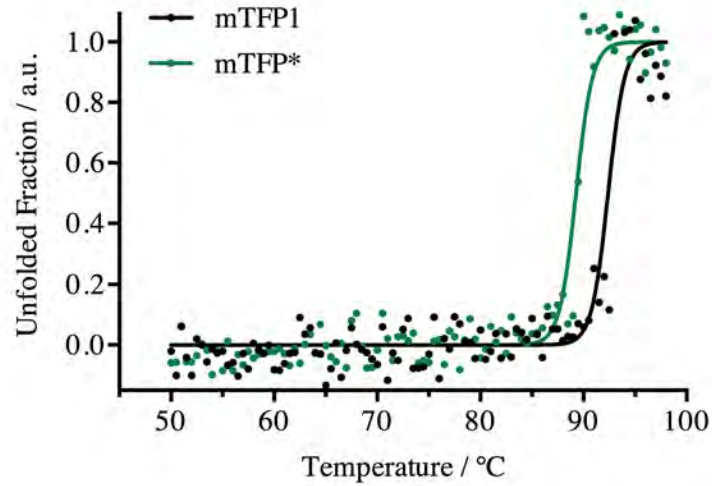
Figure 23 Temperature Stability: mTFP1 versus mTFP*

1.4.4. pH Stability

Further and in prospect to catalysis, pH stabilities were also clarified through a combination of CD and fluorescence measurements. Herein a similar robustness was identified regarding extreme conditions. At pH 2.3 circular dichroism measurements indicated structural perturbation, similarly only at pH 12.6 a sudden decrease in fluorescence could be observed arguing an overall robustness regarding pHs from 2.5 to 12.5 (Figure 24, Figure 25).
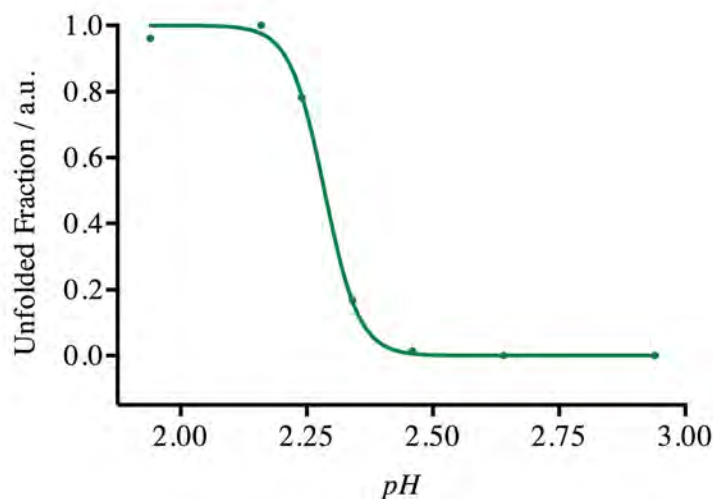
Figure 24 pH Stability: mTFP*, pH < 3, circular dichroism at 198nm indicates unfolded fraction
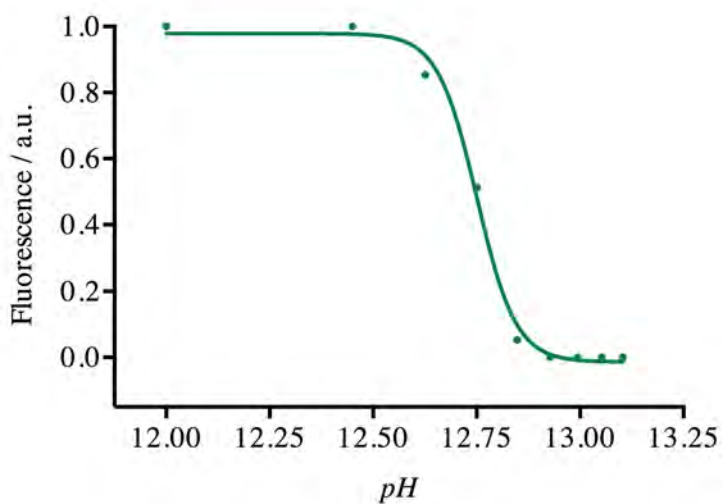
Figure 25 pH Stability: mTFP*, pH > 12, fluorescence (Abs: 468nm, Em: 495nm) indicates stability

1.4.5. Organic Solvent Tolerance

(the work of this Section has been accomplished in collaboration with Arwa Makki)

In the context of the study we proceeded with organic solvent screens to determine the overall capability of our host protein to withstand a more hostile environment that would be present during many catalytic operations. Judged by fluorescence and absorbance measurements after 24 hours, mTFP* remained mostly stable in up to 60% organic solvent such as acetone, 2-butanol, t-butanol, methanol, diglyme, dioxan, dimethylformamide, dimethylsulfoxide, ethanol, hexanol, 2-propanol, tetrafluoroethylene and tetrahydrofuran (Figure 26, Figure 27). Only concentrations of 80% and above succeeded to precipitate more than 50% of protein in the course of 24 h and therefore underlined the sincere robustness that is especially necessary for artificial metalloenzymes[1,13,15,63,97].
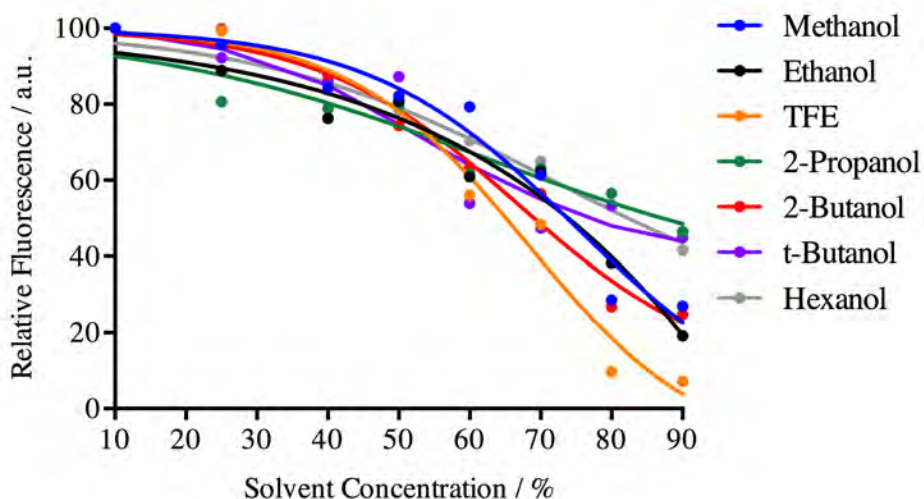
Figure 26 Organic Solvent Screen: Protic Solvents; Fluorescent Measurements indicates stability of mTFP* in respective solvents
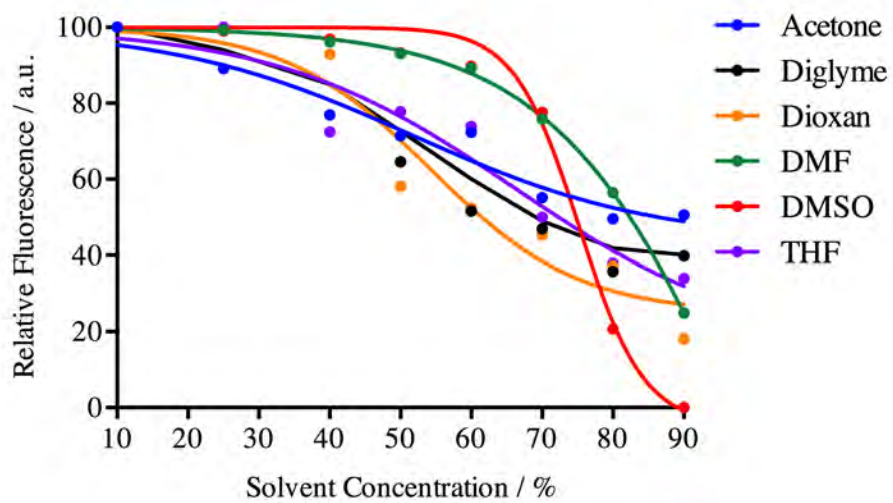
Figure 27 Organic Solvent Screen: Aprotic Solvents; Fluorescent Measurements indicates stability of mTFP* in respective solvents

1.4.6. X-Ray Structure of mTFP*

A further element in the analysis of mTFP* had to be a structural characterization that served several purposes. First we wanted to test our *in silico* design by revealing conformational changes that appeared in the scaffold due to the mutations which were introduced. Second, it remained unclear to what extend some amino acids had stability determining properties and were therefore unsuitable for alterations in the cause of our journey to artificial metalloenzymes. In spite, our analysis was to reveal structural features to grasp a comprehensive understanding of how and where the protein surface, or a present cavity, could serve as template in the formation of ArMs and would thus interact with the catalytically active transition metal. For this purpose we pursued with means of protein crystallography and were able to resolve the crystal structure of mTFP* to 1.00 Å resolution (Figure 28, PDB: 4Q9W, Table S 5).
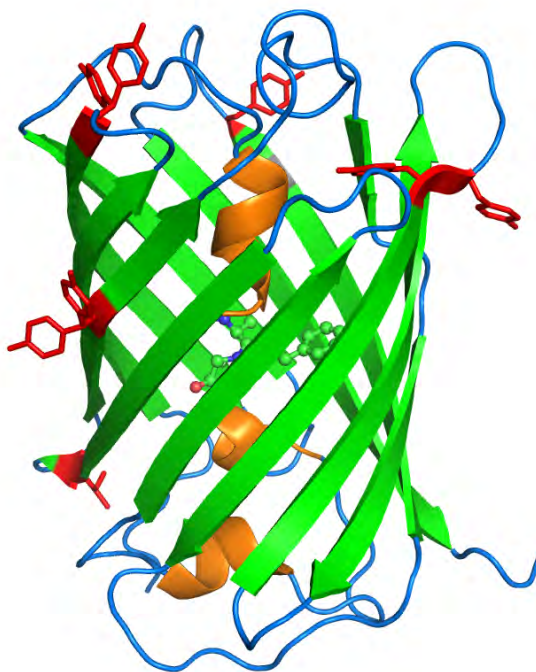
Figure 28 Crystal Structure: mTFP* at 1.00 Å (PDB: 4Q9W, red residues indicate mutations)

Herein and as deduced from earlier mentioned experiments, it appeared that none of the introduced mutations caused great perturbations and thus a destabilization of mTFP*. In general an homologous nature was observed for either mutant, mTFP1 and mTFP* (Figure 30). Each comprising variable regions, within their loops, flanking the barrel structure as well as N- and C-terminally, wherein the chromophore was consistently conjugated by residues: T58, W89, R91, S142 and H159 (Figure 29) without being affected.
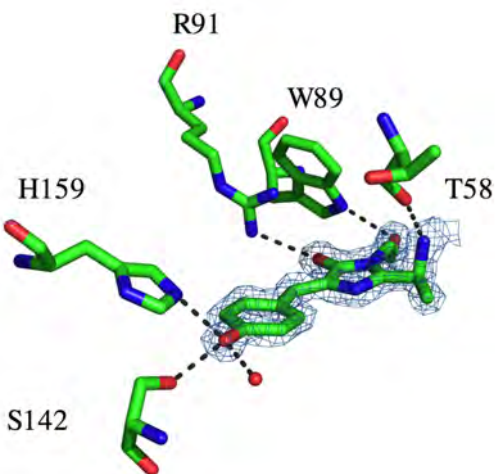
Figure 29 Chromophore of mTFP* with coordinating residues T58, W89, R91, S142, H159 (mesh indicates electron density, PDB: 4Q9W)

Regarding B-Factors and Root Mean Square Deviations (RMSDs), comparisons of mTFP1 and our designed protein mTFP* (Model and XRay Data) further confirmed the earlier described robustness (Figure 30). Only residues E111, G165 and K202, all positions representing the tip of a turning, antiparallel, beta pleated sheet, revealed higher thermal movements within mTFP*, as they appeared not to be stabilized through interactions with neighboring molecules in the crystal. Similarly D150, V186 and A187 within mTFP1 showed greater variability than the same residues within mTFP*. However, either identified residues of the barrel structure, comprising increased dynamics only resembled a region of increased motility, not destabilization, within one variant and the respective packaging in the crystal (Figure S 18). Concluding one might therefore argue a

minor conformational shift from mTFP1 to mTFP*, however not to the extent of a significant

perturbation.
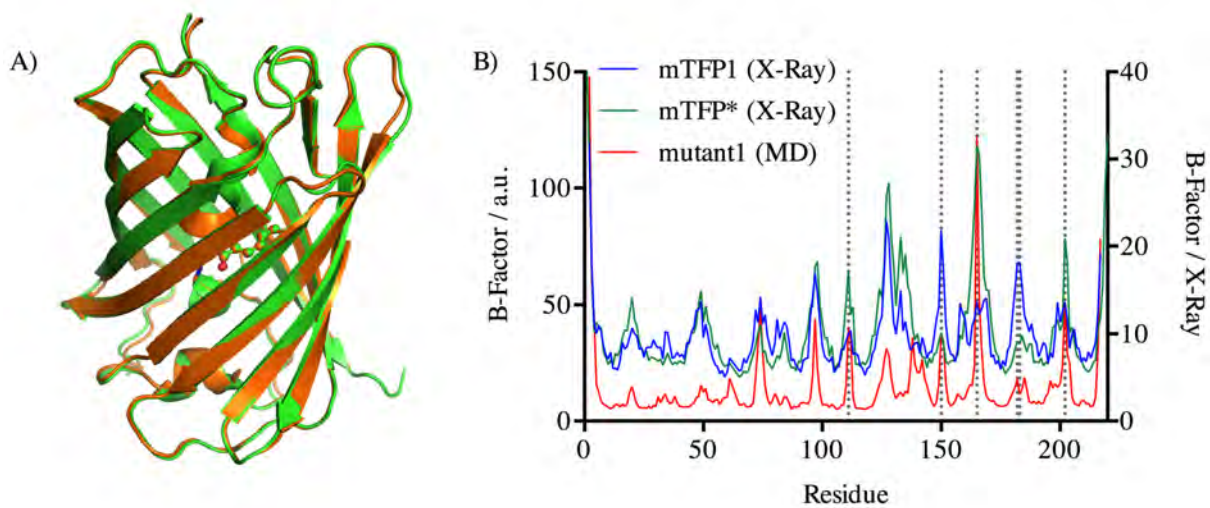
Figure 30 Superposition and B-Factor Comparison: A) mTFP1 (orange) and mTFP* (green) superposition visualizing low structural deviation; B) B-Factor Comparison of mTFP1, mTFP* and mutant1, dashed lines indicate differences between mTFP1 and mTFP* and confirm overall low thermal movement and structural integrity

1.4.7. Metal Affinity of mTFP*

Lastly, we focused on our selective approach to minimize metal binding affinities within our host protein, mTFP*. As described above, we followed our *in silico* design and replaced all surface exposed residues that would show affiliations towards metals (cysteine, histidine and methionine) with respectable other amino acids. Subsequently we needed to evaluate resulting affinities and utilized means of mass spectrometry, the intrinsic fluorescence of mTFP* and X-ray Crystallography.

1.4.7.1. Mass Spectrometry

Indications for minimal interactions were collected as we incubated 25 equivalents of various metal salts (Copper(II)Nitrate, Palladium(II)Chloride, Rhodium(II)Acetat, Nickel(II)Chloride) with mTFP* at room temperature for 1 hour. Samples were then either dialyzed over night, or directly prone to mass spectrometry. To our consent most samples did not show traces of metalation in ESI-TOF measurements (Table 1). The only notable exception were samples that had been incubated with Palladium(II)chloride. Herein we observed an additional mass signal that denoted the addition of a single Palladium species. Nevertheless, this signal disappeared after dialysis of the respective sample and indicated the overall low affinity.

| No | Mutant | Metal | Mass Spectrometry | | Δ (Da) | Metal Conjugation |
			Expected (Da)	Observed (Da)		
1	mTFP*	-	25154	25154	0	o
2	mTFP*	Cu	25154	25154	0	o
3	mTFP*	Pd	25154	25255 ($^\Phi$25154)	101(0)	x/o
4	mTFP*	Rh	25154	25154	0	o
5	mTFP*	Ni	25154	25154	0	o

Table 1 ESI-TOF Mass Spectrometry: mTFP* metalation affinity; $^\Phi$indicates observed mass after dialysis

1.4.7.2. Fluorescence

Coherently we proceeded testing the quenching effect the same transition metals had on the intrinsic fluorescence of mTFP*. Anticipating the multi modal binding sites within mTFP1 (referring to the presence of H30, M118, H128, H177, H178 and H209) we expected differently distributed quenching results in a direct comparison with mTFP*. Following and as expected the lower affinity towards transition metals was confirmed by the general increase in fluorescence despite the presence of a quencher. Also experiments that involved up to 10 equivalents of salts of Copper or Rhodium showed a significant higher fluorescence for mTFP*. This became most apparent as samples that were dialyzed showed full signal recovery for mTFP*, but not for mTFP1 (Figure 31, Figure S 6).
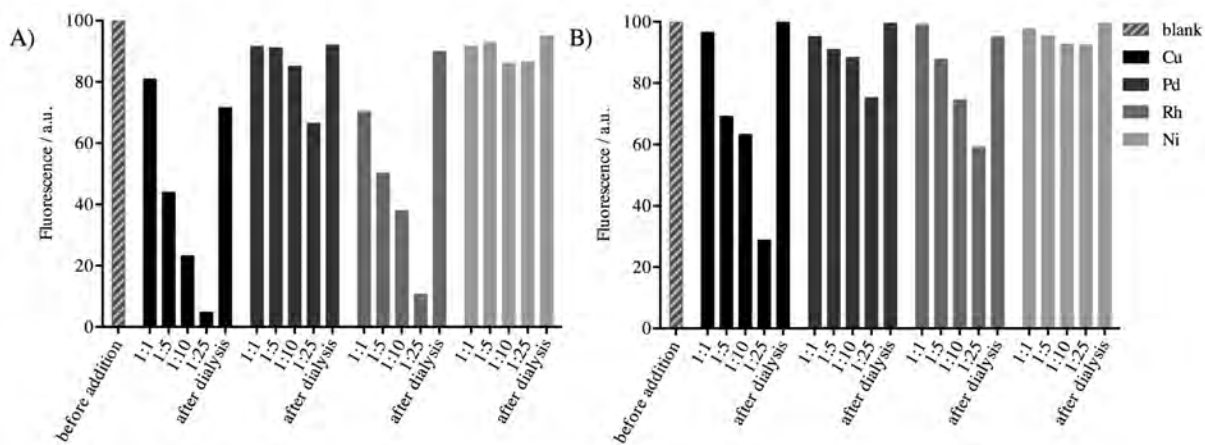
Figure 31 Fluorescence Quenching: A) mTFP1, B) mTFP* with 1 to 25 eq. of transition metal

Concluding, notable exceptions appeared to be experiments that contained Pd^{2+} or Cu^{2+} ions. Herein we observed a concentration dependent addition in ESI-TOF or fluorescence measurements. These adverse effects however, were of reversible nature and disappeared once the samples were dialyzed. Hence in the course we were able to show that most metals do not have significant affinities towards mTFP*.

1.4.7.3. Transition Metal FRET

In the spirit of quantifying interactions of transition metals with our host protein we further referred to the intrinsic fluorescence of mTFP* and thus anticipated transition metal FRET (Foerster Resonance Energy Transfer) principles to evaluate the metalation affinities of our optimized host. Förster resonance energy transfer is a process where excitation energy is transferred by dipole-dipole coupling from a donor to an acceptor fluorophore[98]. Herein the efficiency of this particular energy transfer is strongly dependent on the distance of both dyes, $E = \frac{R_0{}^6}{R_0{}^6 + R^6}$ and R_0 is the distance at which the transfer is 50%[99,100]. This relationship makes FRET an extremely sensitive method to map distances of probes in three-dimensional space. Within classical FRET methodologies the acceptor dye emits at a different wavelength than the donor dye was excited at. Strongly simplifying, this relation can be used to estimate the orientation simply from the amount of light that is detected at a particular wavelength. In tmFRET however, a colored transition metal is scrutinized to act as the energy acceptor and only the reduction of donor fluorescence is evaluated. However because metals generally have a very short R_0 their capability of being the acceptor is strongly limited and even more dependent of a stationary position within a short distance[101,102]. Arguably tmFRET presented itself to be an ideal tool to quantify binding dynamics of our transition metal catalyst to the designed metalloproteins.

In the context of mTFP*, titrations with various concentrations of Copper(II)Nitrate were performed (Figure 32). We observed a substantial difference in fluorescence between our mutant and the original *wild-type* in response to the stepwise addition of quencher up to concentrations of 100 mM. Additionally and as expected, titrations that were performed at pH 7.5, generally appeared to be more sensitive and baselined at about 10-fold lower concentrations. Interestingly

mTFP1 showed a high sensitivity towards the addition of Copper(II)Nitrate and thus confirmed our estimation of various coordinating residues to be present.
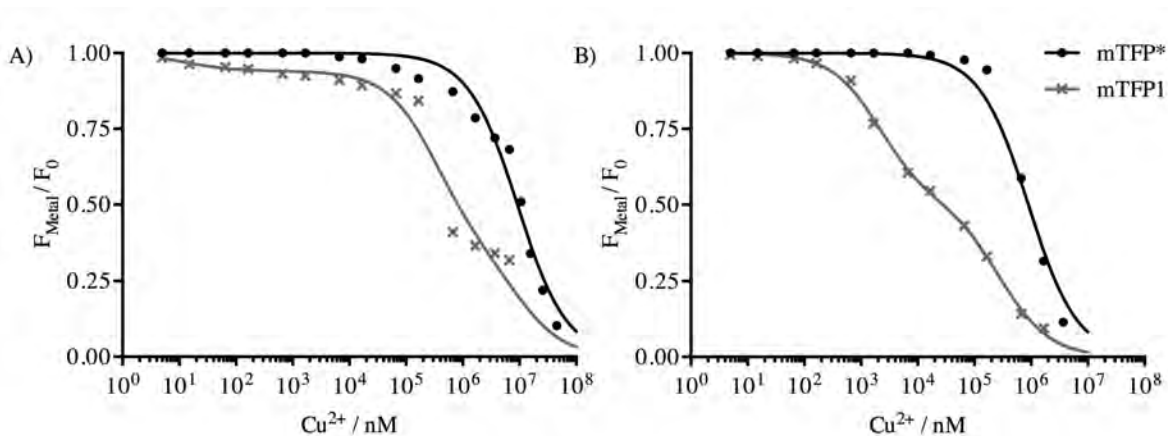
Figure 32 tmFRET: mTFP1 and mTFP* titration against various amounts of Copper(II)Nitrate at pH 6 (A) and pH 7.5 (B)

Nonetheless, to verify these findings and later scrutinize tmFRET methodologies to argue dissociation constants for our ArMs, we also needed to evaluate fluorescence lifetimes; moreover their change upon the addition of transition metal. Evaluating the formulae that we were applying, binding dynamics could only be judged if the correct quenching process was assumed. Hence for proteins that were not supposed to coordinate metals, mTFP*, only static quenching had to be considered. On the contrary upon the introduction of binding motifs, dynamic processes were to be evaluated as well. Since only the latter would affect fluorescence lifetimes we were pleased to observe a drastic change for mTFP1, but not for mTFP* and therefore found further evidence for our design (Figure 33).
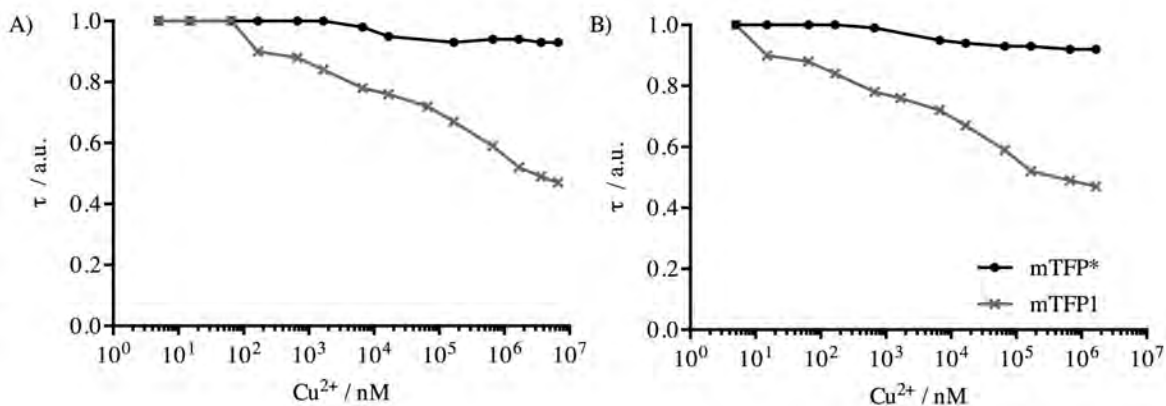
Figure 33 Fluorescence Lifetime Measurement: mTFP* versus mTFP1 upon Copper(II)Nitrate addition.

Anticipating a monophasic model for mTFP*, implying no binding site would be present in the designed host and thus only static quenching taking place, and a bi-phasic model for mTFP1 implying the earlier identified amino acid represented a binding site and thus a combination of static and dynamic quenching would occur, we were able to determine static (K_dStat) and dynamic dissociation constants (K_dDyn) at pH 6.0 and pH 7.5 respectively (Figure 32, for details see MATERIALS AND METHODS Page 118).

Mutant	pH	K_dStat (mM)	K_dDyn (μM)
mTFP1	6.0	8.46	324 / 0.01
	7.5	0.89	269 / 2.14
mTFP*	6.0	8.46	-
	7.5	0.89	-

Table 2 Dissociation Constants: mTFP* (mono-phasic model), mTFP1 (bi-phasic model)

Concluding we established protocols to quantify the affinities of our potential catalytic transition metal, Copper, towards the designed host proteins. We were also able to prove the earlier made observations of a low metalation affinity of mTFP*, and vice versa from mTFP1, from general quenching experiments and mass spectrometry, but also quantified the affinities that our host proteins intrinsically possessed.

1.4.7.4. X-Ray Structure

Further to elucidate its intrinsic ability or disability to coordinate metals we performed co-crystallization and soaking experiments using the same metal salts as in previous evaluations. Herein, initially only co-crystallization principles yielded in usable material for most metal salts. Albeit and as desired, we weren't able to identify relevant coordinations in most of the derived structures and assumed the aforementioned low metalation affinity. Only samples that were co-crystallized with 25 equivalents of Copper(II)Nitrate and thus a vast excess revealed the coordination of a single species by residues D140, H159 and K160 (Figure 34). Referring to the concentration and the lack of copper being present in any other structure derived from co-crystallization experiments with less than 25 equivalents we minored the importance of this finding in the context of our study.

Samples that were incubated with $PdCl_2$ however, did not show any initial crystal formation under various conditions. In spite we continued with soaking experiments and were able to obtain solid crystals in the presence of varying amounts of $PdCl_2$, and could in a few cases highlight sites of coordination within mTFP* (PDB: 4Q9X).
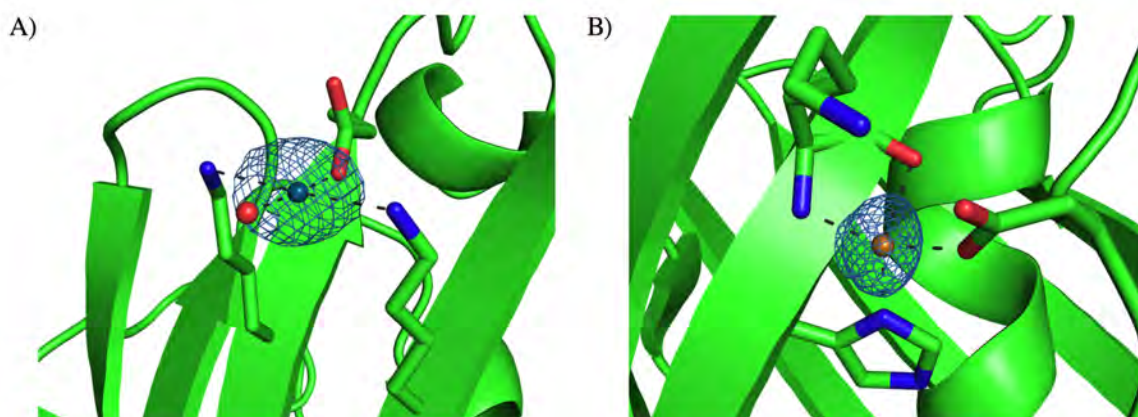
Figure 34 Metal Affinity: Crystal Structures of mTFP* A) Palladium Soak (PDB: 4Q9X), B) Copper Co-Crystallization

From structures containing palladium however we made a few immanent observations. Merely with concentrations of 10 mM metal and above we observed, yet undescribed square planar and to almost octahedral motifs, utilizing ε-amine and γ-carboxyl-groups from lysine, aspartate or glutamate to coordinate palladium (Figure 34). As precisely these coordinating residues seemed to be differently orientated and in close proximity to the pairing molecule in the unit cell of naïve mTFP* (they form the contacts, Table S 4), we comprehended the initial failure of co-crystallization experiments. Taking these and the aforementioned findings into account we concluded weak, kinetically labile interactions of our host with metals and found our hypothesis further supported.

1.5. Discussion

The design of a stable and functional metalloprotein involves two steps: i) the identification of a suitable protein scaffold and ii) the incorporation of the metal binding site. The choice of the right host protein scaffold is fundamental for artificial metalloprotein design. Starting from the highly stable and brightly fluorescent protein mTFP1, we were able to engineer a low metal-affinity variant, mTFP*. Our method was straight forward and involved the selection of surface exposed metal binding residues, FoldX-based prediction of changes in folding energy for mutants and stability evaluations of highest scoring mutants by MD. The simplicity of this method should make it applicable to any other host protein scaffold of choice. Metal binding studies underlined the importance of our approach: ESI-TOF and fluorescence evaluation argued low metal affinity for mTFP* and significantly higher affinities for mTFP1. tmFRET titrations revealed at least two metal binding sites of with K_ds of 2.14 μM and 269 μM at pH 7.5 and K_ds of 0.01 μM and 324 μM at pH 6.0 for the parent mTFP1 protein, while within the investigated pH range mTFP* possessed only a low, unspecific metal affinity of roughly 1 to 10 mM. mTFP* showed an astonishing stability towards temperature (T_m = 89 °C), pH changes (stability range: 2.3 < pH < 12.6), salt concentrations (e.g. stable in 10 mM urea at 80 °C, Figure S 13), and was even stable and soluble in high concentrations of organic solvents. The flappy N- and C-terminus of mTFP1 were removed during the protein engineering process. The design principle of creating of maximizing rigidity enhanced the crystallization tendency of mTFP*. Correspondingly, mTFP* protein and various mutants crystalized readily and provided electron density maps, which could be refined to outstanding resolutions of up to 1.0 Å.

2. MODIFICATION AND CONJUGATION

2.1. Introductory Remarks

Modifying the mTFP1 scaffold to become a metalloprotein required the pre-establishment of a protein host that greatly withstood metalation. Having succeeded relevant measures to functionalize this host had to be considered. We imagined means of dative anchoring and covalent modification and present our findings below.

2.2. Selection of Binding Pocket

Continuing we evaluated potential sites of modification, yet catalysis on the surface of mTFP*. Herein initially identified residues, Y200 and Y204 respective mTFP*, H205 and Y209 respective mTFP1 (GenBank: DQ676819), H204 and Y208 respective deposited crystal structure (PDB: 2HQK) were found to be flanking a 10 x 9 x 9 Å cleft that could be scrutinized in the sense of a second coordination sphere (Figure 35).
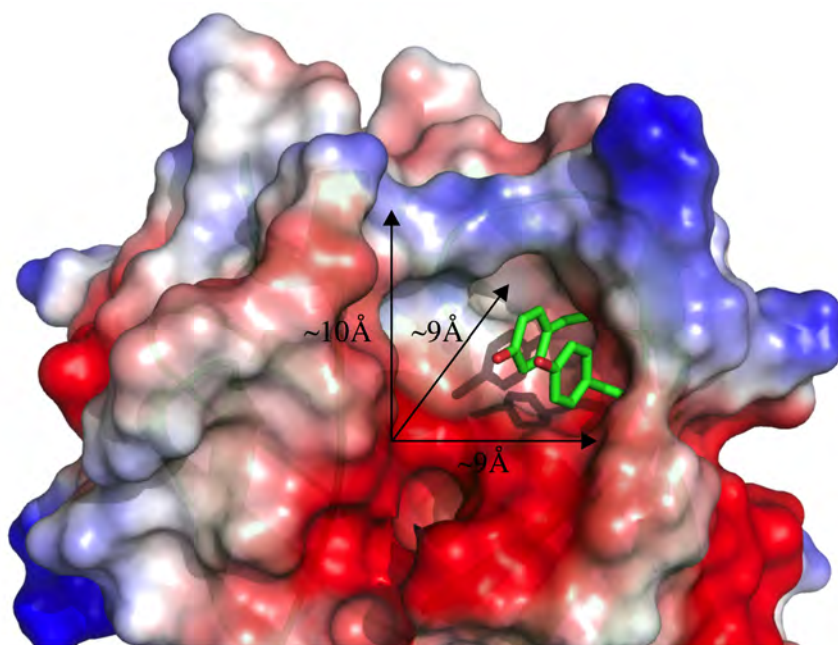
Figure 35 Selection of Binding Pocket: 10 x 9 x 9 Å Cleft, Illustrating Residues Y200, Y204

Within this mentioned cavity, yet working on model scaffolds to establish an artificial metalloenzyme, we envisioned to specifically reintroduce metal binding capabilities via dative or covalent anchoring strategies. Means of site directed mutagenesis (SDM) were employed to introduce either the possibility to station thiols (specifically positioned cysteines and largely employing residue Y204) or a designed combination of metal affine naturally occurring residues, canonical amino acids, to form a binding pocket (dative anchoring)[14]. We targeted to prove modifications and following conjugations with transitions metal species i.e. Cu^{2+} by principle means of spectroscopy, crystallography and/or mass spectrometry and were able to show successful derivatization. A detailed outline will be presented in section below.

2.3. Canonical Amino Acids

In the present study a family of transition metal binding sites was created by introducing coordinating amino acids, cysteine, aspartate/glutamate, histidine or methionine at geometrically appropriate positions. By these means our previously evaluated host protein mTFP* was further converted into a subset of metalloproteins, mTFPmb (metal binder), each comprising the robust nature that had been discovered and evaluated before (Table S 2).

2.3.1. Design and Generation of a mTFPmb Library

The above mentioned information along with careful analysis of the mTFP* crystal structure (PDB: 4Q9W) and the original presence of a histidine residue at position 209 of mTFP1 (GenBank: DQ676819) led us to consider engineering motifs related to the well described 2-his-1-caboxylate triad (His/His/Asp)[85,86,103,104]. The crystal structure of mTFP* suggested an ideal spacing of neighboring residues Y200 and Y204 ($2HQK_{Y204} = 4Q9W_{Y200}$), having roughly 4 Å distance in three-dimensional space[85]. Further, the surrounding loops also prompted residues I197, D55 and Y54 to be taken into consideration for alternative triads (Figure 36).
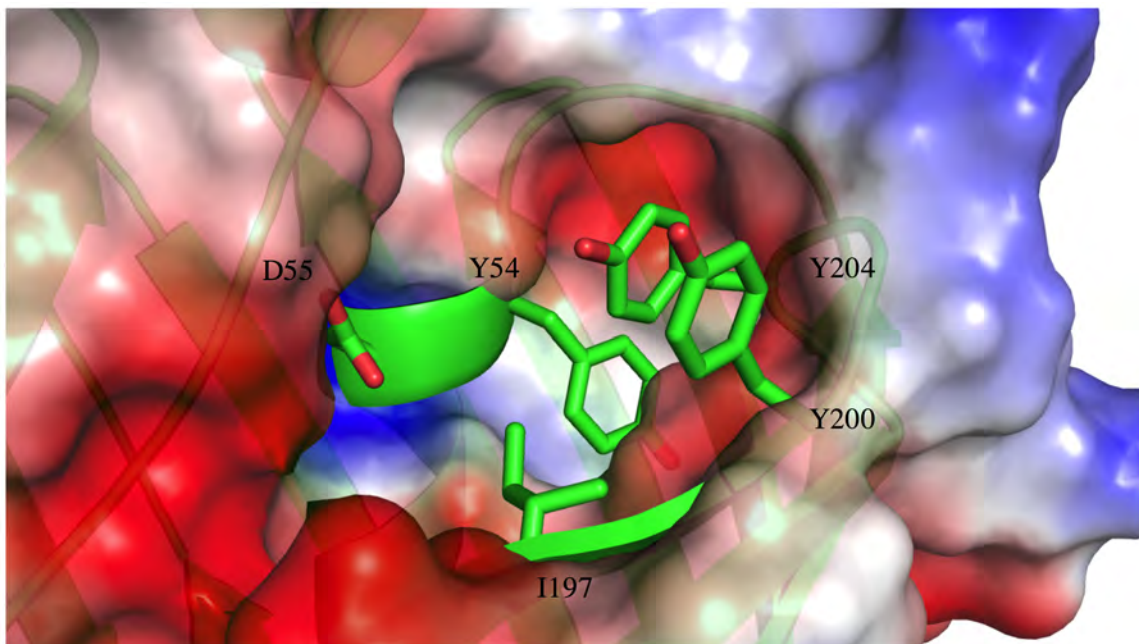
Figure 36 Selection of Binding Pocket: Y54, D55, I197, Y200, Y204

We anticipated the preferential Copper binding by a subset of three out of the five positions. Subsequently residues I197, D55 and Y54 were each permutated with cysteine, aspartate/glutamate, histidine and methionine thereby paired with two consistently present histidines at positions 200 and 204. Ergo we created a small library, starting from position I197, D55 to Y54 that consisted of several metal binding triads (Table 3).

No	Mutant			Mutations		
1	mbYDCHH	Y54	D55	C197	H200	H204
2	mbYDEHH	Y54	D55	E197	H200	H204
3	mbYDHHH^ɸ	Y54	D55	H197	H200	H204
4	mbYDMHH^ɸ	Y54	D55	M197	H200	H204
5	mbYCIHH	Y54	C55	I197	H200	H204
6	mbYEIHH	Y54	E55	I197	H200	H204
7	mbYHIHH	Y54	H55	I197	H200	H204
8	mbYMIHH^ɸ	Y54	M55	I197	H200	H204
9	mbCDIHH	C54	D55	I197	H200	H204
10	mbDDIHH	D54	D55	I197	H200	H204
11	mbHDIHH	H54	D55	I197	H200	H204
12	mbMDIHH^ɸ	M54	D55	I197	H200	H204
13	mbYDIHH	Y54	D55	I197	H200	H204
14	mbYEQHH	Y54	E55	Q197	H200	H204
15	mbYECHH	Y54	E55	C197	H200	H204
16	mbYDIHC	Y54	D55	I197	H200	C204
17	mbYDIMH	Y54	D55	I197	M200	H204
18	mbYDIMC^ɸ	Y54	D55	I197	M200	C204

Table 3 Metal Binding Library: Overview of Mutants, ɸ indicates mutants that were not established or that didn't maturate to intact protein.

Deriving from crystal-data of mTFP* however, a few mutations where eliminated in position 197 as they appeared sterically to be too demanding (Table 3: No 3 - mbYDHHH, No 4 – mbYDMHH; ɸindicates mutants). In both cases we anticipated the limited space present once a histidine or methionine would be incorporated and argued proper metal-binding sites could not be achieved. However in the spirit to analyze the geometrical and chemical influences six additional motifs were included. These showed influences of a fourth binding partner (mbYECHH), a sterically competitive ligand (mbYEQHH), a missing third ligand (mbYDIHH) or a combination of cysteine, histidine or methionine forming a dual anchor (mbYDIHC, mbYDIMH and mbYDIMC).

Concluding a set of 18 mutants was planned initially. Nonetheless in the process of the establishment two aforementioned mutants were eliminated from the design and another 3 mutants did not maturate under any conditions, mbYMIHH, mbMDIHH and mbYDIMC. Hence these were also not considered in our analysis of the first and second coordination sphere on Diels-Alder reactions. Finally we planned to scrutinize the robust nature and the foreseen metalation affinity of this novel metal-binding protein-family to prove our concept of novel artificial metalloenzymes.

2.3.2. Protein Characterization

In the spirit of our in depth analysis of mTFP*, the established host proteins had only to be evaluated on their metalation affinity through mass spectrometry and/or spectroscopy. We argued a similar robustness referring to the minor alterations introduced in our establishment (Figure S 15). Hence we applied the same methodologies for the production and purification as well as the analytics using ESI-TOF mass spectrometry and tmFRET (MATERIALS AND METHODS, Page 118). Herewith we believed to grasp insights of the binding potency and the attached kinetics – a factor of utmost importance when considering catalysis. Due to the overall similarity of all mutants, we appraised scaffolds mbYDCHH and mbYDEHH for their ease of production as templates to evaluate general affinities; thus our protocols heavily focus on these particular mutants. Insights were then transferred to the remaining mutants and helped substantially in subsequent catalysis.

2.3.2.1. Mass Spectrometry

Our mass spectrometry evaluation of all mutants clearly indicated the successful establishment of the envisioned library (Table 4, Figure S 7 - Figure S 10). Despite the lack of some foreseen motifs we continued with ESI-TOF mass spectrometry to prove conjugation with Cu^{2+}. Herein and as outlined in the experimental section, 0.04 mM protein from the metal binding library were incubated with 2 equivalents of Copper(II)Nitrate. Measurements occurred using a C4 column prior to ESI-TOF principles. We could show successful conjugation through an additional signal ($\Delta M = 64Da$) respective to the expected *wild-type* masses, for all mutants, but mbYEIHH, mbYEQHH and mbYDIHC. Owing the well-described difficulty to determine transition metal conjugation to proteins from mass spectrometry data, we continued further with spectroscopic evaluations[15]. Indications towards a successful establishment however were apparent.

No	Mutant	Metal	Mass Spectrometry		Δ (Da)	Metal Conjugation
			Expected (Da)	Observed (Da)		
1	mbYDCHH		25092	25092	0	
		Cu	25156	25155	-1	+
2	mbYDEHH		25118	25115	-3	
		Cu	25182	25177	-5	+
3	mbYCIHH		25090	25090	0	
		Cu	25154	25145	9	+
4	mbYEIHH		25116	25115	-1	
		Cu	25180	25115	-65	-
5	mbYHIHH		25124	25123	-1	
		Cu	25188	25178	-10	+
6	mbCDIHH		25042	25040	-2	
		Cu	25106	25105	-1	+
7	mbDDIHH		25054	25052	-2	
		Cu	25118	25123	5	+
8	mbHDIHH		25076	25073	-3	
		Cu	25140	25133	-7	+
9	mbYDIHH		25102	25099	-3	
		Cu	25166	25162	-4	+
10	mbYEQHH		25131	25131	0	
		Cu	25195	25131	-64	-
11	mbYECHH		25106	25106	0	
		Cu	25170	25169	-1	+
12	mbYDIHC		25068	25067	-1	
		Cu	25132	25067	-65	-
13	mbYDIMH		25096	25095	-1	
		Cu	25160	25152	-8	+

Table 4 mTFPmb Library: Mass Spectrometry Results indicating correctness of mutants and metal conjugation; (see APPENDIX Page 143 to 146 for detailed spectra)

2.3.2.2. Transition Metal FRET

As described above we proceeded with metal binding mutants mbYDCHH and mbYDEHH and compared them with their predecessors mTFP1 and mTFP*. As described earlier we anticipated multiple binding sites for mTFP1, no binding sites for mTFP* and one binding site for our designed mutants. Thus spectral datasets from fluorescence quenching experiments were fitted according to theorems that accounted for their different static and dynamic interactions with transition metals (MATERIALS AND METHODS, Page 118). To reassure their difference fluorescent lifetimes of mbYDCHH were compared to mTFP* and proved the presence of dynamic quenching (Figure S 16).
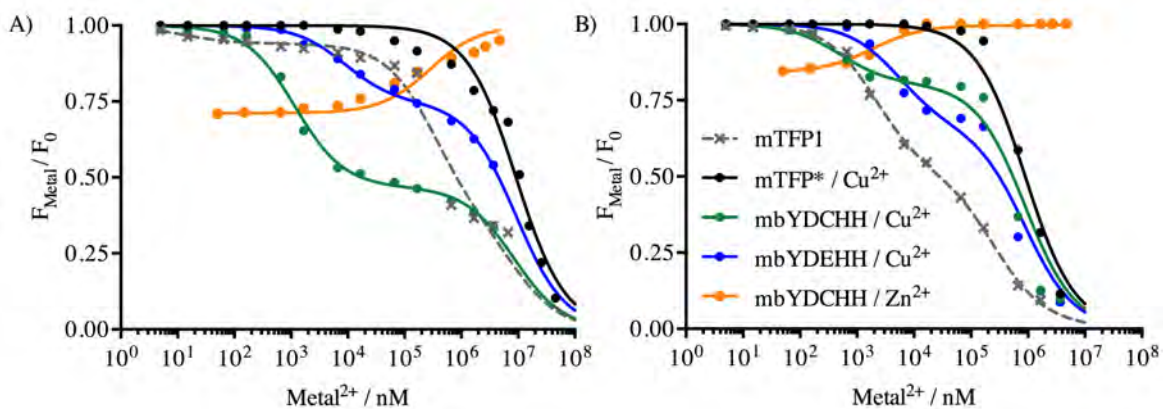
Figure 37 tmFRET: mTFP1, mTFP*, mbYDCHH and mbYDEHH; A) pH 6.0, B) pH7.5

Further, owing the catalytic prominence of several transition metals that do not necessarily embody quenching properties towards our host proteins fluorescence, we advanced our methodologies towards indirect quantification principles as well. Herein, the behavior of Zn^{2+}, a transition metal of great importance in enzymology, was evaluated by using a competitive screen based on our insights from Cu^{2+} titrations[105]. Hence from known concentrations of copper we performed titrations with Zinc(II)Nitrate and were are able to determine dissociation constants through the displacement of copper and the recovery of the fluorescence.

Mutant	Metal	pH	K_dStat (mM)	K_dDyn (μM)
mTFP1	Cu	6.0	8.46	324 / 0.01
		7.5	0.89	269 / 2.14
mTFP*	Cu	6.0	8.46	-
		7.5	0.89	-
mbYDCHH	Cu	6.0	8.46	1.18
		7.5	0.89	0.97
mbYDCHH	Zn	6.0	8.46	4.04
		7.5	0.89	128.34
mbYDEHH	Cu	6.0	8.46	8.86
		7.5	0.89	5.22

Table 5 Dissociation Constant Overview: mTFP1, mTFP*, mbYDCHH and mbYDEHH

In general, our analysis suggested the establishment of a novel metalloprotein family. The derived dissociation constants for both mutants implied a severe increase in the metal affinity with respect to mTFP* by a whole order of magnitude (Table 5). Whereas mTFP* titrations resulted in 8.46 mM at pH 6.0 and 890 μM at pH 7.5, corresponding metalloprotein versions mbYDCHH and mbYDEHH only resulted in 1.18 μM and 0.97 μM, 8.86 μM and 5.22 μM at pH 6.0 and pH 7.5 respectively. On the basis of these experiments, indirect titrations were performed with various concentrations of Zinc(II)Nitrate stock solutions. Herein we anticipated previous insights and were able to derive dissociation constants of 128.34 μM and 4.04 μM at pH 6.0 and pH 7.5.

Interestingly our analysis visualized a drastic disparity of titrations performed with mbYDCHH at pH 6.0 and 7.5. Whereas the experimental setup was not altered between both titrations, except for the pH, the resulted quenching increased almost by a factor of two. We performed further experiments to discriminate pH effects on the general spectral properties of the protein scaffolds. Next to a radical decrease in fluorescence and a shift of the emission maximum, we also evaluated the potentially increased absorption of Copper with respect to more acidic conditions or in response to the binding of histidines (Figure S 14). Since the effect couldn't be explained by these means we assumed a structural rearrangement to take place, either forming a binding site

closer to the chromophore or a ligand derived energy transfer to enhance the quenching process. Further pH resolved titrations as well as high throughput mapping, and the subsequent plotting of estimated E-Factors confirmed these initial observations (Figure 38).
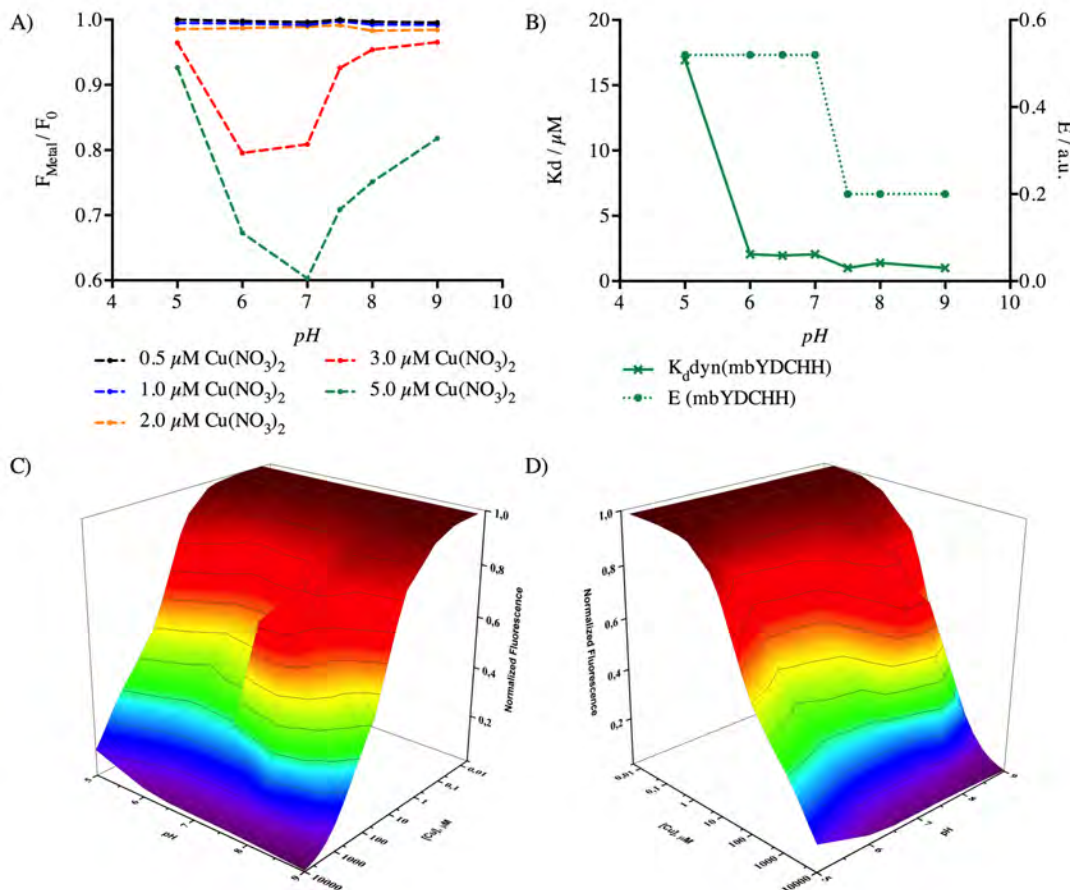
Figure 38 pH Quenching Studies: mbYDCHH titrated with various concentrations of Copper(II)Nitrate over a range of pHs

Supporting these findings, titrations with mutant mbYDEHH behaved differently. Herein the earlier observed shift and increase in fluorescence quenching with respect to changes of pH could not be observed. Thus we gathered our insights and concluded for a change in the ligand structure that coordinates the copper atom within mutant mbYDCHH. However since both mutants only vary in one particular position, we believed the spectroscopic difference to be caused by C197, moreover its participation or non-participation in the coordinating motif depending on the pH

condition. Throughout this analyzes we gained insights towards the metalation affinity of metal binding mutants of mTFP*. Our results indicate structural dynamics in the process of metal coordination and were further evaluated by means of protein crystallography.

2.3.3. X-Ray Structure

In accordance to previously described crystallographic methodologies we were able to obtain solid crystalline material of mutants mbYDCHH and mbYDEHH. Owing to the insights gained from tmFRET studies we also envisioned to crystalize mutant mbYDCHH at pH 6.0 and at pH 7.5. Thus samples of protein were dialyzed against 50 mM HEPES Buffer with the respective pH and then crystallized over night. Crystals showed the same appearance as material from other studies and were established with similar ease. We were able to obtain several structures to elucidate our earlier findings.
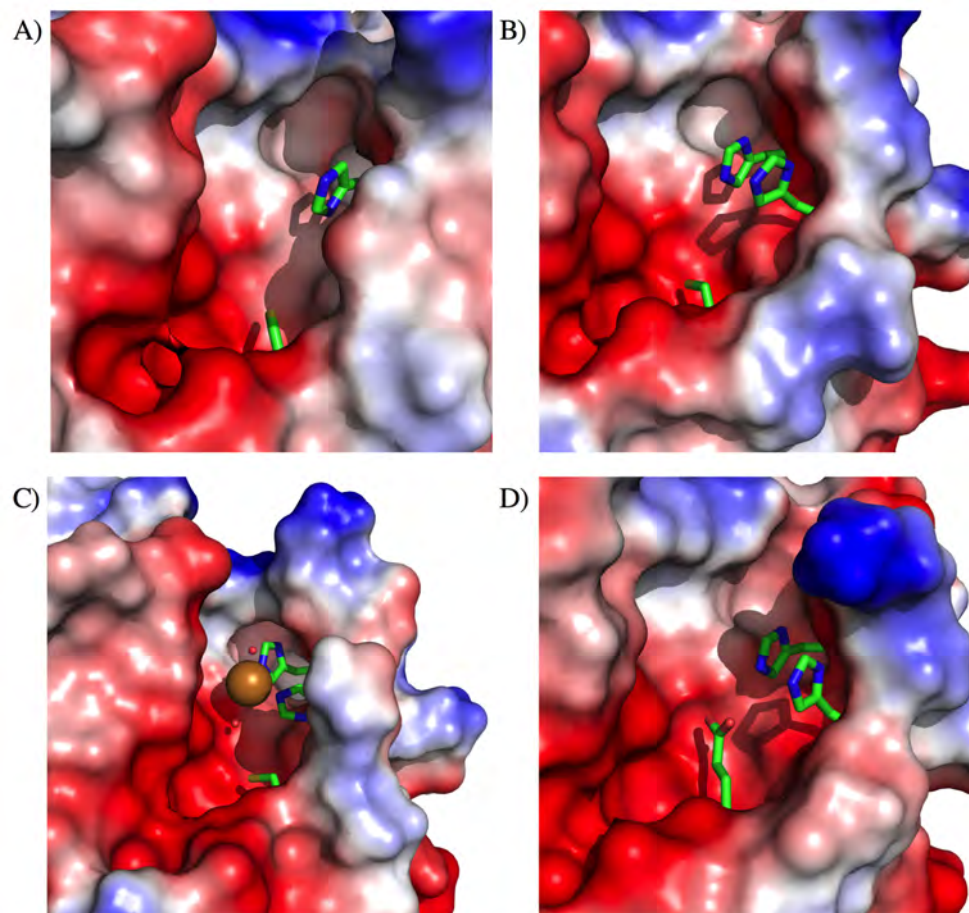
Figure 39 Crystal Structures mbYDCHH, mbYDCHH_Cu, mbYDEHH: A) Binding Pocket of mbYDCHH at pH 6.0 (open conformation); B) Binding Pocket of mbYDCHH at pH 7.5 (closed conformation); C) mbYDCHH_Cu co-crystallization; D) Binding Pocket of mbYDEHH

To our surprise and thus endorsing our first suspicion, we were able to resolve two orientations of the same triad in mutant mbYDCHH (Figure 39). This observation appeared to be conserved since the further evaluation of datasets obtained from crystals grown at pH 6.0 or 7.5, yielded in the same structural orientations. The moiety built by residues C197, H200 and H204 showed an open and a closed conformation in accordance with enhanced thermal movement of the loop built by amino acids 195-205 (Figure 40). Herein especially residue H200 showed increased dynamics, being oriented outwards to the surface (open-conformation) or towards the inside (closed-conformation) of the protein and thus potentially lacked involvement in the earlier described transition metal binding at the lower pH (Figure 40B). Upon an opening of the binding pocket, residues C197 and H204 showed closer proximity (5.2 Å) and could thus account for a planar, bidentate binding motive of its own (Figure 39A, Figure S 19). This movement is stabilized by a hydrogen-bond between the protonated H200 and T208 and reduces the charge repulsion of two positively charged side chains of H200 and H204. Distances of respective residues C197 and H204 (5.7 Å) in the closed confirmation however, showed the anticipated and potential involvement of all three members of the triad (Figure 41, Figure S 19).

Further evaluating the conundrum regarding the dynamics of the binding pocket we proceeded with co-crystallization principles to gain insights how mbYDCHH would make use of the binding triad to coordinate Copper atoms (Figure 39C). We were able to resolve a crystal structure at 1.55 Å resolution (PDB: 4R6D) and found one copper atom to be coordinated by H200 and H204. Herein earlier indications were found to be correct, as C197 did not show any involvement in the binding process. Moreover the distances derived from crystal structures objected the possibility in the first place. C197 showed a distance of 5.7 Å towards the bound Copper that was found in closer proximity, 2.1 Å, regarding H200 and H204 (Figure S 19).
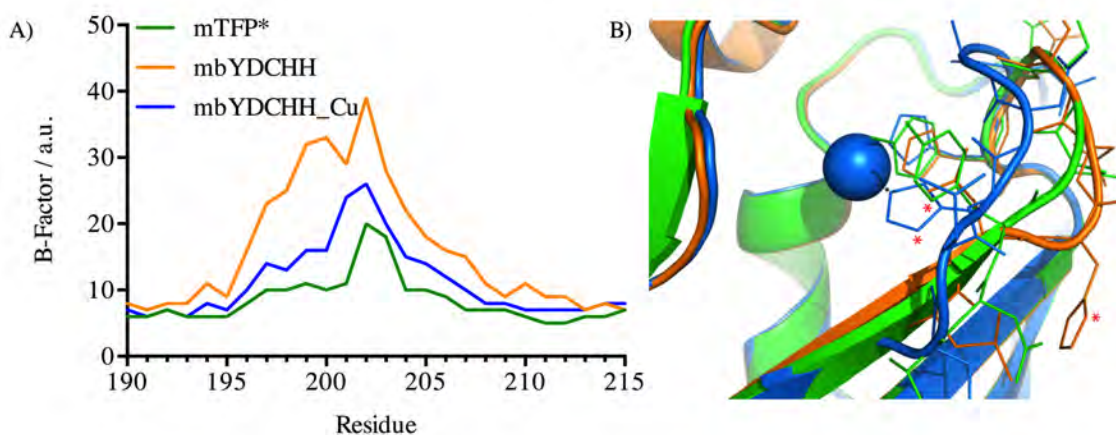
Figure 40 B-Factor Comparison and structural superposition of mbYDCHH open/closed Pocket and Copper co-crystallization; *indicates H200

Evaluating the recorded datasets further, we compared thermal movements of the earlier identified loop region around residues 195-205. Clearly it could be deduced that the introduction of C197, H200 and H204 increased the dynamics of this particular loop (Figure 40A). However paying close attention we also observed that the coordination of a copper atom stabilized the thermal movement. Thus also on the basis of structural superpositions we argued the copper bound state to be favored over a non-bound state explaining the earlier described high affinity towards transition metals (Figure 40B). However, despite these estimations, we anticipated to prove the concept of a flipping loop, the open and closed state of the binding pocket through the solution of yet another crystal structure. We therefore proceeded co-crystallization principles with mbYDCHH at pH 6.0 and obtained solid material. Despite numerous attempts and recorded data-sets, we weren't able to resolve structures that showed the coordination of a copper atom, however the open conformation was consistently present.

Referring to crystals from mutant mbYDEHH we were able to deduced structures up to 1.6 Å resolution (Figure 39). Despite the fact that all measured datasets visualized the anticipated conformation with a suitable average spacing of 4.5 Å between the carboxylate and the amines

(H200, H204), we weren't able to obtain any structures of mbYDCHH or mbYDEHH that showed the believed copper coordinated to the moiety (Figure 41, Figure S 19).
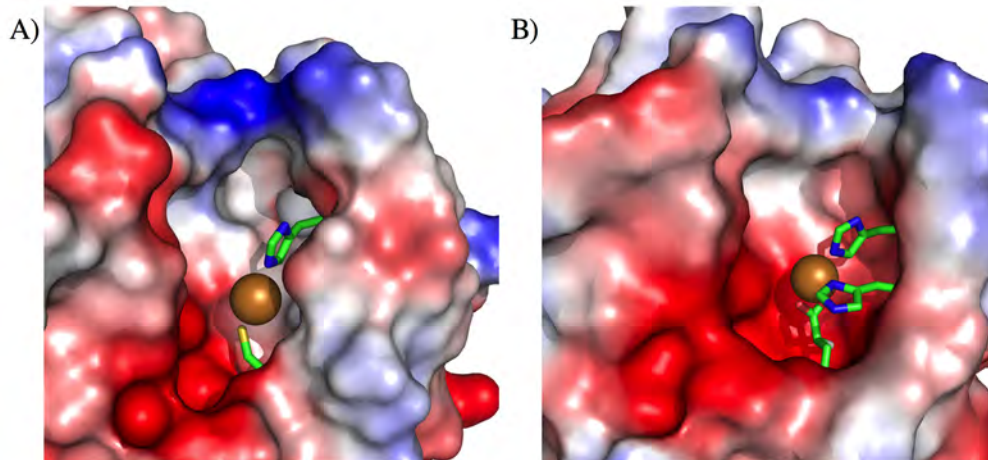
Figure 41 Copper Coordination Model: Showing envisioned Copper coordination A) mbYDCHH open conformation (C197, H204); B) mbYDEHH (E197, H200, H204)

2.4. Co-Factor Conjugation

2.4.1. Design and Generation

Regarding co-factor coordination we planned to functionalize two differently oriented positions within mTPF*. Those were expected to embody different demanding scopes. Amino acids C164 and C204, the first being surface/solvent orientated, the latter being buried in the earlier described cleft were introduced using means of site-directed mutagenesis (Figure 42). We targeted to gain insights on quantitative conjugation methodologies with the solvent accessible Thiol C164 and planned to apply those to the sterically more demanding position C204. In the context of copper based ArMs the well described moiety phenanthroline, herein a 5-maleimide conjugated version (Figure 42D), was believed to functionalize mTFP* and thus create an artificial metalloenzyme on the basis of covalent anchoring (Figure 42C)[2,87,106]. The protein scaffold was envisioned to provide the necessary influence in the form of a second coordination sphere.
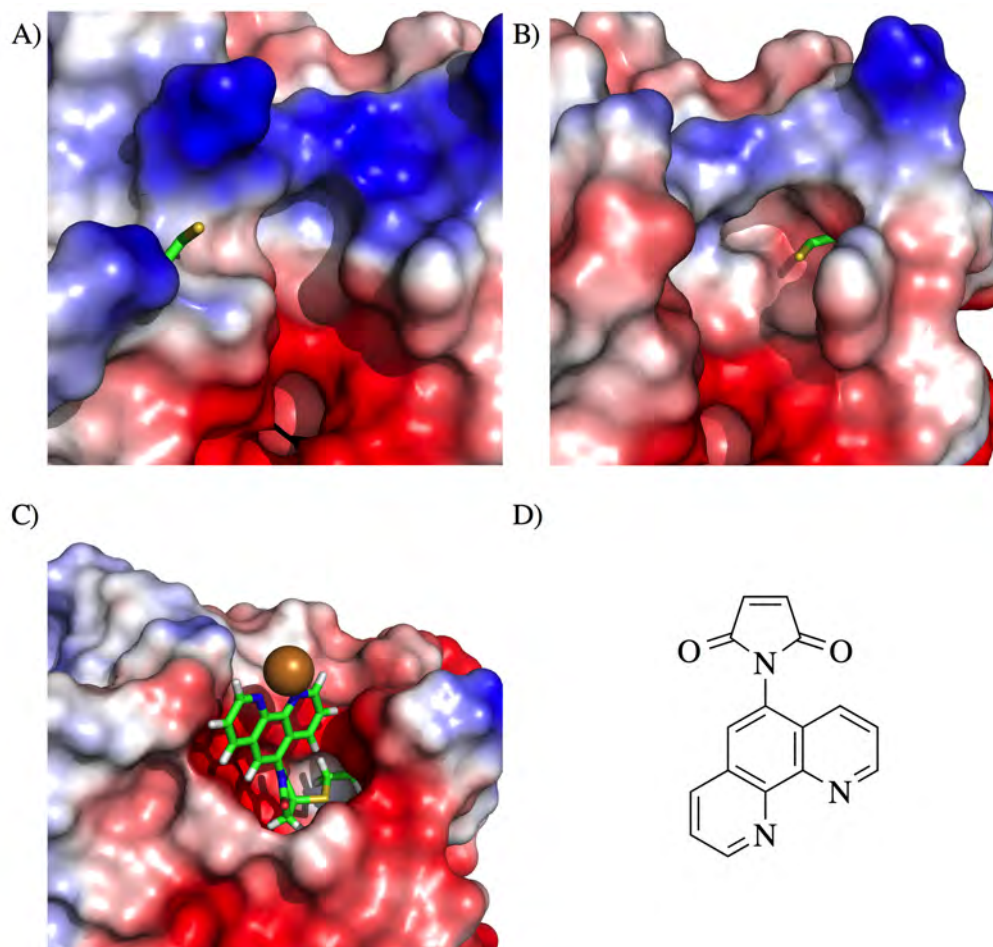
Figure 42 Covalent Conjugation of mTFP*: A) Model mTFP*C164; B) Model mTFP*C204; C) Model of mTFP*C204_phen; D) 1,10-phenanthroline-5-malemide

2.4.2. Protein Characterization

Utilizing protocols from literature we synthesized 1,10-phenanthroline-5-malemide and conjugated mutants of mTFP* according to our optimized protocols (MATERIALS AND METHODS, Page 118). Herein concentrations of 0.32 mM protein dissolved in 100 mM Tris/HCl pH 7.4 were reduced using TCEP and subsequently conjugated with a 10-fold excess under inert atmosphere. Bioconjugates of protein and 1,10-phenthroline-5-malemide were characterized by mass spectrometry. Datasets showed almost full conversion with phenanthroline at the respective sites (Table 6, Figure S 11).

No	Mutant	Ligand	Metal	Mass Spectrometry Expected (Da)	Observed (Da)	Δ (Da)	Conjugation
1	mTFP*C164			25126	25126	0	
		phen		25401	25418	17	+
		phen	Cu	25464	25480	16	+
2	mTFP*C204			25095	25095	0	
		phen		25370	25368	-2	+
		phen	Cu	25433	25429	-4	+

Table 6 ESI-TOF Mass Spectrometry Data: mTFP*C164/204 ± 1,10-phenthroline-5-malemide and conjugation with Copper

In the spirit copper based catalysis we also tried to prove coordinations by means of mass spectrometry. To our consent we could prove coordination of a single copper atom to each mutant, C164_phen and C204_phen (Figure S 11).

2.4.2.1. Transition Metal FRET

Owing the indifferent affinity of phenanthroline towards Cu^{2+} with regards to the site of attachment on the protein, we utilized conjugated mutant mTFP*C204_phen to determine the general metalation affinity[107,108]. We proceeded as outlined earlier and evaluated the overall fluorescence decrease to determine dissociation constants.
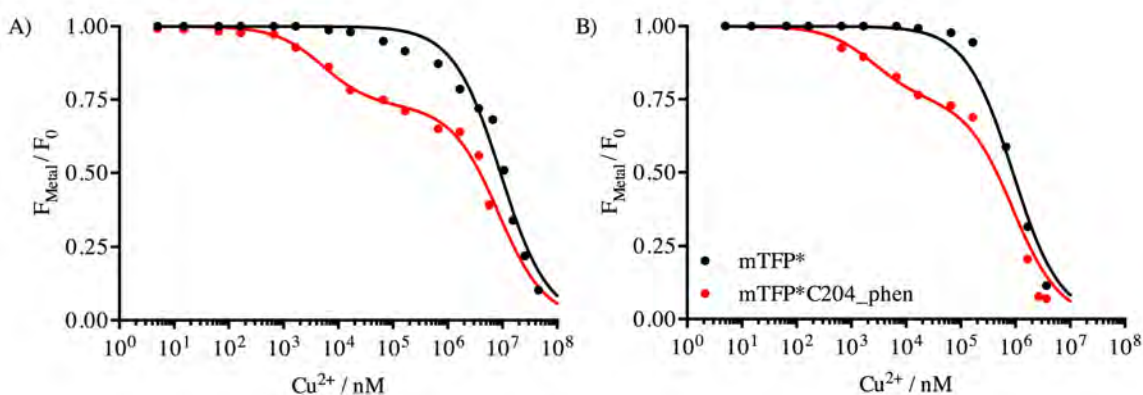
Figure 43 tmFRET Studies of mTFP*C204_phen: A) pH 6; B) pH 7.5

Phenanthroline conjugated protein showed dissociations constants of 5.28 and 2.52 μM at pH 6.0 and 7.5 respectively (Table 7). Similar to earlier titrations we observed a general shift by one order of magnitude to baseline the protein-exhibited fluorescence from pH 6.0 to pH 7.0.

Mutant	Metal	pH	K_dStat (mM)	K_dDyn (μM)
mTFP*C204_phen	Cu	6.0	8.46	5.28
		7.5	0.89	2.52

Table 7 Dissociation Constants Overview: mTFP*C204_phen

2.5. Discussion

Binding motifs on the basis well described 2-his-1-caboxylate triad (His/His/Asp) were successfully integrated into the envisioned and earlier described cleft of mTFP*[85,86,103,104]. Despite missing maturation referring to mutants that contained permutations of methionine at positions 55 and 54 (mbYMIHH and mbMDIHH) or a combination of methionine and cysteine at 200 and 204, and disregarding sterically inappropriate mutations I197M/H, we were able to establish all envisioned metal binding motifs. Results from mass spectrometry argued reasonable affinities towards ions of Copper(II)Nitrate and gave first insights to the successful establishment of metalloproteins. Owing to the low concentration of transition metal used and the described difficulty to obtain mass data from transition metal-protein complexes we were keen to observe adducts of Copper ($\Delta M = 64$ Da), or closely related mass differences in all samples, but mbYEIHH, mbYEQHH and mbYDIHC[109-113]. Applying the same methodologies for the latter approach of covalently linking a phenanthroline moiety to mTFP*C164/204 we were also able to show successful derivatization and data from Copper additions argued low, but successful conjugation. We concluded the establishment of a library of metalloproteins that were further evaluated regarding their metal binding affinities.

Generally, the rational design of a metal binding site was believed to be more than a simple library approach of several triads or the mere introduction of an artificial co-factor. Owing to the literature in which a multitude of triads were identified in naturally occurring proteins, but lacked metalation or catalytic scopes, or covalent anchors conjugated failed to display novel functionality, we targeted show the interplay of first and second coordination sphere by combining both approaches at the same site. Herein respective insights towards metalation affinities were of great importance. Also we anticipated an estimate distance of 4 Å regarding canonical motifs and a reasonable flexibility of the loop region, amino acids 195-205 (mTFP*) to

be necessary for strain-free conformational changes upon metalation or conjugation with phenanthroline. Results obtained from tmFRET studies argued significantly enhanced, by one order of magnitude to the least, interactions irrespective of the modification approach applied (mbYDCHH 1.18 μM and 0.97 μM, mbYDEHH 8.86 μM and 5.22 μM, mTFP*C204_phen 5.28 μM and 2.52 μM at pH 6.0 and 7.5 respectively). Our data clearly indicated this tuning by design, but showed also a pH dependent interaction of copper with respect to mbYDCHH. Metal induced quenching became significantly more pronounced from pH 5.0 to 6.5 and sharply dropped when reaching pH 7.5 or above. Assuming a more or less constant distance from the chromophore AYG_{62-64} to Cu^{2+} binding site, considering a singular binding site, the calculated Förster radii R (Table S 3) of donor and acceptor pair, aligned with FRET efficiencies argued significant distance changes for mbYDCHH. Observing neglectable changes for the glutamic acid containing sister mutant mbYDEHH or phenanthroline conjugated mTFP*C204 over the same pH range, herein respective FRET efficiencies didn't change as severely, we apprehended the influence of C197 and thus a change in the ligand structure coordinating the copper atom (Figure S 17). Putting this into context with the overall monotonous decrease of K_dDyn from pH 6.0 to 7.5 the only probable explanation was a major rearrangement of the metals first coordination sphere. As described earlier and to our consent X-ray structures of the metal free mbYDCHH revealed two different conformations. Acknowledging the bidentate motif of the open conformation that allows a closer proximity between H204 and C197, the postulated triad of the closed conformation, and taking insights from Cu^{2+} co-crystallized mbYDCHH into account, the only probable explanation to major difference in quenching efficiency was a ligand to metal, Cysteine-Copper, charge transfer (LMCT) that is well described for blue copper proteins[114,115]. The proposed coordination mechanism would include two Copper coordinated states (A' and B') that are interchangeable through influences of pH, however require the prior displacement of Copper (A and B).
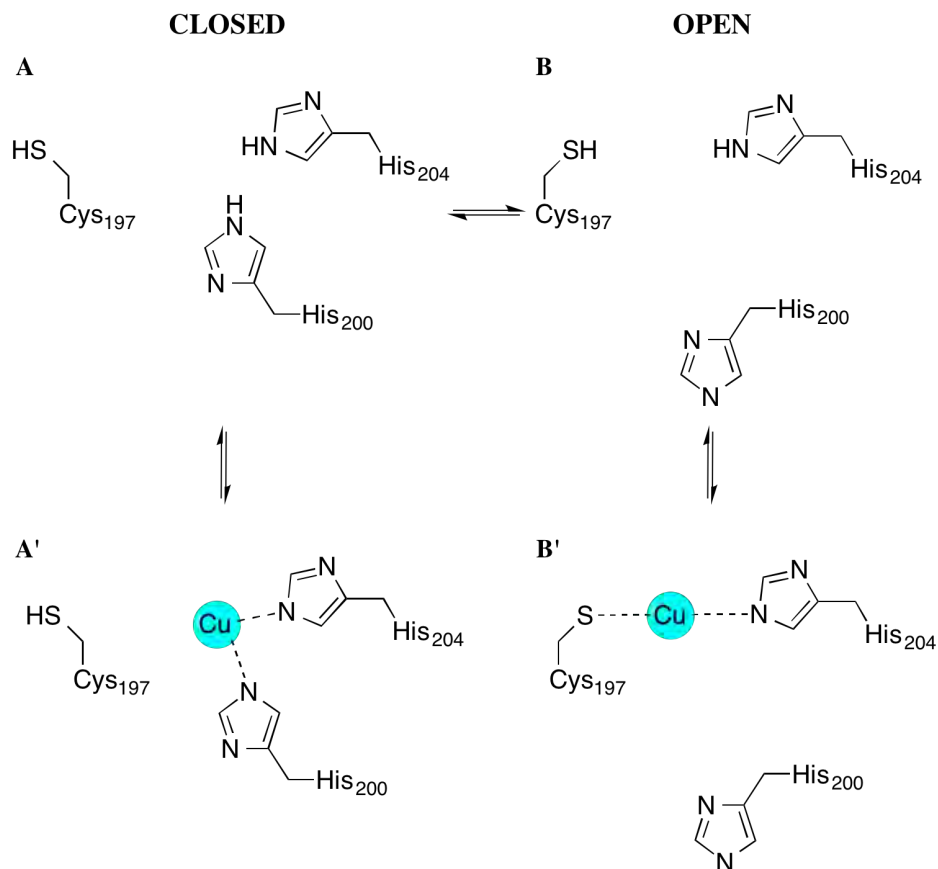
Figure 44 Binding dynamics of mbYDCHH: A' to B' indicates proposed mechanism of Copper coordination

Lastly our evaluation of all crystal structures, but most importantly of Copper co-crystallized mbYDCHH proved the ideal spacing of the projected binding pocket and thus our permutation approach (Figure S 19). Reports Reetz and Ward had argued an ideal spacing < 4.5 Å surrounding the transition metal in order to achieve sufficient means of coordination by classical 2-his-1-carboxylate motifs[85,86]. Observing distances for non mutated residues I197, D55 and Y54 of 5.7 Å, 4.7 Å and 4.6 Å to the coordinated Copper atom argued an ideal spacing for newly introduced cysteines, glutamates and histidines considering average carbon-carbon bond lengths of 1.5 Å (Figure S 20)[116]. Each amino acid of our screen would therefore reach proximities closer than 3.2 Å and would therefore be able to consolidate coordinations with copper and histidines 200 and 204.

3. CATALYSIS

(Results of this section have been accomplished in collaboration with Dr Meina Liu)

The proof of concept, yet the successful establishment of artificial metalloenzymes relied on the important challenge to argue stereoselective conversion in template reactions. Owing the novelty of our approach and the different members of our host protein library, we anticipated comprehending the influences designed binding motifs would comprise. Insights were then believed to identify clear trends on the electrostatic and geometric constitution that could support future work on artificial metalloenzymes by suggesting general design principles.

The catalytic scope of mTFP* derived catalysts was limited to copper based catalysis with respect to this study. Prominent examples of C-C bond forming reactions had been described in the context of Diels-Alder, Michael addition and Friedel-Crafts alkylation reactions in water[117-120]. Referring to the differently constituted artificial metalloenzymes examples regarding presented approach were scarce and thus we initiated our investigation with Diels-Alders cycloadditions.

3.1. Diels-Alder

In the quest to designed metalloenzymes we envisioned to observe product formation through HPLC analytics from azachalcone (1) and cyclopentadiene (2) (Figure 45). From literature we depicted that complexes of Cu^{2+} with an asymmetric ligand catalyzed a variety of Diels-Alder reactions in organic solvents[47,121,122]. Further the compatibility of the below shown model reaction had been described in combination with complexes of amino acids, nucleic acids and proteins and therefore seemed a suitable testing hurdle[110,121,123]. We envisioned screening our successfully established and characterized metalloproteins over a range of conditions. Evaluating the influences of the designed ligand structure at a set of pHs, temperatures and reaction times, also considering the undeniable background reaction, the complex interplay of first and second coordination sphere with the transition metal and the substrates was evaluated.
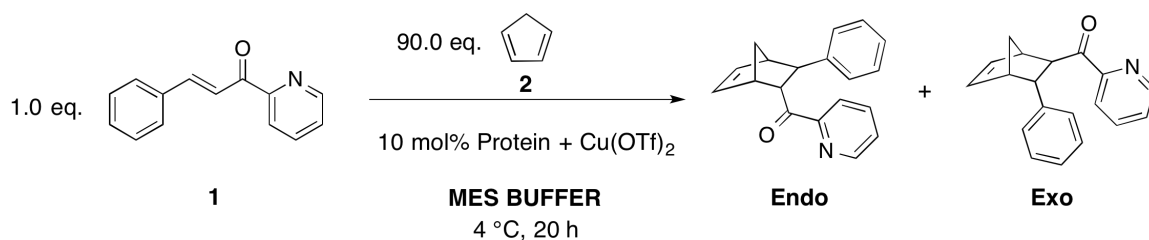
Figure 45 Reaction Conditions – Diels-Alder: 1. Azacalcone, 2. Cyclopentadiene, Cu(OTf)$_2$, in MES Buffer at 4 °C, 20 hours

Initial results obtained from screens of utilizable Cu(II) salts accounted for Cu(OTf)$_2$ to be the salt of choice (APPENDIX/CATALYSIS). Further we agreed on a standard reaction temperature of 4 °C as well as the overall reaction time of 20 hours. These principles were applied to all screens presented in the following.

3.1.1. Canonical Metalloenzymes

Gaining insights in Diels-Alder reactions we observed the formation of product, with a consistent diastereomeric bias of up to 79:21, towards the Endo configuration, in the absence of transition metal catalyst (Figure 46A). Studies related to the background formation of product indicated a reaction of apparent first order, owing the excess of cyclopentadiene, that yielded within 20 hours in up to 34% of product at pH 5 and 4 °C (Figure 46A, Figure S 22). Comparing these insights with results from a negative control, utilizing mTFP* and Cu(OTf)$_2$ in a ratio that accounted for a slight excess of scaffold (0.12 / 0.1 = mTFP* / Cu(OTf)$_2$), we observed a similar diastereomeric bias and thus no influence of the protein scaffold. The resulting full conversion was therefore only attributed to free Copper in solution and confirmed our estimations of a non-binding scaffold.
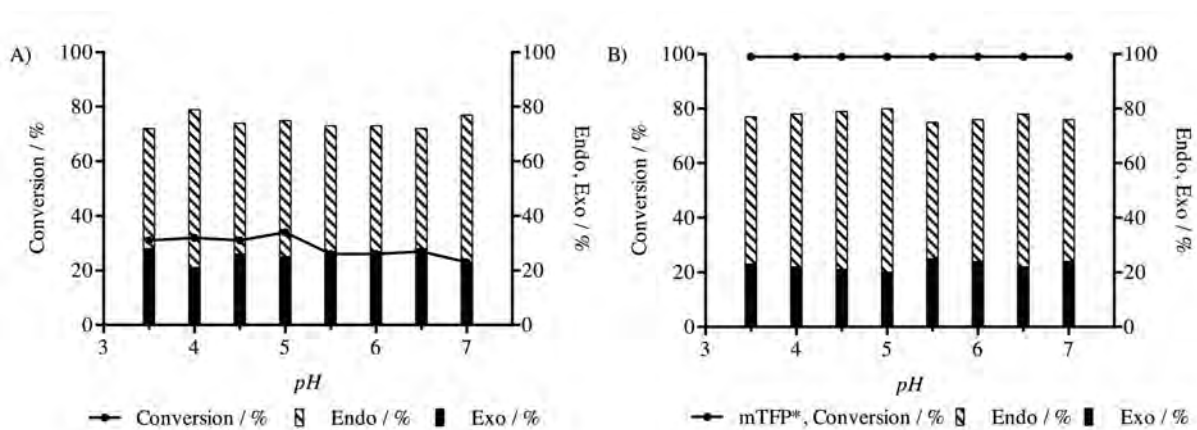
Figure 46 Diels-Alder: A) Evaluation of Diels-Alder background Reaction at 4 °C after 20 hours. B) Evaluation of mTFP* based Diels-Alder reaction shows no stereoselective, but expected fully conversion.

Performing catalytic trials with the earlier presented template mutants, mbYDCHH and mbYDEHH, both being designed on the basis of naturally occurring motifs, we anticipated an alteration in the Diels-Alder activity[86,124]. To our consent we observed a general increase of diastereomeric excess of up to 95% Endo content upon the introduction of our Mutants (Figure 47C, D). Further initially absent stereoselective conversions, with an enantiomeric excess of up to 17%, mbYDEHH (9%, mbYDCHH), were derived from HPLC traces. Regarding the electronic ligand constitution it appeared that the exchange of a cysteine to glutamate, thus the replacement of a soft ligand with a hard ligand, boosted the enantiomeric excess by a factor of 2. Influences regarding pH were also observed for mutant mbYDEHH. Herein pH 5 yielded in the highest stereoselective conversion. Screens referring to mutant mbYDCHH however indicated the highest stereoselectivities at pH 7 paired with a sudden decrease in overall activity.
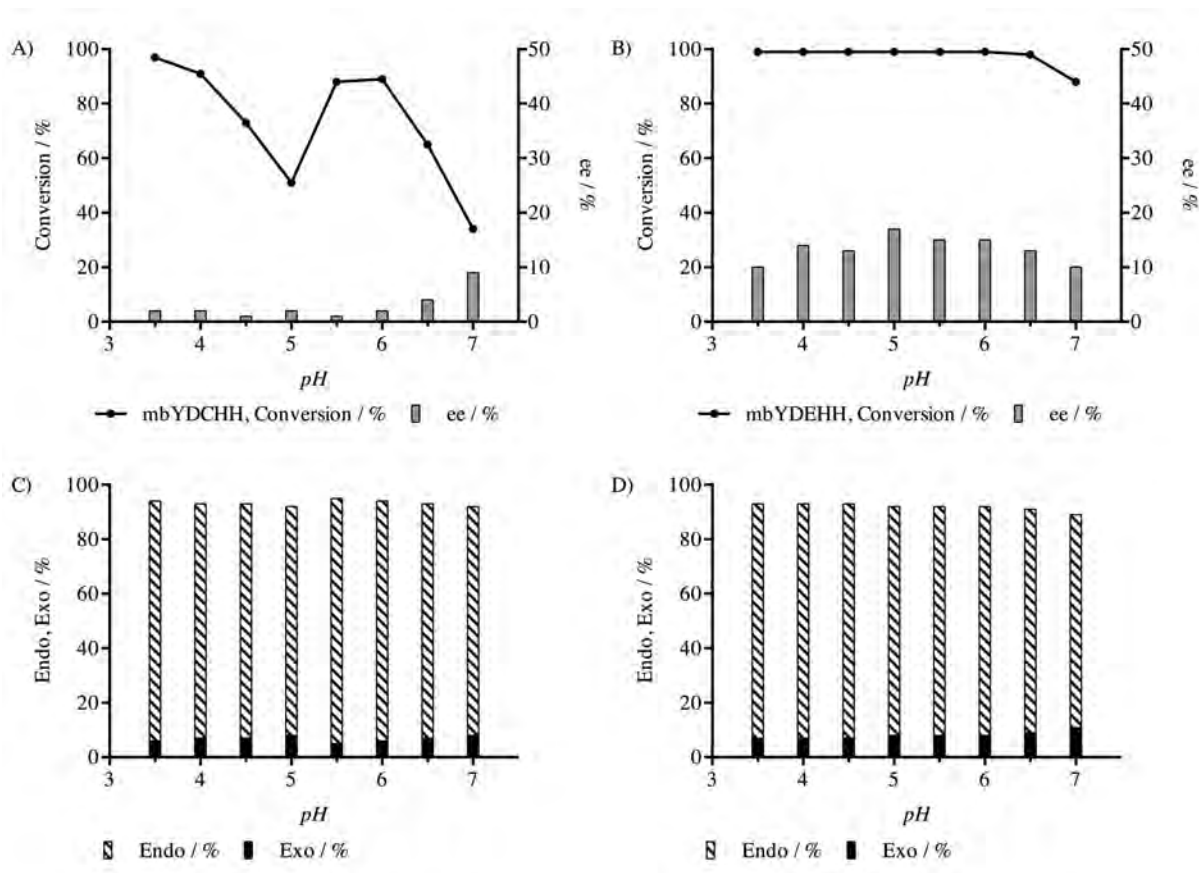
Figure 47 Diels-Alder: A, C) mbYDCHH; B, D) mbYDEHH; Graphs indicate overall conversion at 4 °C after 20 hours; enantiomeric excess and Endo/Exo ratio are indicates by bar graphs.

To further evaluate the influences of the binding motif and the number of coordination sites, catalytic screens utilizing mutants mbYECHH and mbYEQHH were accomplished. Herein and to our consent, mbYECHH rarely converted substrates above yields that were deduced form background reactions. Only trials performed at pH 3.5, 4.0 and 4.5 showed conversions around 40% and therefore exceeded the earlier identified background (Figure 48A). Further, the enantiomeric excess was absent or within the margin of error and lastly the diastereomeric profile resembled the earlier described ratio of 80:20 (Endo:Exo) (Figure 48C). Comparing these results with insights from the sister-binding motif, mbYEQHH, that contained a sterically demanding residue, however not a coordinating one, we found our estimations further supported. Herein conversion reached the anticipated higher scope (close to full conversion), including marginal stereoselectivities, up to 8% and the diastereomeric bias returned.
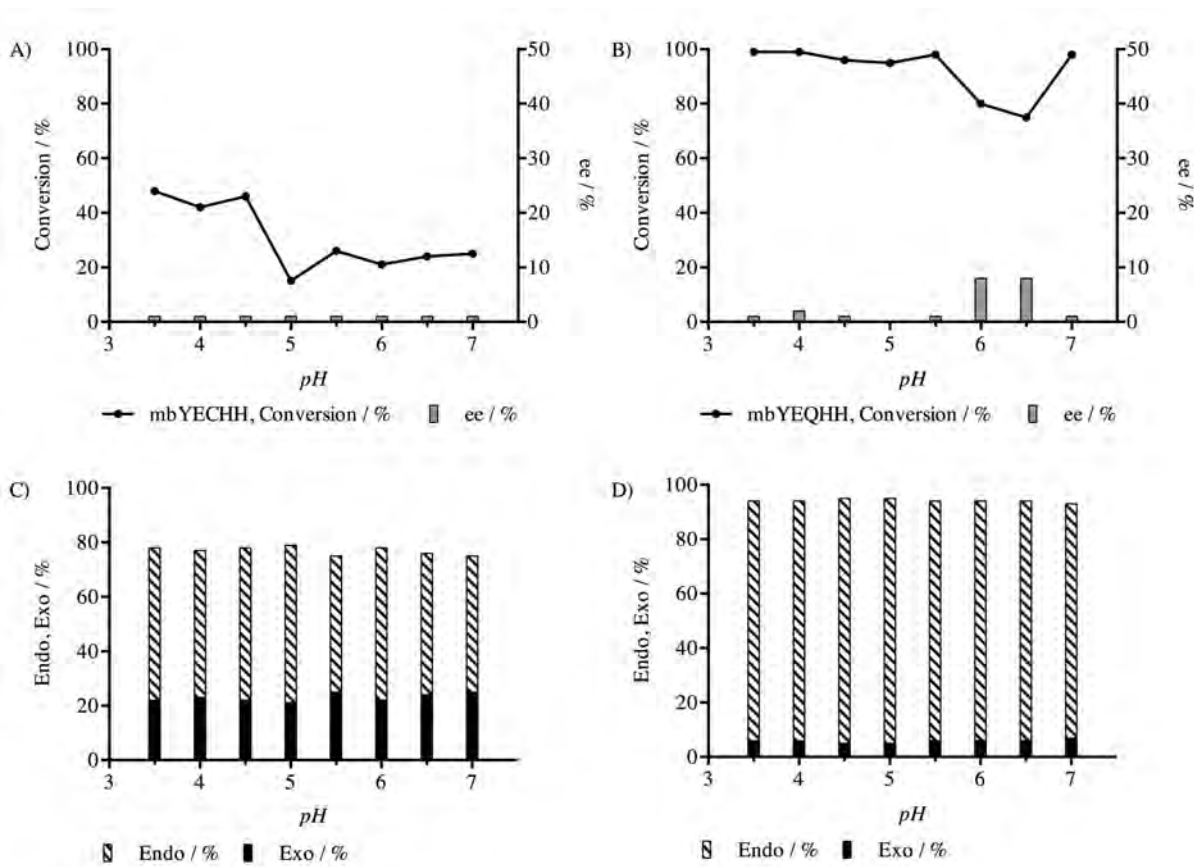
Figure 48 Diels-Alder Screen: A, C) mbYEQHH; B, D) mbYECHH; Data indicates strong influence of ligand constitution and number of residues in the moiety

Evaluating the other envisioned mutants that only comprised two binding partners, thus a dual anchor for the transition metal catalyst (mbYDIHH, mbYDIHC and mbYDMH), we observed a generally present increase in conversions and the introduction of some stereoselectivity (Figure 49).
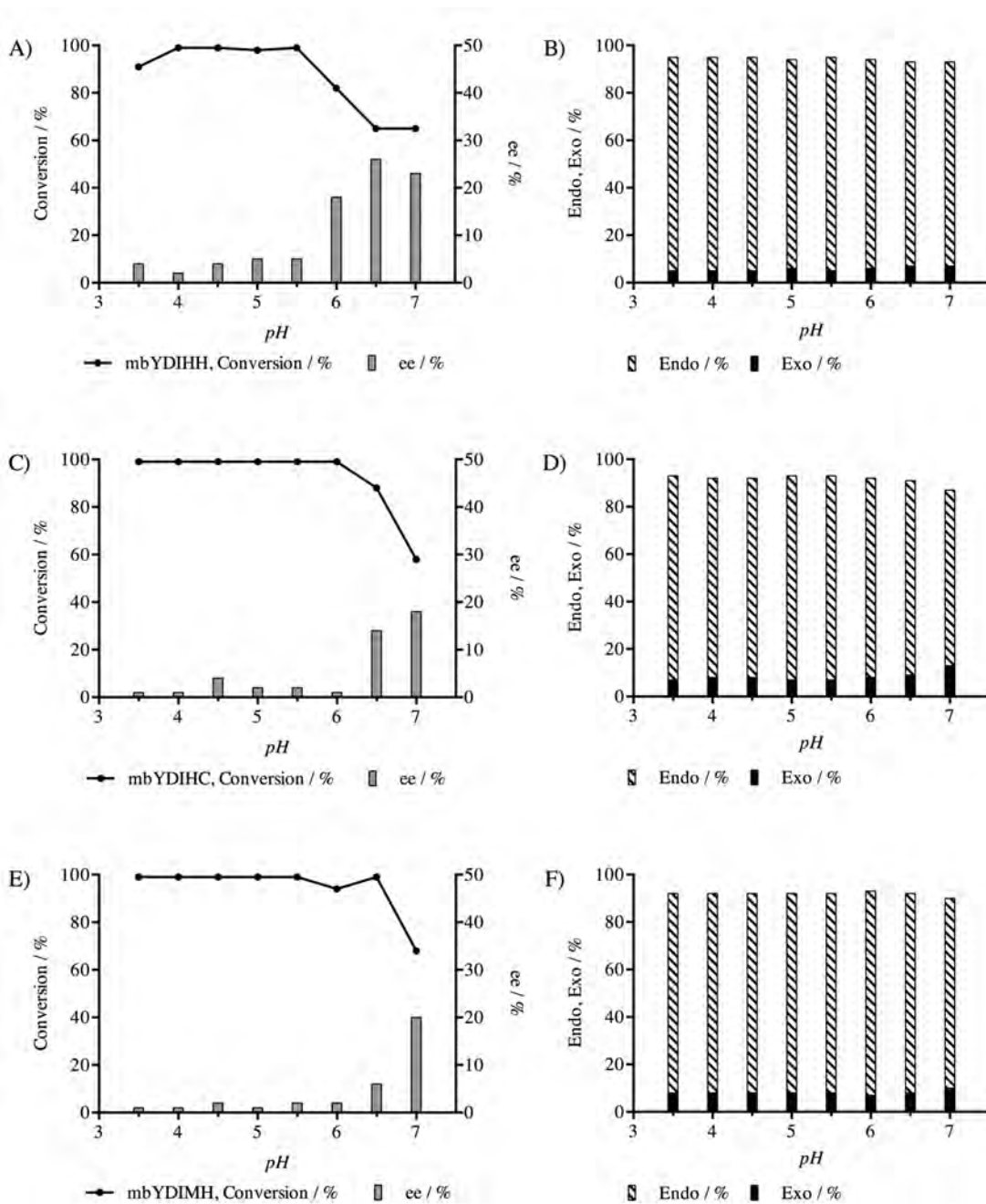
Figure 49 Diels-Alder Screen: Dual Anchoring Mutants A) mbYDIHH, C) mbYDIHC, E) mbYDIMH; increasing pH argues enhances stereoselectivity; HH motif appears more powerful than HC or MH; B, D, F) Diastereomeric excess indicates copper coordination for all motifs

Most obvious appeared to be an increase in enantiomeric excess with increasing pH. However, likewise some conversions dropped significantly at pH 6.5 or above. Like before the ligand constitution showed a slight preference, herein towards a double histidine moiety than the combination of histidine and cysteine, or methionine and histidine. Referring to the earlier described diastereomeric bias no alteration towards previous experiments was observed and we concluded coordinated Copper to be responsible for the catalytic activity.

The mutation screen of identified residue D55 accounted for some interesting insights. Generally speaking the successfully established mutants argued some potency of D55 to be scrutinized as third binding partner in the transition metal anchor. We observed some enantiomeric excess for all three motifs and experienced the earlier described trend regarding optimum catalytic pH (first identified in mbYDCHH and mbYDEHH), respective the electronic properties of the third amino acid. Herein cysteine containing mutant mbYCIHH showed enhanced, 19%, enantiomeric excess towards pH 6, (levels at pH 6.5 and 7.0 are ignored regarding low conversion and altered diastereomeric excess; pH 7.0 indicates diastereomeric excess from background reaction). Differently mutant mbYEIHH, thus contained glutamic acid at position 55 showed a tendency towards pH 5.0 to 6.0 (8% ee), whereas an introduced histidine, mbYDHIHH, accounted for the overall lowest enantiomeric excess (3%) at pH 5.5. Conversions seemed to be more effected by pH regarding mutants that contained cysteine or histidine at position 55, both visualizing stark reductions above pH 6.0. The overall diastereomeric bias showed now difference to previously observed ratios and therefore accounted for coordinated copper to be catalyse Diels-Alder substrates.
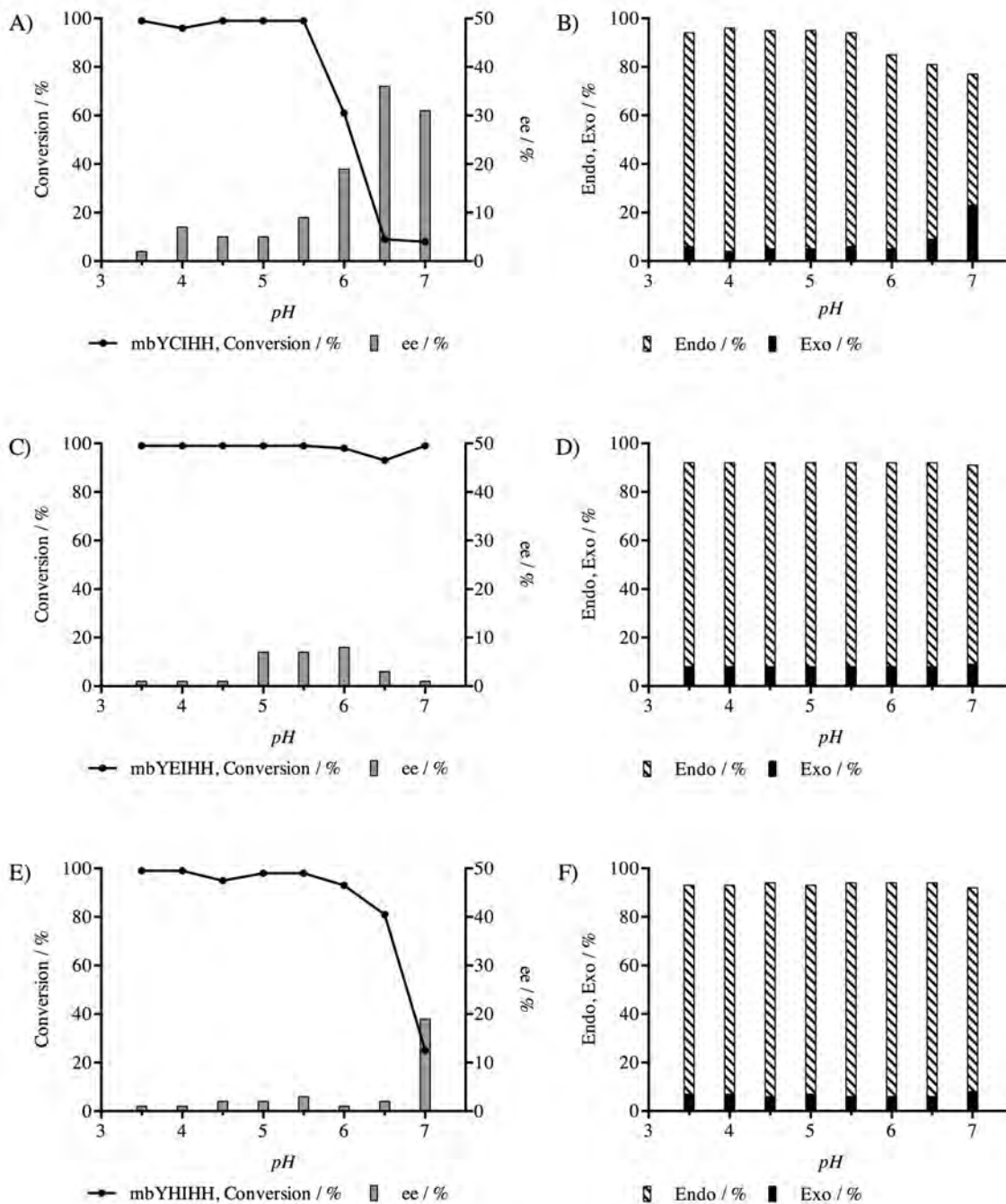
Figure 50 Diels-Alders Permutation Screen D55: A) mbYCIHH, B) mbYEIHH, C) mbYHIHH; B, D, F) respective diastereomeric excess for all motifs;

Position Y54 being permuted argued a general and stronger dependency on pH than previously observed. Conversions of all mutants declined latest at pH 6.0 and inclined to about 50% at pH 7.0. In these cases rising enantiomeric excess was only observed for mutants mbCDIHH and mbHDIHH, thus motifs containing cysteine or histidine. mbCDIHH and mbHDIHH peaked at pH 7.0 with 13% and 9% ee respectively. Mutant mbDDIHH peaked around pH 5.0 (11% ee), however showed a larger spread of enantiomeric excess compared to other mutants. Moreover the sudden decrease in conversion at pH 6.5 and above did not show any increase in enantiomeric excess. Differently to other mutants of position Y54, the diastereomeric bias changed towards 84:16 (Endo:Exo) and indicated uprising background – a tendency that could not be proven for other mutants that showed anticipated ratios of 92:8 (Endo:Exo).
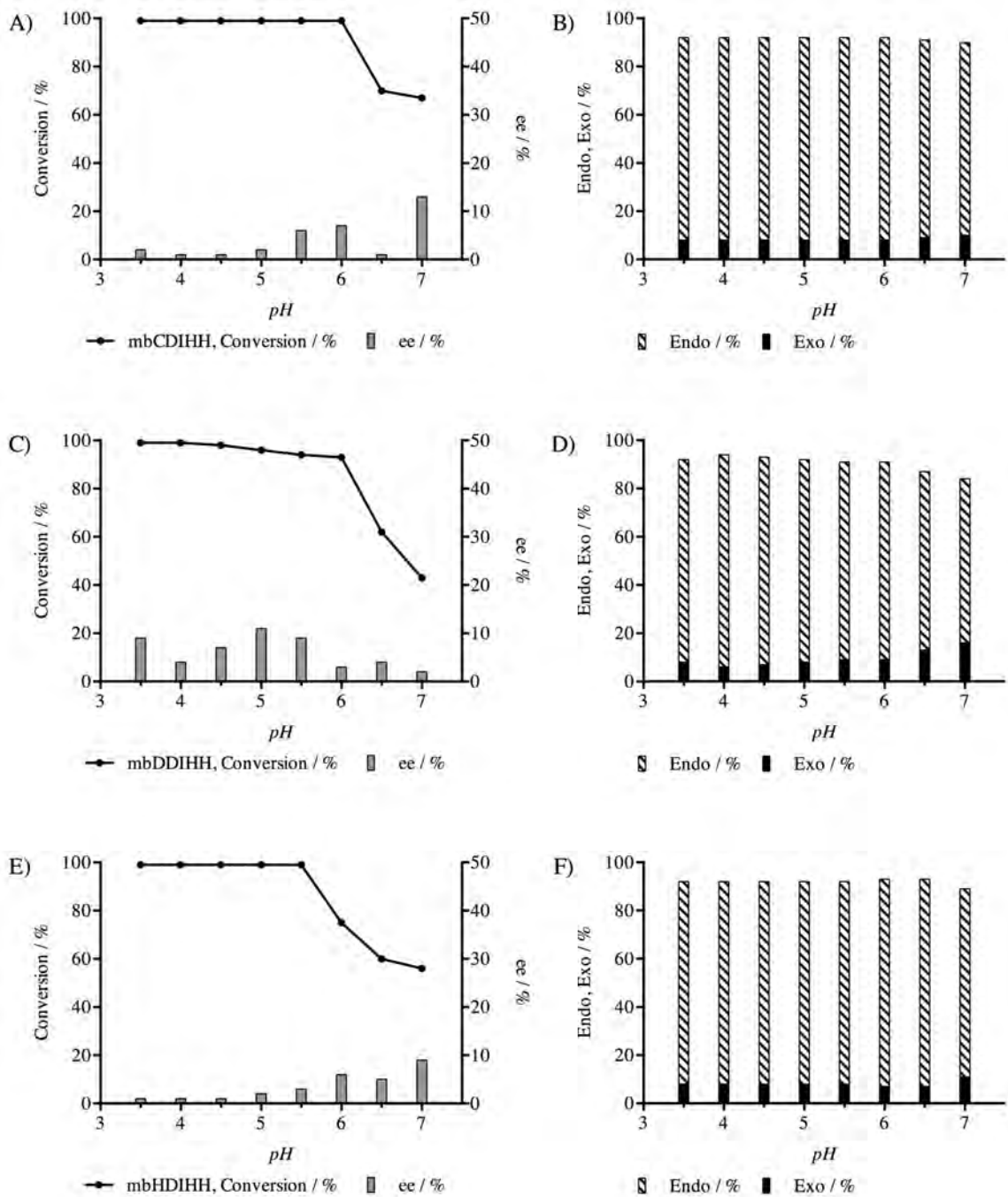
Figure 51 Diels-Alders Permutation Screen Y54: A) mbCDIHH, B) mbDDIHH, C) mbHDIHH; B, D, F) respective diastereomeric excess for all motifs

3.1.2. Covalent Metalloenzymes

Evaluating the performance of our covalently established artificial metalloenzyme, mTFP*C204_phen, we envisioned a decent catalytic performance. Referring to the earlier identified metalation affinities and the introduction of a second coordination sphere by embedding the moiety into the cavity of mTFP*, we hoped to boost enantiomeric excess. We anticipated to advance the constrains reported in literature regarding covalently anchored phenthroline based artificial metalloenzymes[71].
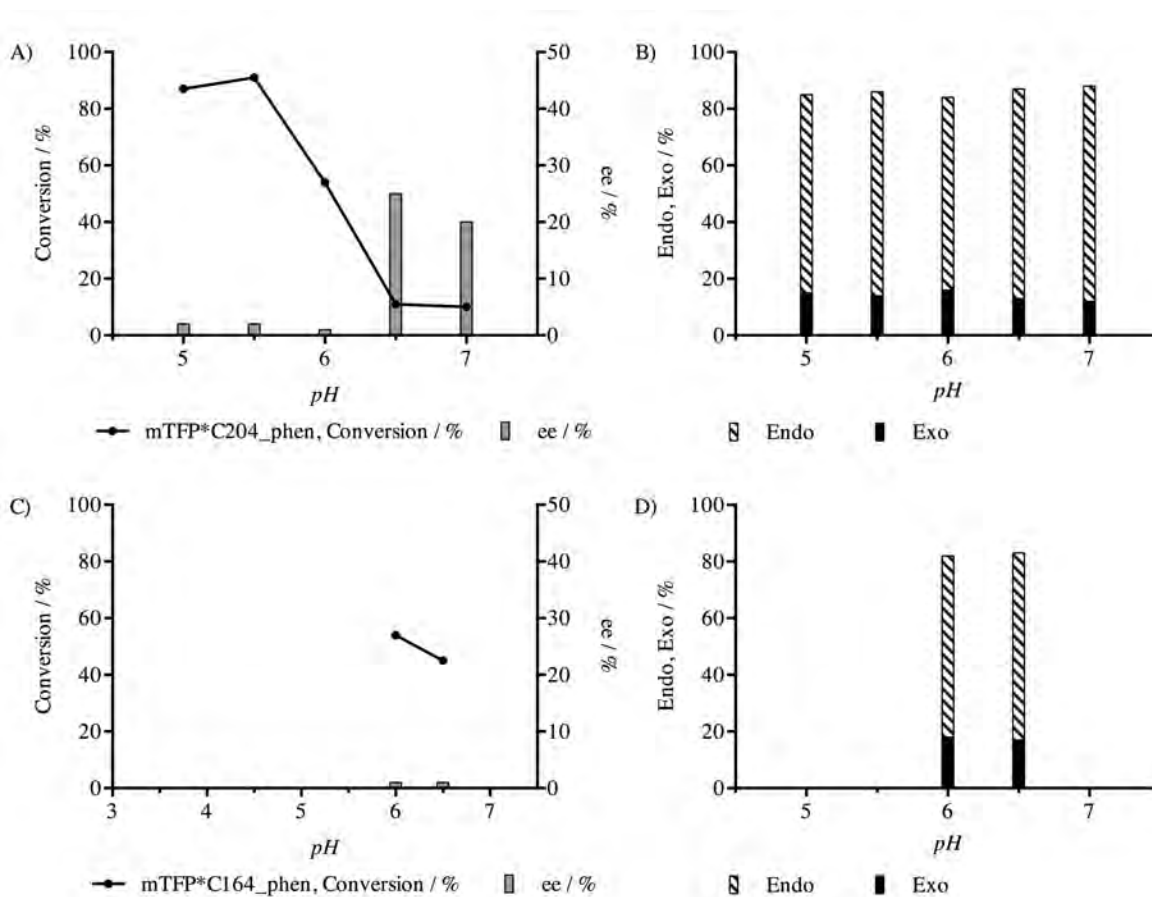
Figure 52 Diels-Alder Screen: mTFP*C204_phen shows mediocre performance; A) Conversions drop significantly with increasing pH; B) Diastereomeric bias settles around 85:15, Endo:Exo for all pHs; C) mTFP*C164_phen also shows low conversion and no ee ; D) Diastereomeric ratio 82:18 (Endo:Exo) indicates catalysis of free copper-phenanthroline complex

Reactions with covalently conjugated mTFP* showed overall mediocre conversions that dropped significantly with rising pH. Whereas on average a very low ee was found, we observed a drastically rising excess at pH 6.5 and 7.0 for mutant mTFP*C204_phen (Figure 52A). With equally reduced conversions however, interpretations were treated with caution. Diastereomeric evaluations revealed a similar but not identical bias of 85:15 (Endo:Exo) for protein embedded copper-phenthroline complex like presented in literature (Figure 52C)[71]. For exposed phenthroline with mutant mTFP*C164_phen we observed a bias of 82:18 (Endo:Exo) and thus reproduced 81:19 (Endo:Exo) reported for unconjugated copper-phenanthroline complex in literature (Figure 52C)[71].

3.2. Discussion

mTFP* clearly showed lacking chiral induction within attempts to catalyze Diels-Alder substrates. The missing enantiomeric excess indicated that conversions were performed by "free" copper in solution and thus supported our theory. With respect to the evaluated background reaction we were able to observe a different bias in the diastereomeric distribution than in reactions performed with metal binding mutants. Generally speaking, "free" copper as well as the brackground reaction showed a diastereomeric bias of the 80:20 (Endo:Exo), whereas conjugated catalyst deviates this ratio to around 95:5 (Endo:Exo).

Mutants mbYECHH and mbYEQHH visualized the influence regarding the number of coordinating residues in the binding pocket. Referring to the overall missing conversion and taking diastereomeric ratios into account, mbYECHH showed solid coordination of Copper and thus only background conversion of Diels-Alder substrate appeared. This argued that all coordination sites of copper were blocked and differed from mbYEQHH, were mutation C197Q had been introduced. Catalytic trials of this mutant showed high conversions and initial chiral induction from the scaffold. Since the diastereomeric bias was seemingly different and indicated coordinated copper, we assumed a free however hindered fourth coordination site.

Dual anchor mutants, mbYDIHH, mbYDIHC and mbYDIMH also showed chiral induction in Diels-Alder catalysis. Their respective diastereomeric bias also indicated coordination of copper. Respective the constitution, mutants containing a combination of histidine, cysteine or methionine appeared less sufficient in the order presented and thus confirmed the literature reported two-histidine containing mutants[124].

Utilizing our template mutants mbYDCHH and mbYDEHH, as well as considering members of the library that followed the same mutagenic order (mbYCIHH, mbYEIHH, mbYHIHH and mbCDIHH, mbDDIHH, mbHDIHH), several general assumptions became prevalent. Both, geometric and electronic constitution of the binding motif appeared to influence enantiomeric conversions drastically. However especially the combination of the aforementioned properties appeared to have greatest influence. Clearly position I197 mutated to glutamic acid empowered mutants of mTFP* more than similar mutations (to carboxylates) at D55 or Y54. Herein mbYDEHH showed an enantiomeric excess of 17% without further ado. Respective other mutants only reached mediocre 8% (mbYEIHH) or 11% (mbDDIHH). Differently the introduction of a cysteine at I197 did not result in high enantiomeric excess (9%), whereas the same mutation accounted for 13% at Y54 and exciting 19% at D55. Indifferently towards all positions was the low enantiomeric output regarding introduced histidines, 3% and 9%, mbYHIHH and mbHDIHH respectively. Taking these insights into account another observation showed great importance. Motifs comprising carboxylates showed less influence towards rising pH conditions than all others – they showed greatest stereoselective output around pH 5.0. Interestingly and differently with decreasing conversions appearing at higher pHs, enantiomeric excess especially of cysteine containing mutants gained. In this context, the apparent outlier to the trend, mbDDIHH, that also showed the progress of less conversion with rising pH, was believed to be coordinate copper through a fourth residue, D55 (this residues was ignored in the establishment referring to its distance > 4 Å), and thus lacked catalytic potency. Respective alterations in the diastereomeric bias further supported this concept on the basis of a catching up background reaction. Comparing these findings with previous reports, we concluded and extended what had been described earlier. Both cysteine and aspartate/glutamate, depending on positioning in the scaffold, suffice the purpose to coordinate Copper(II) with pairs of histidines and thus perform stereoselective Diels-Alder catalysis[85,125]. Further chiral induction with respect

to the second coordination sphere of mTFP* or respective mutant was prevalent and proved the establishment of novel artificial metalloenzymes on the basis of canonical amino acids.

Covalently conjugated mutant mTFP*C204_phen showed mediocre, however chiral induced conversions. With respect to singular experimentation with mTFP*C164_phen we estimated that our findings demonstrated the chiral induction performed by the protein scaffold, thus the cavity and it became more evident that the position of the coordinating moiety was of great importance. In this context literature reports two extremes of apparent or missing chiral induction. Kamer et al. reported minute to enhanced induction of phenanthroline conjugated sterol carrier protein type 2 like domain (SCP-2L) in Diels-Alder cycloadditions depending on the positioning of the moiety[71]. In coherence to our findings they were able to retrieve up to 25% enantiomeric excess at pH 6.0, however reducing overall conversions to minimal 19.6% (±9.2%). Generally and in context to our study, the observations made argue a reduced capability of copper conjugated phenanthroline to effectively catalyze Diels-Alder cycloadditions at the utilized and preferred, "physiological" conditions. However to our consent again, chiral induction and therefore enantioselective catalysis in Diels-Alder cycloadditions can clearly be propagated through the scaffold of mTFP*.

4. OPTIMIZATION

The subject of artificial metalloenzymes initiated with the premise that the second coordination sphere, provided by the biomolecular scaffold, could reflect enzyme-like properties[63]. Resulting, the versatile embedded transition metal catalyst would then introduce attractive properties that could merge with the sustainable and environmentally benign, yet selective nature of the host, anticipating the best of both worlds[3]. Referring to the advancements of the field means of optimizing the created artificial metalloenzymes became of great importance. Largely, chemo-genetic approaches are utilized focusing on the parallel and combinatorial adaptation of first and second coordination sphere. Herein the coordinating moieties are modified and interchanged with respect to seize and ligand constitution, whereas structural variants of the scaffold are generated using advanced mutagenesis methodologies[1,4,7,126]. While these advances are highly encouraging and accounted for the uplift of turnover numbers and enantiomeric access, repeating cycles of optimization only enhance individual scaffold and transition metal complexes regarding singular applications[7]. Thus although successful, the procedures were believed to be labor intensive as qualitative methodologies needed to meet quantitative high throughput principles. In this context Ward and co-workers initiated designed evolution principles that limited the number of potential modifications from structural insights gained at an earlier stage[127,128]. Resulting artificial metalloenzymes were optimized with a strongly reduced number of cycles as the apparent anchoring of the transition metal was not affected, but only the environment around it. This of course referred more to supramolecular and covalently established artificial metalloenzymes but appeared more difficult for dative anchoring approaches largely presented in this study. Herein problematic perturbations of the binding motif may be introduced upon the mutagenic optimization of the second coordinations sphere. Hence there appeared to be a bigger influence of the second, to the first coordination sphere than reported for other classes of hybrids[85]. Expanding this thought a great limitation is also attributed to the general nature of the second coordination

sphere – referring substrate coordination. The mere positioning of a transition metal catalyst, especially in the context of dative anchoring approaches only partially accounted for potency. Relating to the hydrophobic nature of many substrates, not only sterically demanding, but ideally coordinating pockets are envisioned. Since the latter was absent within initial artificial metalloenzymes on the basis of mTFP*, we anticipated one simplistic approach to overcome the issue of substrate attraction. Referring to the generally apparent substrate availability problem and enhanced background reactivity of Diels-Alder cycloadditions in aqueous buffers, we also progressed with means to modify our protein, creating more versatile scaffolds. The respective results are presented below:

4.1. Altering the Second Coordination Sphere

In the spirit of substrate attraction we believed a more hydrophobic and sterically demanding binding pocket, moreover the replacement of those residues at the edge of the earlier described cleft to have significant influence on substrate coordination. We identified residues K135, T137, E164, G165, I197, N199, D201 and K202 and believed their replacement with more polar and hydrophobic amino acids would suffice. Neglecting iterative principles however accounting for the space the Diels-Alder substrate would require we envisioned to introduce mutations K135A, T137S, E164G, G165K, I197Y, N199Y, D201K and K202Y to shrink the binding pocket, however increasing the attraction towards the substrate. Simplistic energy minimizations utilizing crystal structure mbYDCHH_Cu (PDB: 4R6D) and YASARA Dynamics, with YAMBER force field methodologies argued reasonable stabilities of the introduces mutations[129-131]. However more importantly they indicated a stronger coordination of Diels-Alder substrate, azachalcone.
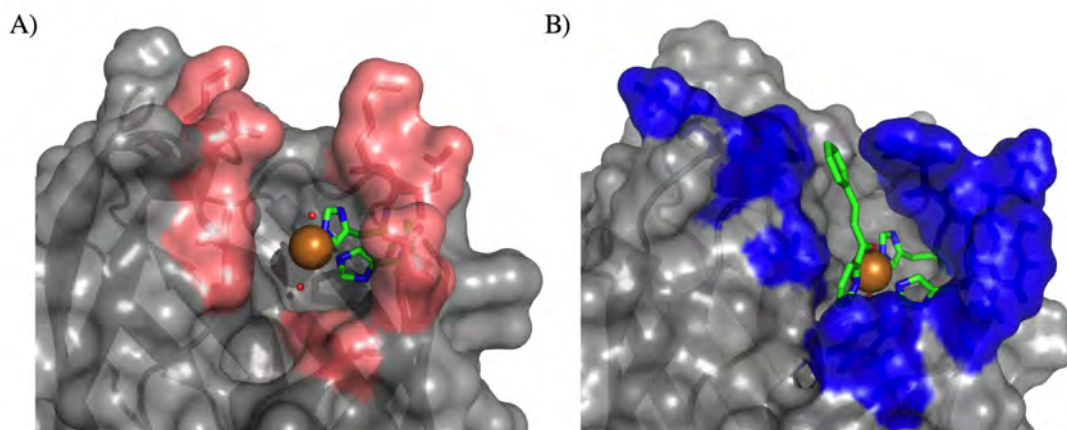
Figure 53 Second Coordination Sphere Evaluation: A) Binding pocket of mbYDCHH_Cu derived from crystal structure (PDB: 4R6D), red color indicates residues forming the binding pocket; B) Binding pocket of mbYDCHH derived from simulation, Diels-Alder substrate azachalcone is coordinated within optimized binding pocket, indicated by blue color

The indications mentioned above lasted to introduce mutations by means of site-directed mutagenesis. We proceeded from mutant mbYDCHH (and mbYDEHH), however did account for the presence of C197 in the binding motif, which was therefore not replaced in the establishment of mutant mbYDCHH[e]. Since no significant perturbation was observed within initial protein productions, the aforementioned methodologies were applied. However within larger scale protein expression we observed a drastic decrease in yield to less than 10 mg/L of LB culture. Differently mbYDEHH[e] did not yield in any maturated protein and was further disregarded. We succeeded to extract pure fractions of mbYDCHH[e], suitable for the application within Diels-Alder reactions and confirmed correctness through mass spectrometry and fluorescence measurements (Table 8, Figure S 10E). Since the latter was indifferent in spectroscopic terms towards mbYDCHH, we estimated correct folding and maturation to take place. Concluding we reported the successful establishment of an enhanced ([e]) version of mbYDCHH that was to be tested in asymmetric Diels-Alder reactions.

No	Mutant	Mass Spectrometry		Δ (Da)
		Expected (Da)	Observed (Da)	
1	mbYDCHH[e]	25117	25115	2

Table 8 Mass Spectrometry Data: mbYDCHH[e]

4.2. Host Protein PEGylation

Despite the advancements to genetically optimizing host proteins towards more stereoselectivity and increased turnovers, the earlier described chemo-genetic approach, we anticipated more universal means of protein modification to enhance the overall capability of artificial metalloenzymes. However not being limited to one class of artificial metalloenzyme we argued for a general tool that could address several of the apparent issues, i.e. protein aggregation during catalysis, solubility and stability in organic solvents or insufficient scope of the second coordination sphere and thus introduced means of N-hydroxysuccinimide ester modifications. Owing to the effectiveness of this class of modifiers to overcome the limitations, we believed to complement all surface exposed primary amines of the respective mutants of mTFP* and performed modifications with PEG-conjugated NHS-Esters[132].

Figure 54 NHS-Ester Modification: mTFP* PEGylation through modification of primary amines

Herewith we anticipated not only resolving solubility and stability matters, but also estimated for more interactions between Diels-Alder substrates and the novel environment provided by the protein. Therefore being able to increase parts of organic solvents that are indispensible to some substrates, we believed to enhance single-phase catalysis throughout a combined effect –

decreasing the solubility of Copper, forcing it into the binding site, however solubilizing substrates making them more available. We also envisioned scrutinizing lower reaction temperatures in accordance to the lower freezing points of the organic solvents used. The resulting conversions were believed to exceed previously determined selectivities.

Modifications with two different PEG types were performed (see MATERIALS AND METHODS). Herein we utilized protocols available from literature, however adapted those with respect to the 24 primary amines present in mTFP*, excess factor of NHS-Ester and overall reaction time. Resulting we performed conjugations of 0.2 mM protein solutions at pH 8.2 for a total of 20 hours with a 10-fold excess of PEG-conjugated NHS-Ester per primary amine. We varied the amounts of repeating ethylene glycol units between four and twelve (PEG4, PEG12) and anticipated to evaluate the consequential chain length difference on catalysis. Our envisioned derivate of mutants of mTFP* is illustrated below.
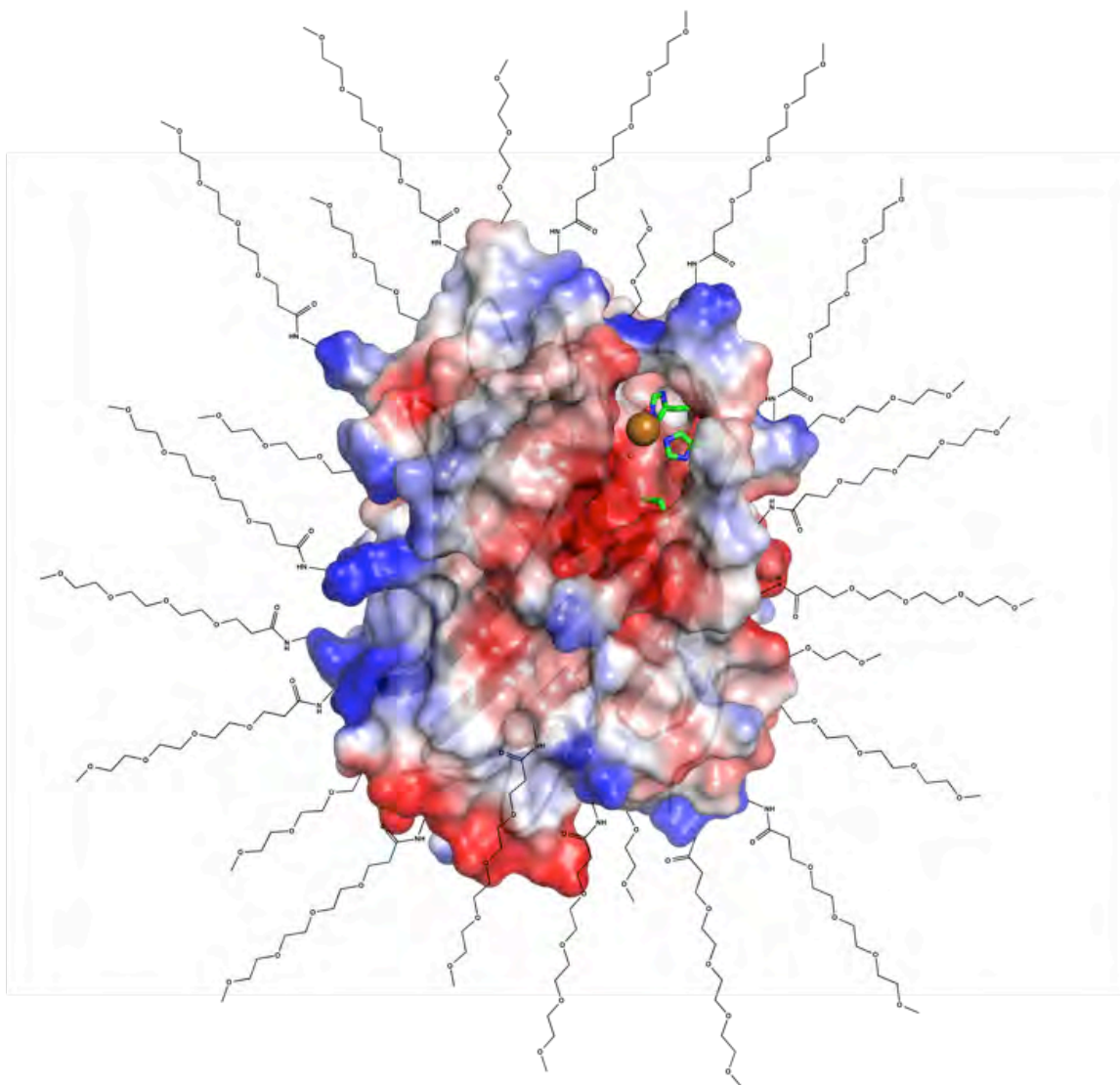
Figure 55 mbYDCHH-PEG4 Conjugated: Figure illustrates the modification of primary amines on the surface of mbYDCHH with NHS-PEG4 Ester

4.3. Catalysis

Considering the means of modification that were introduced to optimize the potency of mutants of mTFP*, we performed catalytic trials in accordance to the earlier described principles.

4.3.1. mbYDCHH[e]

Mutant mbYDCHH[e] comprising the altered second coordination sphere achieved impressive results in Diels-Alder cycloadditions. With respect to mbYDCHH we observed a general increase of conversions and enantiomeric excess from pH 5 - 7. Most obvious however was the increase at pH 6, where the introduced mutations consistently accounted for a boost from 2 to 26% enantiomeric excess. The overall diastereomeric bias towards the Endo configuration appeared not to be influenced and remained constant at 95:5 (Figure S 24).
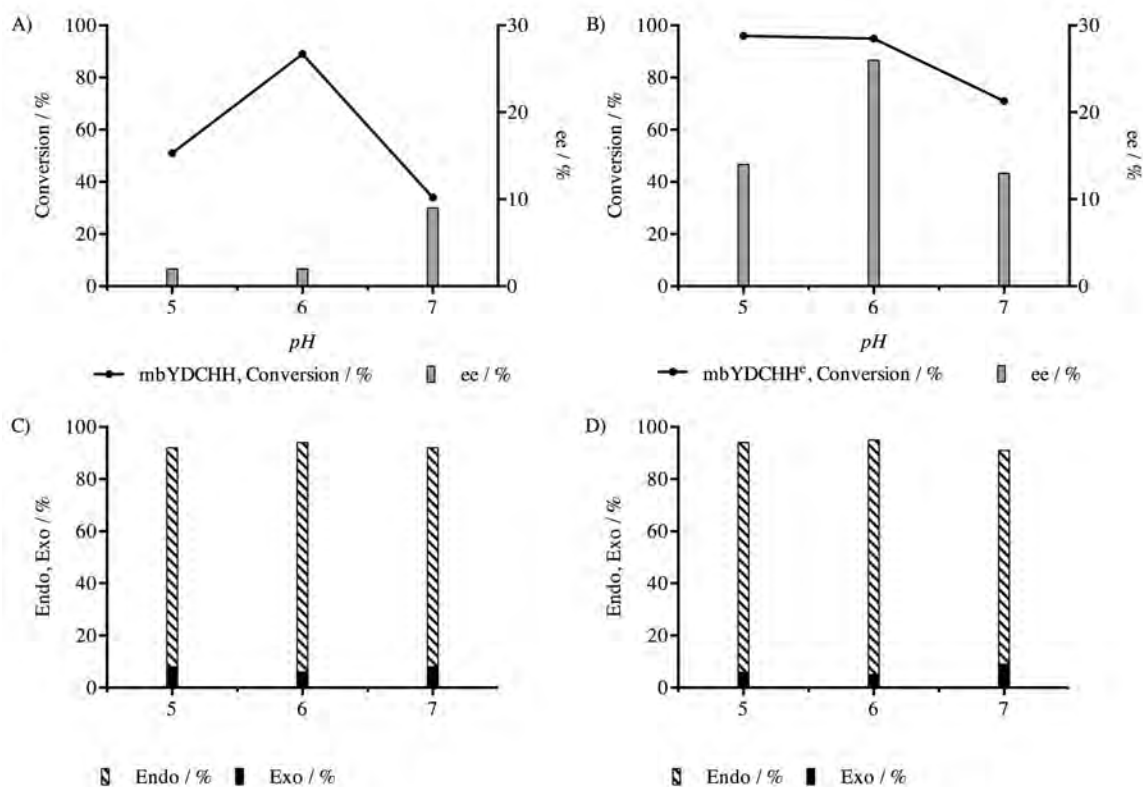
Figure 56 Diels-Alder Screen: Influences of enhanced second coordination sphere are indicated through an increase of conversion and enantiomeric excess

4.3.2. PEGylation

Screens of PEGylated mutants of mTFP* revealed the potency modifications of this kind have on artificial metalloenzymes. Our initial attempts of Diels-Alder cycloadditions, performed with the same catalytic conditions that were utilized earlier (Catalysis, Page 85), revealed a clear increase of conversions, but moreover boosted enantioselectivities.
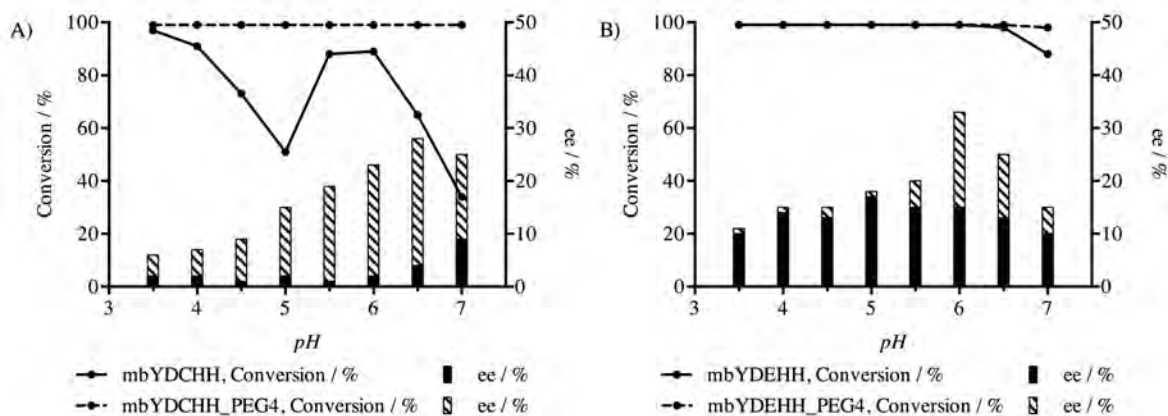
Figure 57 Diels-Alder Screen: A) mbYDCHH ± PEG4; A) mbYDEHH ± PEG4; PEGylation of host protein accounts for enhanced enantioselectivity

We observed that both mutants mbYDCHH and mbYDEHH, that had been described earlier as our template metal binding mutants with already existing enantioselectivities, were enhanced up to 30% enantiomeric excess upon conjugation with PEG4. Interestingly the introduced modification seemed to reduce influences of pH regarding conversions of mbYDCHH. We referred this to the structural fixation successful PEGgylation would cause for. The earlier crystallographically described rearrangement of the binding pocket of mbYDCHH was therefore believed to be hindered. Indifferently for both mutants was a clear trend of enhanced enantiomeric excess - mbYDCHH_PEG4 peaked at pH 6.5 and mbYDEHH_PEG4 peaked at pH

6.0. Despite these advancements the diastereomeric bias was not found to be altered. Both variants showed ratios up to 95:5 (Endo:Exo) over all pHs tested (Figure S 25).

Testing mutants that were modified with PEG12-conjugated NHS-Esters showed almost no enantiomeric excess, however the diastereomeric bias of conjugated Cu^{2+}. Considering that repetitive trials of catalysis failed to display any stereoselectivity we concluded PEG12 to be inappropriate for the purpose of optimizing reaction parameters (Figure 58).
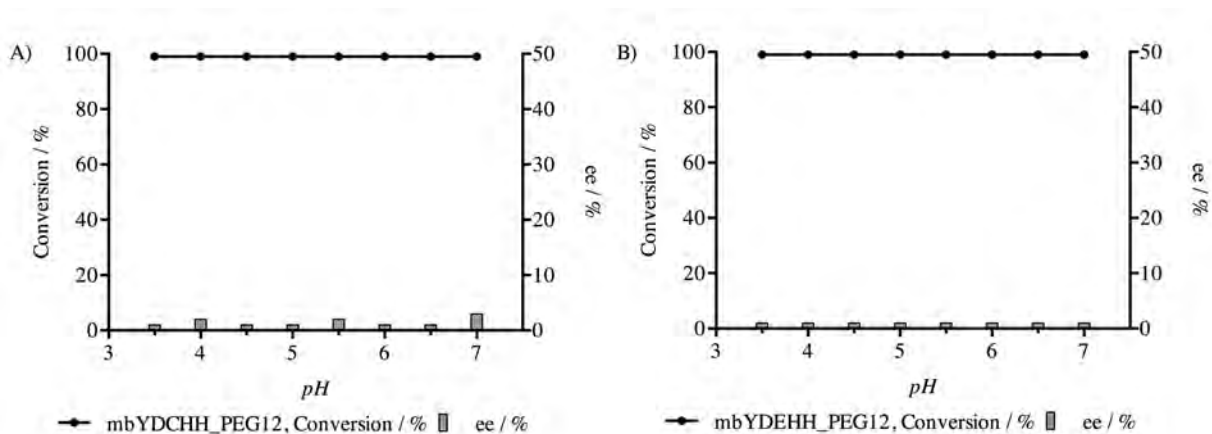
Figure 58 Diels-Alder Screen: A) mbYDCHH_PEG12; A) mbYDEHH_PEG12; PEG12 conjugation accounts for loss of enantioselectivity.

In continuation of our PEG approach we also envisioned to scrutinize means of enhanced solvent tolerance. As described earlier we believed organic solvents to be able to improve catalytic output drastically for a multitude of reasons. Accounting for the solvent tolerance we utilized MES Buffer at pH 6.5, the earlier identified optimal pH of mbYDCHH_PEG4, and increased amounts of Acetone up to reaction conditions that only contained the organic solvent. We performed Diels-Alder reactions with the same substrates and observed enantiomeric excess of up to 45% at a mixture of 50% MES / Acetone and 4 °C within 20 hours (Figure 59A). Higher concentrations of Acetone appeared to lower enantiomeric output so we deduced optimum ratios from 60:40 to

30:70, MES:Acetone. Lowering temperatures further to -15 °C improved enantiomeric conversions to 58%, however accounting for a halving of the overall conversion (Figure 59A). Thus increasing reaction times to 48 hours at -15 °C we were able to retain high enantiomeric excess around 60% and equally converting 100% of substrates (Figure 59B). Evaluating the diastereomeric output it became clear that again ratios of 95:5 (Endo:Exo) were present for reactions performed at 4 °C. At -15 °C however, we deduced a slight decrease towards 90:10, (Endo:Exo) that appeared to vanish with higher contents of Acetone (Figure 59D).
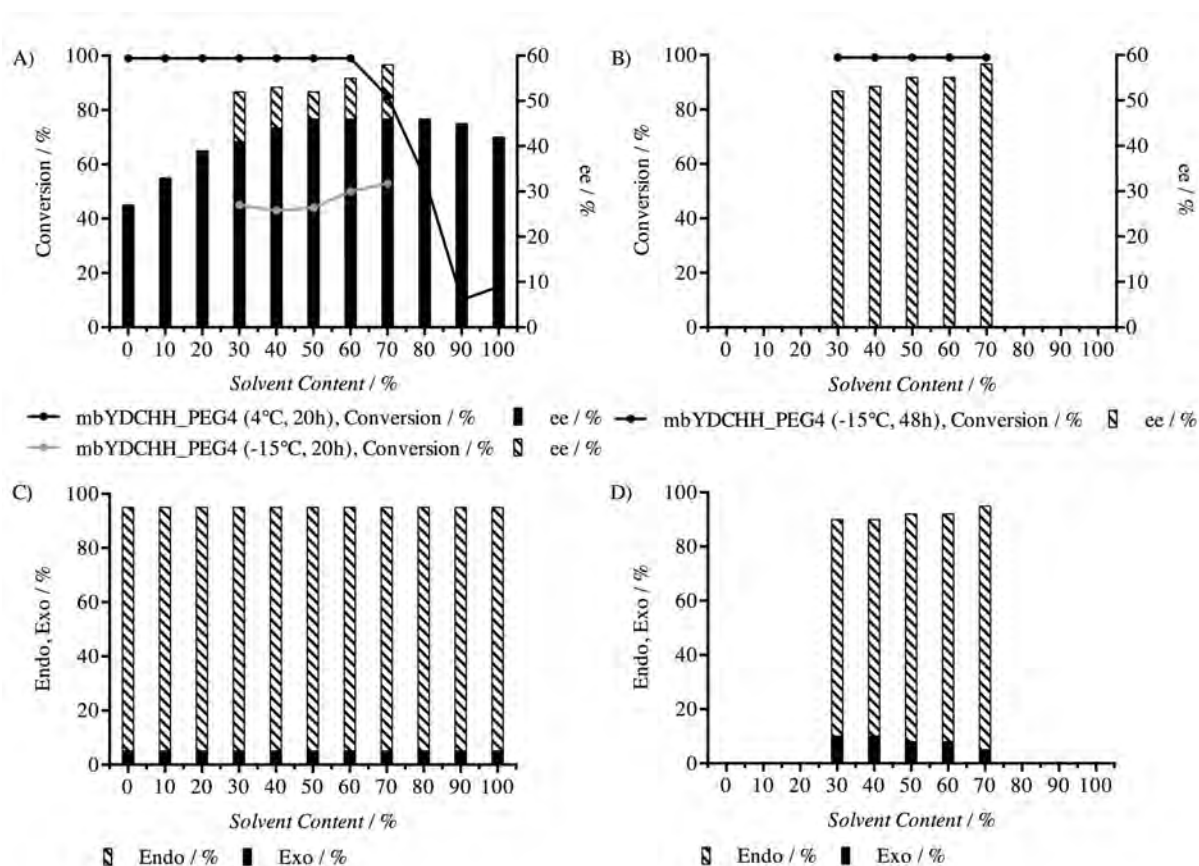
Figure 59 Diels-Alder Screen: A) mbYDCHH_PEG4 with enantiomeric excess up to 45% at 4 °C and 50% Acetone/MES pH 6.5 after 20 hours; At -15 °C enantiomeric excess peaks at 55%; B) Reactions performed at -15 °C show full conversion after 48 hours. C) Endo:Exo ratio at 4 °C constant at 95:5; D) Endo:Exo ratio at -15 °C constant at 95:5

4.4. Discussion

Whereas initially established mutants of mTFP* visualized significant insights towards the electrostatic and geometric influences of the first coordination sphere, the above presented approaches largely focused to optimize means of the second coordination sphere. In our evaluation of the potential binding pocket of mTFP*, that was performed prior to the establishment of converting artificial metalloenzymes, mostly steric properties, that would limit substrate entry with respect to specific orientations, were taken into consideration. The combination with a positioned transition metal therefore envisioned to form novel artificial metalloenzymes on the basis of a fluorescent protein. Owing to our findings and the recent literature on potent candidates, especially in asymmetric Copper catalyzed reactions, hydrophobic second coordination spheres gained much attention[118,133]. Roelfes et. al reviewed variants of Lactococcal multidrug resistance Regulator (LmrR) for this purpose and argued a positive correlation between conversion and enantiomeric excess - hence an acceleration of stereoselective catalysis within a hydrophobic pocket. Comparing these insights to our approach of replacing residues around the cleft of mTFP* and respective mutants, with polar and hydrophobic residues, we were able to obtain similar results. Indifferently to the fully hydrophobic pocket of LmrR, mbYDCHH[e] showed enhanced conversions and an increase in enantiomeric excess from 2 - 26% in comparison to its predecessor mbYDCHH. As the binding motif was not altered we presumed enhanced substrate attraction and coordination to take place and therefore concluded a general success of this principle. Despite our excitement, mutagenic advancements of this kind comprise the great limitation of unpredictable perturbation and thus folding. With respect to further mutants that were anticipated individual combinations didn't maturate in the process of protein expression, or showed earlier described decrease in yield. This limitation however may be overcome throughout small-scale libraries that can be screened utilizing the intrinsic fluorescence of mTFP*

or co-crystallization studies with transition metal and substrate that reveal the importance of individual positions. The latter is currently conducted.

Host protein PEGylation appeared to be a powerful tool to overcome lacking stereoselectivity in protein based Diels-Alder catalysis. Both PEG4 modified host proteins revealed significantly higher stereoselective conversions and more distinct trends towards optimal pH conditions. We referred this to the limited structural constraints that PEGgylation introduced[132]. Therewith flexibilities of the first coordination sphere were believed to be strongly limited and thus the earlier described rearrangement of mbYDCHH hindered. In consequence the actual potency of the individual binding motifs seemed apparent and further confirmed the earlier identified trend regarding the electrostatic constitution of the first coordination sphere. Considering the change length we observed an abrupt lack of improvement once PEG12-conjugated NHS-Ester were used. Herein again either structural constrains put onto the proteins or steric constrains from PEG12 were believed to account for the findings. Generally speaking PEG12 comprised three times the chain length of PEG4 and could account for a deviation in the three dimensional structure of the protein, thus a hindering of proper coordination at the envisioned sites. Estimating the surface area of PEG4 and PEG12 conjugated mTFP, respective the individual chain length and anticipating a spherical protein, mutants showed a drastic increase of 8-fold when conjugated with PEG12[132]. Thus most probably substrates and transition metal catalyst were not only hindered from entering the active site, but reacted earlier in the PEG-mesh on the surface. Chiral induction was therefore hindered.

Introducing parts of organic solvents to catalysis with PEG-conjugates, showed great potential and provides means to enhance enantiomeric excess. According to our insights the potential relies on 4 principle factors. Firstly using organic solvents readily dissolves substrates that may possess limited solubility under aqueous reactions conditions. Hence they become more available during

catalysis. Secondly, a general problem in artificial metalloenzymes refers to leaching catalysts from the active site that account for unspecific conversion. This holds great importance in the utilization of designed binding motives on the basis of canonical amino acids, as there dative coordination may not be as strong as the one from artificial co-factors like phenthroline[107]. Introducing organic solvent like acetone however decreases the solubility of the transition metal, enhancing its interactions with the coordinating moiety. Leaching is therefore reduced and paired with the earlier mentioned argument accounts for enhanced reactivity. Thirdly, PEG conjugated proteins show good solubility in high quantities of organic solvent. Therefore the already described advancements can also be paired with new reaction parameters i.e. lower reaction temperature that account for more specific conversions. Lastly, the apparent background reaction is significantly decelerated with the introduction of organic solvents. Thus unspecific conversions are less significant in the overall evaluation. In the context of our study we were able to show that increasing solvent concentrations, paired with lowering the reaction temperature boosted enantiomeric excess from 30 to 58%. Since mutant mbYDCHH originally only showed 4% enantiomeric excess at the respective pH, our means of modification argued a powerful 10-fold enhancement.

Summarizing, the introduction of an optimized binding pocket or means of modifying the artificial metalloenzyme by PEGylation show great potential and provide guidelines to boost other members of the field to new levels of functionality.

D. CONCLUSION

The presented study deals with the formation of artificial metalloenzymes on the basis of the fluorescent protein mTFP1. For this purpose, means of establishing a host protein system were developed, further advanced to functionalize respective scaffolds and targeting novel catalytic activity in Diels-Alder cycloadditions, lastly optimized for their catalytic output.

Optimizing mTFP1 resulted in the establishment and characterization of our host protein mTFP*. We were able to obtain high expression levels and harvested an extremely robust protein that showed high stability in various organic solvents, temperatures of up to 80 °C and over a broad pH range. Insights from crystallographic studies further confirmed our success of diminishing intrinsic metalation affinities and we thus concluded the establishment of a highly suitable scaffold for catalytic applications.

The intrinsic fluorescence that mutants of mTFP* comprised, acted not only as a reporter for quantification but allowed direct and indirect evaluation of binding dynamics with respective transition metal catalysts. The described mutagenic approach introduced variants of reported facial triads to show the electronic and geometric influences of the first coordination sphere. Single thiol modifications conjugated to well-described phenanthroline moieties argued influences the second coordination sphere could perform. Successful derivatization was shown by mass spectrometry and protein-catalyst dynamics were evaluated on the basis of two mutants. tmFRET and crystallographic methods provided a combined view that further elucidated interactions of the transition metal copper with the anticipated first coordination spheres. Structural rearrangements of the binding site of one mutant highlight the overall importance of an holistic evaluation and showed the simple utilization of triads may not be sufficient.

Library screens of permutated triads as well as with the introduced phenanthroline cofactor argued chiral induction of Diels-Alder substrates. In both cases, influences on diastereomeric and enantiomeric excess were observed. Protein conjugated to its cofactor however showed insufficient catalytic output despite reasonable indications of chiral induction. We concluded that the spacing of the provided cleft is insufficient to perform enantioselective conversions at increased rates and found similar evidence in recent reports. With respect to the introduced canonical triads however we concluded that the mere electronic or geometric constitution had a great influence on asymmetric Diels-Alder catalysis. Arguably, hard and soft ligand structures of the first coordination sphere, provided either by carboxylates or cysteine, altered stereoselective conversions with regards to the pH of the catalytic reaction. Respective dissociation constants supported these findings further. However, during optimization screens this trend could not be confirmed and we deduced geometric means in non-optimized scaffold to exercise their influence with changing proton concentration. We could show that the combination of both features, the electronic and geometric structure of the first coordination sphere, encompassed more influence than the individual feature alone. Thus referring to our library of metal binding mutants of mTFP* and their application in Diels-Alder cycloadditions we were able to derive the following general design principles targeting dative anchoring methodologies. 1) The number of residues coordinating the transition metal catalyst have great influence on stereoselective conversions; 2) two binding partners show limited stereoselectivity, however ideally comprise two histidines; 3) triads derived from 2-his-1-caboxylate motifs embody the greatest potency with three coordinating residues; 4) four binding partners block catalysis and diminish Diels-Alder activity and 5) triple histidine motifs appear inappropriate in Copper catalyzed cycloadditions.

Optimizing mutants of mTFP* followed two simplistic yet powerful scenarios. We focused on apparently limited influences of the second coordination sphere within initial metal binding mutants of mTFP* and thus introduced polar and hydrophobic amino acids to amplify

interactions between the protein and the substrates. Results indicated rate accelerations and enhanced stereoselective conversions throughout the tested conditions and we concluded that our efforts had succeeded. Introducing means of modification with NHS-Ester proved to be a general tool to overcome classical limitations of artificial metalloenzymes. Regarding to the stark increase in stereoselective conversions and the enhanced applicability of our scaffold with respect to reaction conditions, PEGylation was understood to be a solid accomplishment. Lastly, combining the insights from both optimizations showed that electronic and geometric means of the first coordination sphere are indisputably connected to the second coordination sphere and only the combined exploitation leads to successful catalysis at adaptable reaction conditions.

E. OUTLOOK

Creating catalytic function from non-catalytic scaffolds is exceedingly more challenging than the introduction of a mere metal binding motif. Concerted catalytic activity of the coordinated metal center not only requires a well-defined geometry of the first coordination sphere, with at least one free coordination site and a suitable structure, but coherently an appropriate second coordination sphere that provides means of substrate attraction, coordination and guidance to the active site. It's the mere interaction of both that facilitates stereoselective conversion with exceeding rates. Evaluating this complex interplay, the presented study intended to provided individual and combined insights for the first and second coordination sphere and therefore followed the rational to introduce facial triad motifs known from enzymes as well as covalently linked co-factor phenthroline that had been studied excessively in literature. Means of optimization open the possibility to advance insights further. Considering the limited catalytic scope of asymmetric Diels-Alder cycloadditions that was tested, future work could draw connections between the potency of individual motifs and means of optimization in other Lewis Acid catalyzed reactions. Preliminary results from Friedel-Craft alkylations or Tsuji-Trost reactions argue more suitable applications with already determined stereoselectivities exceeding values from this study. Moreover referring to the enhanced output of optimized mutants a whole new library approach could offer more details on the catalytically important hotpots in the second coordination sphere. Guided evolution would then provide ways to extend those findings even further. Our general approach to enhance functionality through protein modification could lastly be tested with other examples from literature. In any event expanding the findings hereof anticipates to advance the catalytic scope beyond what is known from nature. Applications target principles of metabolic engineering to whole cell catalysis and open plethora of possibilities that just started to uncover the wealth of options.

MATERIALS AND METHODS

General Remarks: Unless otherwise noted, all chemicals were purchased from Sigma Aldrich or VWR and were used without further purification. LB-Media was obtained from Luria Broth Ready Mix (Sigma Aldrich).

Computational Approach: Structure analysis was pursued with Pymol by Schrödinger INC. or YASARA (Yet Another Scientific Artificial Reality Application) by YASARA Biosciences GmbH.

Cloning and Mutagenesis: The gene of mTFP1[90] (monomeric Teal Fluorescent Protein) was ordered from Geneart[TM] (Life Technologies GmbH) and amplified using the following Oligonucleotides (Eurofins MWG Operon): 5'-ATTACAGGATCCGGCGTAATCAAGCCCGACATGAAG-3' and 5'-ATTACACTCGAG TTAGTCGGTGGAGTTGCGGGCCAC-3'. The amplification product was digested with BamH1 and Xho1 (New England Biolabs Inc.) and subsequently fused to a modified version of Champion[TM] pET303/CT-His, (Invitrogen Life Technologies GmbH) that had been supplemented with a SUMO protein coding region (Smt3p from *Saccharomyces cervisiae*). The resulting plasmid pET303/SUMO_mTFP1.1 was then electrotransformed into *E. Coli* BL21 (DE3) Gold (Stratagene[TM], Agilent Technologies) for further plasmid purification and mutagenesis.

Site-directed mutagenesis: Site-directed mutagenesis was performed on pET303/SUMO_mTFP1.1 (denoted as wild-type) to obtain our designed mutant mTFP* - the basis to all relevant mutants of this study. A detailed outline of all Mutants and Primers is shown elsewhere (APPENDIX/Molecular Biology, Page 137). Primers were designed according to the guidelines of the QuikChange Kit (StratageneTM, Agilent Technologies) and subsequently

obtained from Eurofins MWG Operon. Mutant plasmids were transformed into E. Coli BL21 (DE3) Gold (StratageneTM, Agilent Technologies) and purified using peqGOLD Plasmid MiniPrep Kit II (peqlab Biotechnologie GmbH). Purities and successful mutagenesis were checked by 1% Agarose Electrophoresis and Sanger Sequencing (KAUST Core Facilities).

Expression and Purification: For production of mTFP*, LB Medium that contained 180mg L^{-1} ampicillin was inoculated with *E. Coli* BL21 (DE3) Gold cells, purchased from Agilent Technologies, that had been transformed with pET303/SUMO_mTFP*. Expression yields were improved by picking fluorescent colonies, from LB Agar containing 180 mg L^{-1} ampicillin and 1 mM IPTG, for pre-culture. Pre-cultures were left to grow overnight at 37 °C and were further used to inoculate expression cultures under standard protocol. Induction occurred at OD 0.5 – 0.6, using 1 mM IPTG. Cells were left to express for 48 hours at 20 °C. Cultures were then centrifuged at 4500 rpm for 30 minutes and cooled to 4 °C. Pellets were washed with Lysis Buffer A, containing 100 mM Tris/HCl pH 7.4, 500 mM NaCl and 20 mM Imidazole. Before lysis c0mplete protease Inhibitor cocktail (Roche), was added together with DNase. Lysis occurred using Frenchpress. Lysates were immediately centrifuged at 25000 rpm and also cooled to 4 °C. Respective supernatant was prawn to Ni-Affinity Chromatographic principles and eluted from the column between 20 and 35% of Elution Buffer B containing 100 mM Tris/HCl pH 7.4, 500 mM NaCl and 500 mM Imidazole. SUMO protease was added to the eluted protein and the mixture then dialyzed overnight, at 4 °C, against Buffer A. Further Ni-Affinity Chromatography followed to remove the SUMO-Tag. Pure Protein was collected from the flow-through whereas elution with Buffer B showed a distinct elution of residual SUMO-Tag and Protease. If necessary, Batches of almost pure protein were further purified using Anion Exchange Chromatography. Anion Exchange Chromatography occurred using Q-Sepherose Colum. Protein samples were dialyzed against 100 mM Tris/HCl pH 7.4 and loaded onto the column. Elution occurred with a

smooth gradient up 20% of the same Buffer containing additional 1 M NaCl. Purity was determined by SDS-PAGE gel electrophoresis at 12.5% acrylamide.

Heat Purification: Alternatively to Anion Exchange Chromatography, Heat Purification principles were applied to obtain purest protein. Up to 5% of Glycerol added to almost pure protein and subsequent heating to 85 °C for 15 minutes caused protein based impurities to precipitate. Centrifugation at 7100 rpm allowed the separation of impurities and condensed pure samples.

Protein Storage: After protein purification pure protein samples were dialyzed against 50 mM Tris/HCl pH 7.4 or 50 mM HEPES pH 7.9 depending on further usage. Samples that were to be stored for a longer period were frozen at -80 °C in either Buffer. Samples of protein that were utilized for catalytic screens were dialyzed at least two consecutive times against H_2O to remove all traces of Buffers. Subsequently removing all water through lyophilization resulted in solid, yellow protein powder.

Mass Spectrometry: Protein mass spectrometry was carried out on a BRUKER maXis HD™ ESI-TOF. For ESI-TOF 0.04 mM of pure protein sample was dialyzed against H_2O or 5% ACN, 0.1% FA and prone to either direct injection or HPLC (Agilent Technologies), C4 Column (Column volume 5ml). Elution occurred with a flow rate of 0.5 μl/min and a gradient to 80% ACN, 0.1% FA at 8min. Subsequently fractions were recorded according to standard procedure.

Spectral Analysis: Absorbance and Fluorescence measurements were performed with pure protein samples, 0.04 mM mTFP* or respective mutant in 50 mM Tris/HCl, at mentioned pH using a TECAN INFINITE M1000 according to standard procedure.

tmFRET Measurements: All measurements were recorded on a Spectrofluorometer (PTI, New Jersey). Protein Samples were diluted to the final concentration of 1 μM using 50 mM MES pH 6.0 and 7.5 and heated to 25 °C. Copper and Zinc titrations were accomplished with a series of $Cu(NO_3)_2$ and $Zn(NO_3)_2$ stock solutions, ranging from 100 to 0.01 mM. Indirect titrations were fitted with 1.5 μM and 3 μM $Cu(NO_3)_2$. Spectra were recorded from 480 to 510 nm with a bandwidth filter of 5nm. Data analysis regarding static and dynamic quenching was performed as described by Tarasaka and co-workers using the following formula[98,99,101,102]:

Static Quenching:

$$\frac{F(Metal)}{F_0} = \left(\frac{1}{1 + \frac{[Metal]}{Kd1}} \right)$$

Combination of Static and Dynamic Quenching (One binding Site):

$$\frac{F(Metal)}{F_0} = \left(\frac{1}{1 + \frac{[Metal]}{Kd1}} \right)\left(1 - \frac{E}{1 + \frac{Kd2}{[Metal]}} \right)$$

Estimation of FRET Efficiency (R values are deduced from crystal structure PDB: 4R6D and model, Figure S 19)

$$E = \frac{1}{1 + (R/R_0)^6}$$

Data analysis regarding multiple binding sites or competitive titrations was performed using the following formulae:

Combination of Static and Dynamic Quenching (Multiple binding Sites):

$$\frac{F(Metal)}{F_0} = \left(\frac{1}{1 + \frac{[Metal]}{K_d^{stat}}} \right)\prod_{i=1}^{n}\left(1 - \frac{E_i}{1 + \frac{K_d^{dyn,i}}{[Metal]}} \right)$$

Competitive titration with $Cu(NO_3)_2$ and $Zn(NO_3)_2$ (One binding Sites)

$$\frac{F(Metal)}{F_0} = \left(1 - \frac{E_{Cu}}{1 + \frac{Kd_{2,Cu}}{[Cu]} + \frac{Kd_{2,Cu}}{Kd_{2,Zn}} * \frac{[Zn]}{[Cu]}}\right)\left(\frac{1}{1 + \frac{[Cu]}{Kd_{1,Cu}}}\right)$$

Fluoresce net Lifetimes: Lifetimes measurements were recorded on a Spectrofluorometer (PTI, New Jersey) with white laser illumination (WhiteLase) at 20 MHz (λ_{ex} = 462 nm; λ_{em} = 495 nm). Intensity measurements were done on the same instrument with Xenon light illumination.

Stability Studies: Melting curves of mTFP* or respective mutant were obtained from circular dichroism measurements using a JASCO J-815 Spectropolarimeter. 400 μL of protein solution, 4 μM mTFP* or respective mutant in 50 mM Tris/HCl pH 7.4, was prepared and given into a Hellma Precision Cell (Type no. 110 QS, 1mm light path). Temperature resolved (50 – 98 °C) far UV Spectra (210 – 200 nm) were recorded.

Solvent Screen: 2 mM mTFP* in 50 mM Tris/HCl, pH 7.4 was diluted to 0.05 mM with a mixture of water and organic solvent (acetone, 2-butanol, t-butanol, methanol, diglyme, dioxan, dimethylformamide, dimethylsulfoxide, ethanol, hexanol, 2-propanol, tetrafluoroethylene and tetrahydrofuran). Concentrations varied from 10 to 90% organic solvent. Fluorescence readings were accomplished with a TECAN INFINITE M1000.

Metal Incubation: 50 μl of protein solution, 0.04 mM mTFP* or respective mutant in 50 mM Tris/HCl pH 7.4, was mixed with the according metal at a ratio of 1:1, 1:5, 1:10 and 1:25. Incubation occurred at 25 °C for 1 hour. Metal salts of Copper(II)Nitrate, Palladium(II)Chloride, Rhodium(II)Acetat, Nickel(II)Chloride were primarily dissolved in 50 mM Tris/HCl pH 7.4 ±

DMSO, or H_2O to 1 M stock solutions. Metal addition was tested using Fluorescence or ESI-TOF measurements as described above.

Crystallography: mTFP* or respective mutants (in 50 mM HEPES, pH 7.9) were concentrated to 50 mg/mL using a 10 kDa NMWL Amicon Ultra Centrifugal Filter Device (Millipore, Billerica, MA). Crystals of mTFP* or respective mutants were grown at 20 °C, overnight to their final size of about 0.5 x 0.1 x 0.1 mm³, using the sitting drop vapour diffusion method. Drops contained 0.2 μL protein and 0.2 μL of reservoir buffer (100 mM MES, pH 6.5 and 21.5% PEG 3000). Co-crystallisations were performed by adding metal salts to a final concentration of 25 mM. For the mTFP*Pd dataset, mTFP* crystals were soaked for 24 h in 10 mM $PdCl_2$. For X-ray measurements, crystals were soaked for 1 hour in a mixture of mother liquor and 50% glycerol (1:1. v/v) and subsequently flash-frozen in liquid nitrogen. Datasets were either recorded using synchrotron radiation at $\lambda = 1.00$ Å at the beam line X06SA, Swiss Light Souce (SLS), Villigen, Switzerland or a using a Bruker CuKα rotating anode at 1.54 Å. X-ray intensities were evaluated with XDS.[134] The space group of mTFP* or respective mutants was P2$_1$ (monoclinic) with unit cell dimensions outlined in the supplementary information (Table S 5). Phases were obtained by molecular replacement using PHASER and the coordinates of mTFP1 mTFP* (PDB: 2HQK, 4Q9W)[90,135]. Model building was performed with Coot. Rigid body, TLS (Translation/Libration/Screw) and positional refinements with REFMAC5 resulted in the final models (Table S 5)[136]. The quality of the stereochemistry was confirmed by the Ramachandran plot determined with PROCHECK[137].

Thiol Modification: 0.32 mM of mTFP*C164/204, dissolved in 100 mM Tris/HCl pH 7.4 was reduced using 10 eq. TCEP for 30min. Dialysis under inert atmosphere for at least 4 hours at 4 °C was performed to remove residual TCEP. Ligand, 5-Maleimido-1,10-phenanthroline (phen) was dissolved in ACN added to the protein with a final solute

concentration of 10%. Addition reactions occurred for 24 hours at 25 °C in the dark. Harvested samples were then prone to further dialysis against 100 mM Tris/HCl pH 7.4 or H_2O.

Synthesis of 5-Maleimido-1,10-phenanthroline: Synthesis occurred according to the protocol published by Trammell and with amendments of Reetz and corworkers[15,138].

Diels-Alder Activity: Cyclopentadiene (2) was freshly prepared from dicyclopentadiene and stored at -80 °C. Azachalcone (1) was prepared according to literature[139]. Hybrid catalysts on the basis of mTFP* or respective mutant were prepared by weighing appropriate amounts of lyophilized catalyst and dissolving in appropriate MES Buffer, or mixing a solution of the desired variant (970 μL, 3 mg/ml of Protein in MES Buffer, pH as anticipated) with $Cu(OTf)_2$ solution (10 μL 10 mM $Cu(OTf)_2$) and incubation for 1 h (400 rpm, 20 °C, Thermomixer comfort, Eppendorf). These hybrid catalysts were immediately used for Diels-Alder reactions: a solution of 1 (0.1 M in Acetone, 10 μL) were added to the catalyst solution and mixed immediately by inverting the tube 3 times. Then, a solution of 2 (10 M in Acetone, 9 μL) was added and mixed immediately as in the last step. The tube was placed immediately in a pre-cooled shaking incubator (4 °C, 400 rpm, Thermomixer comfort, Eppendorf). The standard reaction time was 20 h (Figure S 21). Reactions were extracted with diethyl ether (2 × 1 ml). The combined organic phase was dried by filtering over $MgSO_4$ and the solvent was evaporated. The samples were analyzed by HPLC using anisole as internal standard (column: 250 mm Chiralcel OD-H, 4.6 mm inner diameter; n-heptane/2-propanol = 99:1; 0.5 ml/min, 25 °C; UV-detector 220 nm; retention times: 10.4 min (anisole), 14.2 min (exo-4), 16.1 min (exo-4`), 20.1 min (endo-3), 25.4 min (endo-3`), 31.7 min (3)). The absolute configuration of the enantiomers 3 has not been established in literature[121,140,141].

N-Hydroxy-succinimide-Ester Conjugation: mTFP* or respective mutant were dissolved in 100 mM NaHCO$_3$ pH 8.2 to a final concentration of 0.2 mM. MS(PEG)$_4$ and MS(PEG)$_{12}$ (Thermo Scientific) were dissolved in DMF to a final concentration of 2.5 M. A 240 fold excess of Ester was added to mixtures of protein at room temperature. This accounted for 10 eq. for each of the 24 primary amines (23 lysine residues + N-Terminus) present in mTFP* or respective mutants. Conjugations were performed for 20 hours, gently shaking flasks at 200 rpm. Excess ester was removed by double dialysis against H$_2$O for at least 4 hours.

BIBLIOGRAPHY

1   Reetz, M. T. Biocatalysis in organic chemistry and biotechnology: past, present, and future. *Journal of the American Chemical Society* 135, 12480-12496, (**2013**).

2   Jaeger, K. E., Eggert, T., Eipper, A. & Reetz, M. T. Directed evolution and the creation of enantioselective biocatalysts. *Applied microbiology and biotechnology* 55, 519-530, (**2001**).

3   Lewis, J. C. Artificial Metalloenzymes and Metallopeptide Catalysts for Organic Synthesis. *Acs Catal* 3, 2954-2975, (**2013**).

4   Reetz, M. T., Rentzsch, M., Pletsch, A. & Maywald, M. Towards the directed evolution of hybrid catalysts. *Chimia* 56, 721-723, (**2002**).

5   Reiner, T., Jantke, D., Marziale, A. N., Raba, A. & Eppinger, J. Metal-Conjugated Affinity Labels: A New Concept to Create Enantioselective Artificial Metalloenzymes. *Chemstryopen* 2, 50-54, (**2013**).

6   Jantke, D. *et al*. Synthetic strategies for efficient conjugation of organometallic complexes with pendant protein reactive markers. *J Organomet Chem* 744, 82-91, (**2013**).

7   Deuss, P. J., den Heeten, R., Laan, W. & Kamer, P. C. Bioinspired catalyst design and artificial metalloenzymes. *Chemistry* 17, 4680-4698, (**2011**).

8   C. Malan, T. R. W. Phosphorus Ligands in Asymmetric Catalysis: Synthesis and Applications. Vol. 3, pp. 1103–1131, (**2008**).

9   Sawamura, M. & Ito, Y. Catalytic Asymmetric-Synthesis by Means of Secondary Interaction between Chiral Ligands and Substrates. *Chem Rev* 92, 857-871, (**1992**).

10   Rowlands, G. J. Ambifunctional cooperative catalysts. *Tetrahedron* 57, 1865-1882, (**2001**).

11   DeSantis, G. *et al*. Creation of a productive, highly enantioselective nitrilase through gene site saturation mutagenesis (GSSM). *Journal of the American Chemical Society* 125, 11476-11477, (**2003**).

12   Jiang, L. *et al*. De novo computational design of retro-aldol enzymes. *Science* 319, 1387-1391, (**2008**).

13   Humble, M. S. & Berglund, P. Biocatalytic Promiscuity. *Eur J Org Chem*, 3391-3401, (**2011**).

14   Ringenberg, M. R. & Ward, T. R. Merging the best of two worlds: artificial metalloenzymes for enantioselective catalysis. *Chemical communications* 47, 8470-8476, (**2011**).

15   Reetz, M. T. *et al*. A robust protein host for anchoring chelating ligands and organocatalysts. *Chembiochem : a European journal of chemical biology* 9, 552-564, (**2008**).

16   Lee, H. S. & Schultz, P. G. Biosynthesis of a site-specific DNA cleaving protein. *Journal of the American Chemical Society* 130, 13194-13195, (**2008**).

17   van Santen, R. A., van Leeuwen, P. W. N. M., Moulijn, J. A. & Averill, B. A. History of catalysis. *Stud Surf Sci Catal* 123, 3-28, (**1999**).

18   Anastas, P. T. & Crabtree, R. H. *Handbook of green chemistry*. (Wiley-VCH, **2009**).

19   Carey, F., A. *Advanced Organic Chemistry*. (Springer, **2008**).

20   Leach, B., E. *Industrial Catalysis: Chemistry applied to your life-style and environment*. (New York Academic Press, **1983**).

21   Swiegers, G. F. *Mechanical catalysis : methods of enzymatic, homogeneous, and heterogeneous catalysis*. (John Wiley, **2008**).

22   Knowles, W. S. Asymmetric hydrogenations (Nobel lecture). *Angew Chem Int Edit* 41, 1999-2007, (**2002**).

23   Noyori, R. Asymmetric catalysis: Science and opportunities (Nobel lecture). *Angew Chem Int Edit* 41, 2008-2022, (**2002**).

24   Sharpless, K. B. Searching for new reactivity (Nobel lecture). *Angew Chem Int Edit* 41, 2024-2032, (**2002**).

25   Chauvin, Y. Olefin metathesis: The early days (Nobel lecture). *Angew Chem Int Edit* 45, 3740-3747, (**2006**).

26   Grubbs, R. H. Olefin-metathesis catalysts for the preparation of molecules and materials (Nobel lecture). *Angew Chem Int Edit* 45, 3760-3765, (**2006**).

27   Schrock, R. R. Multiple metal-carbon bonds for catalytic metathesis reactions (Nobel lecture). *Angew Chem Int Edit* 45, 3748-3759, (**2006**).

28   Ertl, G. Reactions at surfaces: From atoms to complexity (Nobel lecture). *Angew Chem Int Edit* 47, 3524-3535, (**2008**).

29   Suzuki, A. Cross-Coupling Reactions Of Organoboranes: An Easy Way To Construct C-C Bonds (Nobel Lecture). *Angew Chem Int Edit* 50, 6722-6737, (**2011**).

30   Negishi, E. I. Magical Power of Transition Metals: Past, Present, and Future (Nobel Lecture). *Angew Chem Int Edit* 50, 6738-6764, (**2011**).

31   Chorkendorff, I., Niemantsverdriet, J. W. *Concepts of Modern Catalysis and Kinetics (Book)*. Vol. 41 1/8p (**2004**).

32   Durrenberger, M. *et al*. Artificial Transfer Hydrogenases for the Enantioselective Reduction of Cyclic Imines. *Angew Chem Int Edit* 50, 3026-3029, (**2011**).

33   Petsko, G. A. Structure and mechanism in protein science: A guide to enzyme catalysis and protein folding. *Nature* 401, 115-116, (**1999**).

34   Pisarewicz, K., Mora, D., Pflueger, F. C., Fields, G. B. & Mari, F. Polypeptide chains containing D-gamma-hydroxyvaline. *Journal of the American Chemical Society* 127, 6207-6215, (**2005**).

35   Maier, W. A. Thalidomide Embryopathy and Limb Defects - Experiences in Habilitation of Children with Ectromelias. *Arch Dis Child* 40, 154-&, (**1965**).

36   Stephens, T. D., Bunde, C. J. W. & Fillmore, B. J. Mechanism of action in thalidomide teratogenesis. *Biochem Pharmacol* 59, 1489-1499, (**2000**).

37   Thomas, C. M. & Ward, T. R. Artificial metalloenzymes: proteins as hosts for enantioselective catalysis. *Chemical Society reviews* 34, 337-346, (**2005**).

38   Jacobsen, E. *Comprehensive Asymmetric Catalysis*. (Springer, **1999**).

39   Li, Y. G., Li, L., Yang, M. Y., Qin, H. L. & Kantchev, E. A. B. Computational modelling of the enantioselectivity in the asymmetric 1,4-addition reaction catalyzed by a Rh complex of a S-chiral disulfoxide. *Rsc Adv* 5, 5250-5255, (**2015**).

40   Schneebeli, S. T., Hall, M. L., Breslow, R. & Friesner, R. Quantitative DFT Modeling of the Enantiomeric Excess for Dioxirane-Catalyzed Epoxidations. *Journal of the American Chemical Society* 131, 3965-3973, (**2009**).

41   Reetz, M. T. Artificial metalloenzymes as catalysts in stereoselective diels-alder reactions. *Chemical record* 12, 391-406, (**2012**).

42   Kagan, H. B. & Riant, O. Catalytic Asymmetric Diels-Alder Reactions. *Chem Rev* 92, 1007-1019, (**1992**).

43   Nicolaou, K. C., Snyder, S. A., Montagnon, T. & Vassilikogiannakis, G. The Diels-Alder reaction in total synthesis. *Angew Chem Int Edit* 41, 1668-1698, (**2002**).

44   Yates, P. & Eaton, P. Acceleration of the Diels-Alder Reaction by Aluminum Chloride. *Journal of the American Chemical Society* 82, 4436-4437, (**1960**).

45   Corey, E. J., Weinshen.Nm, Schaaf, T. K. & Huber, W. Stereo-Controlled Synthesis of Prostaglandins F2alpha and E2 (Dl). *Journal of the American Chemical Society* 91, 5675-&, (**1969**).

46   Evans, D. A. *et al*. Bis(oxazoline) and bis(oxazolinyl)pyridine copper complexes as enantioselective Diels-Alder catalysts: Reaction scope and synthetic applications. *Journal of the American Chemical Society* 121, 7582-7594, (**1999**).

47   Reymond, S. & Cossy, J. Copper-Catalyzed Diels-Alder Reactions. *Chem Rev* 108, 5359-5406, (**2008**).

48   MacMillan, D. W. C. The advent and development of organocatalysis. *Nature* 455, 304-308, (**2008**).

49   Kim, H. J., Ruszczycky, M. W., Choi, S. H., Liu, Y. N. & Liu, H. W. Enzyme-catalysed [4+2] cycloaddition is a key step in the biosynthesis of spinosyn A. *Nature* 473, 109-112, (**2011**).

50   Ose, T. *et al*. Insight into a natural Diels-Alder reaction from the structure of macrophomate synthase. *Nature* 422, 185-189, (**2003**).

51   Kennedy, J. *et al*. Modulation of polyketide synthase activity by accessory proteins during lovastatin biosynthesis. *Science* 284, 1368-1372, (**1999**).

52   Chelikani, P., Fita, I. & Loewen, P. C. Diversity of structures and properties among catalases. *Cell Mol Life Sci* 61, 192-208, (**2004**).

53   Cheung, H. Ullmann's Encyclopedia of Industrial Chemistry. *Choice: Current Reviews for Academic Libraries* 50, 452-452, (**2012**).

54   Lu, Y., Yeung, N., Sieracki, N. & Marshall, N. M. Design of functional metalloproteins. *Nature* 460, 855-862, (**2009**).

55   Thomson, A. J. & Gray, H. B. Bio-inorganic chemistry. *Current opinion in chemical biology* 2, 155-158, (**1998**).

56   Blaser, H. U. Enantioselective catalysis in fine chemicals production. *Chemical communications*, 293-296, (**2003**).

57   Meggers, E. From conventional to unusual enzyme inhibitor scaffolds: the quest for target specificity. *Angewandte Chemie* 50, 2442-2448, (**2011**).

58   Willmann, J. K., van Bruggen, N., Dinkelborg, L. M. & Gambhir, S. S. Molecular imaging in drug development. *Nat Rev Drug Discov* 7, 591-607, (**2008**).

59   Razgulin, A., Ma, N. & Rao, J. H. Strategies for in vivo imaging of enzyme activity: an overview and recent advances. *Chemical Society reviews* 40, 4186-4216, (**2011**).

60   Caravan, P. Protein-Targeted Gadolinium-Based Magnetic Resonance Imaging (MRI) Contrast Agents: Design and Mechanism of Action. *Accounts of chemical research* 42, 851-862, (**2009**).

61   Martic, S., Labib, M., Shipman, P. O. & Kraatz, H. B. Ferrocene-peptido conjugates: From synthesis to sensory applications. *Dalton T* 40, 7264-7290, (**2011**).

62   Wilson, M. E. & Whitesides, G. M. Conversion of a protein to a homogeneous asymmetric hydrogenation catalyst by site-specific modification with a diphosphinerhodium(I) moiety. *Journal of the American Chemical Society* 100, 306-307, (**1978**).

63   Rosati, F. & Roelfes, G. Artificial Metalloenzymes. *Chemcatchem* 2, 916-927, (**2010**).

64   Ward, T. R. Designed evolution of artificial metalloenzymes for enantioselective catalysis based on the biotin-avidin technology. *Abstr Pap Am Chem S* 233, 492-492, (**2007**).

65   Mao, J. C. & Ward, T. R. Artificial Metalloenzymes for Enantioselective Catalysis Based on the Biotin-Avidin Technology. *Chimia* 62, 956-961, (**2008**).

66   Ward, T. R. Artificial enzymes made to order: Combination of computational design and directed evolution. *Angew Chem Int Edit* 47, 7802-7803, (**2008**).

67   Pordea, A., Mathis, D. & Ward, T. R. Incorporation of biotinylated manganese-salen complexes into streptavidin: New artificial metalloenzymes for enantioselective sulfoxidation. *J Organomet Chem* 694, 930-936, (**2009**).

68   Pierron, J. *et al*. Artificial metalloenzymes for asymmetric allylic alkylation on the basis of the biotin-avidin technology. *Angew Chem Int Edit* 47, 701-705, (**2008**).

69   Rioz-Martinez, A. & Roelfes, G. DNA-based hybrid catalysis. *Current opinion in chemical biology* 25, 80-87, (**2015**).

70   Kaiser, E. T. & Lawrence, D. S. Chemical Mutation of Enzyme Active-Sites. *Science* 226, 505-511, (**1984**).

71   Deuss, P. J., Popa, G., Slawin, A. M. Z., Laan, W. & Kamer, P. C. J. Artificial
        Copper Enzymes for Asymmetric Diels–Alder Reactions. *Chemcatchem* 5, 1184-
        1191, (**2013**).

72   Deuss, P. J., Popa, G., Botting, C. H., Laan, W. & Kamer, P. C. J. Highly
        Efficient and Site-Selective Phosphane Modification of Proteins through
        Hydrazone Linkage: Development of Artificial Metalloenzymes. *Angew Chem Int
        Edit* 49, 5315-5317, (**2010**).

73   Wang, L., Xie, J. & Schultz, P. G. Expanding the genetic code. *Annual review of
        biophysics and biomolecular structure* 35, 225-249, (**2006**).

74   Hu, C., Chan, S. I., Sawyer, E. B., Yu, Y. & Wang, J. Y. Metalloprotein design
        using genetic code expansion. *Chemical Society reviews* 43, 6498-6510, (**2014**).

75   Drienovska, I., Rioz-Martinez, A., Draksharapu, A. & Roelfes, G. Novel artificial
        metalloenzymes by in vivo incorporation of metal-binding unnatural amino acids.
        Chemical Science 6, 770-776, (**2015**).

76   Young, T. S., Ahmad, I., Yin, J. A. & Schultz, P. G. An Enhanced System for
        Unnatural Amino Acid Mutagenesis in E. coli. *Journal of molecular biology* 395,
        361-374, (**2010**).

77   Liu, C. C. & Schultz, P. G. Adding New Chemistries to the Genetic Code. *Annual
        Review of Biochemistry, Vol 79* 79, 413-444, (**2010**).

78   Roelfes, G., Bos, J. & Drienovska, I. New artificial metalloenzymes based on the
        transcription factor LmrR. *J Biol Inorg Chem* 19, S744-S744, (**2014**).

79   Fernandez-Gacio, A., Codina, A., Fastrez, J., Riant, O. & Soumillion, P.
        Transforming carbonic anhydrase into epoxide synthase by metal exchange.
        Chembiochem : a European journal of chemical biology 7, 1013-1016, (**2006**).

80   Okrasa, K. & Kazlauskas, R. J. Manganese-substituted carbonic anhydrase as a
        new peroxidase. *Chem-Eur J* 12, 1587-1596, (**2006**).

81   Bruijnincx, P. C. A., van Koten, G. & Gebbink, R. J. M. K. Mononuclear non-
        heme iron enzymes with the 2-His-1-carboxylate facial triad: recent developments
        in enzymology and modeling studies. *Chemical Society reviews* 37, 2716-2744,
        (**2008**).

82   Hegg, E. L. & Que, L. The 2-His-1-carboxylate facial triad - An emerging
        structural motif in mononuclear non-heme iron(II) enzymes. *Eur J Biochem* 250,
        625-629, (**1997**).

83   Koehntop, K. D., Emerson, J. P. & Que, L. The 2-His-1-carboxylate facial triad: a
        versatile platform for dioxygen activation by mononuclear non-heme iron(II)
        enzymes. *J Biol Inorg Chem* 10, 87-93, (**2005**).

84   Parkin, G. Synthetic analogues relevant to the structure and function of zinc enzymes. *Chem Rev* 104, 699-767, (**2004**).

85   Podtetenieff, J., Tagliaber, A., Bill, E., Reijerse, E. J. & Reetz, M. T. An Artificial Metalloenzyme: Creation of a Designed Copper Binding Site in a Thermostable Protein. *Angew Chem Int Edit* 49, 5151-5155, (**2010**).

86   Amrein, B. *et al*. Identification of two-histidines one-carboxylate binding motifs in proteins amenable to facial coordination to metals. *Metallomics* 4, 379-388, (**2012**).

87   Ward, T. R. Latest Developments in Metalloenzyme Design and Repurposing. *Eur J Inorg Chem*, (**2015**).

88   Yang, H., Srivastava, P., Zhang, C. & Lewis, J. C. A general method for artificial metalloenzyme formation through strain-promoted azide-alkyne cycloaddition. *Chembiochem : a European journal of chemical biology* 15, 223-227, (**2014**).

89   Ward, W. Green Fluorescent Protein, Properties, Applications and Protocols. *Wiley-Liss*, 45-75, (**1998**).

90   Ai, H. W., Henderson, J. N., Remington, S. J. & Campbell, R. E. Directed evolution of a monomeric, bright and photostable version of Clavularia cyan fluorescent protein: structural characterization and applications in fluorescence imaging. *The Biochemical journal* 400, 531-540, (**2006**).

91   Armon, A., Graur, D. & Ben-Tal, N. ConSurf: an algorithmic tool for the identification of functional regions in proteins by surface mapping of phylogenetic information. *Journal of molecular biology* 307, 447-463, (**2001**).

92   Van Durme, J. *et al*. A graphical interface for the FoldX forcefield. *Bioinformatics* 27, 1711-1712, (**2011**).

93   Guerois, R., Nielsen, J. E. & Serrano, L. Predicting changes in the stability of proteins and protein complexes: a study of more than 1000 mutations. *Journal of molecular biology* 320, 369-387, (**2002**).

94   Janin, J. Surface and inside Volumes in Globular Proteins. *Nature* 277, 491-492, (**1979**).

95   Wilkins, M. R. *et al*. Protein identification and analysis tools in the ExPASy server. *Methods in molecular biology* 112, 531-552, (**1999**).

96   Wachter, R. M. *et al*. Crystal structure and photodynamic behavior of the blue emission variant Y66H/Y145F of green fluorescent protein. *Biochemistry* 36, 9759-9765, (**1997**).

97   Turner, N. J. Directed evolution drives the next generation of biocatalysts. *Nature chemical biology* 5, 567-573, (**2009**).

98   Helms, V. *Principles of Computational Cell Biology*. (WILEY-VCH Verlag GmbH & Co. KgaA, **2008**).

99   Yu, X. Z., Wu, X. W., Bermejo, G. A., Brooks, B. R. & Taraska, J. W. Accurate High-Throughput Structure Mapping and Prediction with Transition Metal Ion FRET. *Biophys J* 104, 547A-547A, (**2013**).

100   Forster, T. Experimentelle Und Theoretische Untersuchung Des Zwischenmolekularen Ubergangs Von Elektronenanregungsenergie. *Z Naturforsch A* 4, 321-327, (**1949**).

101   Taraska, J. W., Puljung, M. C. & Zagotta, W. N. Short-distance probes for protein backbone structure based on energy transfer between bimane and transition metal ions. *Proceedings of the National Academy of Sciences of the United States of America* 106, 16227-16232, (**2009**).

102   Taraska, J. W., Puljung, M. C., Olivier, N. B., Flynn, G. E. & Zagotta, W. N. Mapping the structure and conformational movements of proteins with transition metal ion FRET. *Nat Methods* 6, 532-U594, (**2009**).

103   Ellis, M. J., Dodd, F. E., Sawers, G., Eady, R. R. & Hasnain, S. S. Atomic resolution structures of native copper nitrite reductase from Alcaligenes xylosoxidans and the active site mutant Asp92Glu. *Journal of molecular biology* 328, 429-438, (**2003**).

104   Messerschmidt, A. *et al*. Refined Crystal-Structure of Ascorbate Oxidase at 1.9 a Resolution. *Journal of molecular biology* 224, 179-205, (**1992**).

105   McCall, K. A., Huang, C. C. & Fierke, C. A. Function and mechanism of zinc metalloenzymes. *J Nutr* 130, 1437s-1446s, (**2000**).

106   Trammell, S. A. *et al*. Synthesis and characterization of a ruthenium(II)-based redox conjugate for reagentless biosensing. *Bioconjugate chemistry* 12, 643-647, (**2001**).

107   Fullerton, R. Stability constants of some M(I)- and M(II)- 1,10-phenanthroline complexes. *Retrospective Theses and Dissertations*, (**1959**).

108   Bystroff, R., I. The substituent effect in transition metal complexes of 1, 10-phenanthroline. *Retrospective Theses and Dissertations*, (**1959**).

109   Deuss, P. J., Popa, G., Slawin, A. M. Z., Laan, W. & Kamer, P. C. J. Artificial Copper Enzymes for Asymmetric Diels-Alder Reactions. *Chemcatchem* 5, 1184-1191, (**2013**).

110   Reetz, M. T. & Jiao, N. Copper-phthalocyanine conjugates of serum albumins as enantioselective catalysts in Diels-Alder reactions. *Angew Chem Int Edit* 45, 2416-2419, (**2006**).

111   Davies, R. R. *et al*. Artificial metalloenzymes based on protein cavities: Exploring the effect of altering the metal ligand attachment position by site directed mutagenesis. *Bioorg Med Chem Lett* 9, 79-84, (**1999**).

112   Davies, R. R. & Distefano, M. D. A semisynthetic metalloenzyme based on a protein cavity that catalyzes the enantioselective hydrolysis of ester and amide substrates. *Journal of the American Chemical Society* 119, 11643-11652, (**1997**).

113   Bos, J., Fusetti, F., Driessen, A. J. M. & Roelfes, G. Enantioselective Artificial Metalloenzymes by Creation of a Novel Active Site at the Protein Dimer Interface. *Angew Chem Int Edit* 51, 7472-7475, (**2012**).

114   Farver, O. & Pecht, I. Electron transfer in blue copper proteins. *Coordin Chem Rev* 255, 757-773, (**2011**).

115   Lancaster, K. M. *et al*. Electron Transfer Reactivity of Type Zero Pseudomonas aeruginosa Azurin. *Journal of the American Chemical Society* 133, 4865-4873, (**2011**).

116   Lippert, E. C. v., T.L. The Strengths of Chemical Bonds. *Angewandte Chemie* 72, 602, (**1960**).

117   Roelfes, G. & Feringa, B. L. DNA-based asymmetric catalysis. *Angew Chem Int Edit* 44, 3230-3232, (**2005**).

118   Bos, J., Browne, W. R., Driessen, A. J. & Roelfes, G. Supramolecular Assembly of Artificial Metalloenzymes Based on the Dimeric Protein LmrR as Promiscuous Scaffold. *Journal of the American Chemical Society* 137, 9796-9799, (**2015**).

119   Drienovska, I. & Roelfes, G. Artificial Metalloenzymes for Asymmetric Catalysis by Creation of Novel Active Sites in Protein and DNA Scaffolds. *Isr J Chem* 55, 21-31, (**2015**).

120   Coquiere, D., Feringa, B. L. & Roelfes, G. DNA-Based catalytic enantioselective Michael reactions in water. *Angew Chem Int Edit* 46, 9308-9311, (**2007**).

121   Otto, S., Boccaletti, G. & Engberts, J. B. F. N. A chiral Lewis-acid-catalyzed Diels-Alder reaction. Water-enhanced enantioselectivity. *Journal of the American Chemical Society* 120, 4238-4239, (**1998**).

122   Otto, S. & Engberts, J. B. F. N. A systematic study of ligand effects on a Lewis-acid-catalyzed Diels-Alder reaction in water. Water-enhanced enantioselectivity. *Journal of the American Chemical Society* 121, 6798-6806, (**1999**).

123   Ward, T. R. *Topics in Organometallic Chemistry: Bio-inspired Catalysts*. (Springer-Verlag Berlin Heidelberg, **2009**).

124   Fujieda, N. *et al*. Enzyme repurposing of a hydrolase as an emergent peroxidase upon metal binding. *Chemical Science* 6, 4060-4065, (**2015**).

125   Solomon, E. I., Sundaram, U. M. & Machonkin, T. E. Multicopper oxidases and oxygenases. *Chem Rev* 96, 2563-2605, (**1996**).

126   Haring, D. & Distefano, M. D. Enzymes by design: Chemogenetic assembly of transamination active sites containing lysine residues for covalent catalysis. *Bioconjugate chemistry* 12, 385-390, (**2001**).

127   Creus, M. & Ward, T. R. Designed evolution of artificial metalloenzymes: protein catalysts made to order. *Organic & biomolecular chemistry* 5, 1835-1844, (**2007**).

128   Petrounia, I. P. & Arnold, F. H. Designed evolution of enzymatic properties. *Curr Opin Biotech* 11, 325-330, (**2000**).

129   Krieger, E., Darden, T., Nabuurs, S. B., Finkelstein, A. & Vriend, G. Making optimal use of empirical energy functions: Force-field parameterization in crystal space. *Proteins* 57, 678-683, (**2004**).

130   Wiederstein, M. & Sippl, M. J. ProSA-web: interactive web service for the recognition of errors in three-dimensional structures of proteins. *Nucleic Acids Res* 35, W407-W410, (**2007**).

131   Vriend, G. & Sander, C. Quality-Control of Protein Models - Directional Atomic Contact Analysis. *J Appl Crystallogr* 26, 47-60, (**1993**).

132   Morar, A. S., Schrimsher, J. R. L. & Chavez, M. D. PEGylation of proteins: A structural approach. *Biopharm Int* 19, 34-+, (**2006**).

133   Bos, J. & Roelfes, G. Artificial metalloenzymes for enantioselective catalysis. *Current opinion in chemical biology* 19, 135-143, (**2014**).

134   Kabsch, W. Xds. *Acta Crystallogr*. *D Biol*. *Crystallogr*. 66, 125-132, (**2010**).

135   Mccoy, A. J. *et al*. Phaser crystallographic software. *J Appl Crystallogr* 40, 658-674, (**2007**).

136   Murshudov, G. N., Vagin, A. A. & Dodson, E. J. Refinement of macromolecular structures by the maximum-likelihood method. *Acta Crystallogr D* 53, 240-255, (**1997**).

137   Laskowski, R. A., Macarthur, M. W., Moss, D. S. & Thornton, J. M. Procheck - a Program to Check the Stereochemical Quality of Protein Structures. *J Appl Crystallogr* 26, 283-291, (**1993**).

138   Trammell, S. A. *et al*. Synthesis and characterization of a ruthenium(II)-based redox conjugate for reagentless biosensing. *Bioconjugate chemistry* 12, 643-647, (**2001**).

139   Otto, S., Bertoncin, F. & Engberts, J. B. F. N. Lewis acid catalysis of a Diels-Alder reaction in water. *Journal of the American Chemical Society* 118, 7702-7707, (**1996**).

140   Otto, S., Engberts, J. B. F. N. & Kwak, J. C. T. Million-fold acceleration of a Diels-Alder reaction due to combined Lewis acid and micellar catalysis in water. *Journal of the American Chemical Society* 120, 9517-9525, (**1998**).

141   Meijer, A., Otto, S. & Engberts, J. B. F. N. Effects of the hydrophobicity of the reactants on Diels-Alder reactions in water. *J Org Chem* 63, 8989-8994, (**1998**).

APPENDIX

1. MOLECULAR BIOLOGY

```
>mTFP1    711 bp              (GenBank: DQ676819)
ATGGTGAGCAAGGGCGAGGAGACCACAATGGGCGTAATCAAGCCCGACATGAAGATCAAG
CTGAAGATGGAGGGCAACGTGAATGGCCACGCCTTCGTGATCGAGGGCGAGGGCGAGGGC
AAGCCCTACGACGGCACCAACACCATCAACCTGGAGGTGAAGGAGGGAGCCCCCCTGCCC
TTCTCCTACGACATTCTGACCACCGCGTTCGCCTACGGCAACAGGGCCTTCACCAAGTAC
CCCGACGACATCCCCAACTACTTCAAGCAGTCCTTCCCCGAGGGCTACTCTTGGGAGCGC
ACCATGACCTTCGAGGACAAGGGCATCGTGAAGGTGAAGTCCGACATCTCCATGGAGGAG
GACTCCTTCATCTACGAGATACACCTCAAGGGCGAGAACTTCCCCCCCAACGGCCCCGTG
ATGCAGAAGAAGACCACCGGCTGGGACGCCTCCACCGAGAGGATGTACGTGCGCGACGGC
GTGCTGAAGGGCGACGTCAAGCACAAGCTGCTGCTGGAGGGCGGCGGCCACCACCGCGTT
GACTTCAAGACCATCTACAGGGCCAAGAAGGCGGTGAAGCTGCCCGACTATCACTTTGTG
GACCACCGCATCGAGATCCTGAACCACGACAAGGACTACAACAAGGTGACCGTTTACGAG
AGCGCCGTGGCCCGCAACTCCACCGACGGCATGGACGAGCTGTACAAGTAA
```

Figure S 1 Sequence mTFP1 (deleted nucleotides)

```
mTFP1     ATGGTGAGCAAGGGCGAGGAGACCACAATGGGCGTAATCAAGCCCGACATGAAGATCAAG 60
mTFP1.1   ------------------------------GGCGTAATCAAGCCCGACATGAAGATCAAG 30
                                        ****************************
mTFP1     CTGAAGATGGAGGGCAACGTGAATGGCCACGCCTTCGTGATCGAGGGCGAGGGCGAGGGC 120
mTFP1.1   CTGAAGATGGAGGGCAACGTGAATGGCCACGCCTTCGTGATCGAGGGCGAGGGCGAGGGC 90
          ************************************************************
mTFP1     AAGCCCTACGACGGCACCAACACCATCAACCTGGAGGTGAAGGAGGGGAGCCCCCCTGCCC 180
mTFP1.1   AAGCCCTACGACGGCACCAACACCATCAACCTGGAGGTGAAGGAGGGGAGCCCCCCTGCCC 150
          ************************************************************
mTFP1     TTCTCCTACGACATTCTGACCACCGCGTTCGCCTACGGCAACAGGGCCTTCACCAAGTAC 240
mTFP1.1   TTCTCCTACGACATTCTGACCACCGCGTTCGCCTACGGCAACAGGGCCTTCACCAAGTAC 210
          ************************************************************
mTFP1     CCCGACGACATCCCCAACTACTTCAAGCAGTCCTTCCCCGAGGGCTACTCTTGGGAGCGC 300
mTFP1.1   CCCGACGACATCCCCAACTACTTCAAGCAGTCCTTCCCCGAGGGCTACTCTTGGGAGCGC 270
          ************************************************************
mTFP1     ACCATGACCTTCGAGGACAAGGGCATCGTGAAGGTGAAGTCCGACATCTCCATGGAGGAG 360
mTFP1.1   ACCATGACCTTCGAGGACAAGGGCATCGTGAAGGTGAAGTCCGACATCTCCATGGAGGAG 330
          ************************************************************
mTFP1     GACTCCTTCATCTACGAGATACACCTCAAGGGCGAGAACTTCCCCCCCAACGGCCCCGTG 420
mTFP1.1   GACTCCTTCATCTACGAGATACACCTCAAGGGCGAGAACTTCCCCCCCAACGGCCCCGTG 390
          ************************************************************
mTFP1     ATGCAGAAGAAGACCACCGGCTGGGACGCCTCCACCGAGAGGATGTACGTGCGCGACGGC 480
mTFP1.1   ATGCAGAAGAAGACCACCGGCTGGGACGCCTCCACCGAGAGGATGTACGTGCGCGACGGC 450
          ************************************************************
mTFP1     GTGCTGAAGGGCGACGTCAAGCACAAGCTGCTGCTGGAGGGCGGCGGCCACCACCGCGTT 540
mTFP1.1   GTGCTGAAGGGCGACGTCAAGCACAAGCTGCTGCTGGAGGGCGGCGGCCACCACCGCGTT 510
          ************************************************************
mTFP1     GACTTCAAGACCATCTACAGGGCCAAGAAGGCGGTGAAGCTGCCCGACTATCACTTTGTG 600
mTFP1.1   GACTTCAAGACCATCTACAGGGCCAAGAAGGCGGTGAAGCTGCCCGACTATCACTTTGTG 570
          ************************************************************
mTFP1     GACCACCGCATCGAGATCCTGAACCACGACAAGGACTACAACAAGGTGACCGTTTACGAG 660
mTFP1.1   GACCACCGCATCGAGATCCTGAACCACGACAAGGACTACAACAAGGTGACCGTTTACGAG 630
          ************************************************************
mTFP1     AGCGCCGTGGCCCGCAACTCCACCGACGGCATGGACGAGCTGTACAAGTAA         711
mTFP1.1   AGCGCCGTGGCCCGCAACTCCACCGACTAA--------------------         660
          ***************************...
```

Figure S 2 Sequence Alignment mTFP1, mTFP1.1

```
mTFP1.1    GGCGTAATCAAGCCCGACATGAAGATCAAGCTGAAGATGGAGGGCAACGTGAATGGCCAC 60
mTFP*      GGCGTAATCAAGCCCGACATGAAGATCAAGCTGAAGATGGAGGGCAACGTGAATGGCTAT 60
           ******************************************************* *
mTFP1.1    GCCTTCGTGATCGAGGGCGAGGGCGAGGGCAAGCCCTACGACGGCACCAACACCATCAAC 120
mTFP*      GCCTTCGTGATCGAGGGCGAGGGCGAGGGCAAGCCCTACGACGGCACCAACACCATCAAC 120
           ************************************************************
mTFP1.1    CTGGAGGTGAAGGAGGGAGCCCCCCTGCCCTTCTCCTACGACATTCTGACCACCGCGTTC 180
mTFP*      CTGGAGGTGAAGGAGGGAGCCCCCCTGCCCTTCTCCTACGACATTCTGACCACCGCGTTC 180
           ************************************************************
mTFP1.1    GCCTACGGCAACAGGGCCTTCACCAAGTACCCCGACGACATCCCCAACTACTTCAAGCAG 240
mTFP*      GCCTACGGCAACAGGGCCTTCACCAAGTACCCCGACGACATCCCCAACTACTTCAAGCAG 240
           ************************************************************
mTFP1.1    TCCTTCCCCGAGGGCTACTCTTGGGAGCGCACCATGACCTTCGAGGACAAGGGCATCGTG 300
mTFP*      TCCTTCCCCGAGGGCTACTCTTGGGAGCGCACCATGACCTTCGAGGACAAGGGCATCGTG 300
           ************************************************************
mTFP1.1    AAGGTGAAGTCCGACATCTCCATGGAGGAGGACTCCTTCATCTACGAGATACACCTCAAG 360
mTFP*      AAGGTGAAGTCCGACATCTCCCTGGAGGAGGACTCCTTCATCTACGAGATATATCTCAAG 360
           *********************.**************************** * ******
mTFP1.1    GGCGAGAACTTCCCCCCCAACGGCCCCGTGATGCAGAAGAAGACCACCGGCTGGGACGCC 420
mTFP*      GGCGAGAACTTCCCCCCCAACGGCCCCGTGATGCAGAAGAAGACCACCGGCTGGGACGCC 420
           ************************************************************
mTFP1.1    TCCACCGAGAGGATGTACGTGCGCGACGGCGTGCTGAAGGGCGACGTCAAGCACAAGCTG 480
mTFP*      TCCACCGAGAGGATGTACGTGCGCGACGGCGTGCTGAAGGGCGACGTCAAGCACAAGCTG 480
           ************************************************************
mTFP1.1    CTGCTGGAGGGCGGCGGCCACCACCGCGTTGACTTCAAGACCATCTACAGGGCCAAGAAG 540
mTFP*      CTGCTGGAGGGCGGCGGCTATTATCGCGTTGACTTCAAGACCATCTACAGGGCCAAGAAG 540
           ****************** *  * **********************************
mTFP1.1    GCGGTGAAGCTGCCCGACTATCACTTTGTGGACCACCGCATCGAGATCCTGAACCACGAC 600
mTFP*      GCGGTGAAGCTGCCCGACTATCACTTTGTGGACCACCGCATCGAGATCCTGAACTATGAC 600
           ***************************************************** * ***
mTFP1.1    AAGGACTACAACAAGGTGACCGTTTACGAGAGCGCCGTGGCCCGCAACTCCACCGACTAA 660
mTFP*      AAGGACTACAACAAGGTGACCGTTTACGAGAGCGCCGTGGCCCGCAACTCCACCGACTAA 660
           ************************************************************
```

Figure S 3 Sequence Alignment mTFP1.1; mTFP*

MUTATION (mTFP1 to mTFP*)	POSITION (2HQK)	PRIMER
H30Y	H25	5'-GGGCAACGTGAATGGCTATGCCTTCGTGATCGAGG-3' 5'-CCTCGATCACGAAGGCATAGCCATTCACGTTGCCC-3'
M118L	M113	5'-AGTCCGACATCTCCTTGGAGGAGGACTCC-3' 5'-GGAGTCCTCCTCCAAGGAGATGTCGGACT-3'
H128Y	H123	5'-CTCCTTCATCTACGAGATATATCTCAAGGGCGAGAACTTC-3' 5'-GAAGTTCTCGCCCTTGAGATATATCTCGTAGATGAAGGAG-3'
H177Y, H178Y	H172, H173	5'-TGCTGGAGGGCGGCGGCTATTATCGCGTTGACTTCAAGAC-3' 5'-GTCTTGAAGTCAACGCGATAATAGCCGCCGCCCTCCAGCA-3'
H209Y	H204	5'-CCGCATCGAGATCCTGAACTATGACAAGGACTACAACAAGG-3' 5'-CCTTGTTGTAGTCCTTGTCATAGTTCAGGATCTCGATGCGG-3'

Table S 1 Oligonucleotides to establish mTFP*

```
mTFP1    MVSKGEETTMGVIKPDMKIKLKMEGNVNGHAFVIEGEGEGKPYDGTNTINLEVKEGAPLP
2HQK     ----------GVIKPDMKIKLKMEGNVNGHAFVIEGEGEGKPYDGTNTINLEVKEGAPLP
mTFP*    ---------SGVIKPDMKIKLKMEGNVNGYAFVIEGEGEGKPYDGTNTINLEVKEGAPLP
                   *******************:****************************


mTFP1    FSYDILTTAFAYGNRAFTKYPDDIPNYFKQSFPEGYSWERTMTFEDKGIVKVKSDISMEE
2HQK     FSYDILTTAFAYGNRAFTKYPDDIPNYFKQSFPEGYSWERTMTFEDKGIVKVKSDISMEE
mTFP*    FSYDILTTAFAYGNRAFTKYPDDIPNYFKQSFPEGYSWERTMTFEDKGIVKVKSDISLEE
         ********************************************************:**


mTFP1    DSFIYEIHLKGENFPPNGPVMQKKTTGWDASTERMYVRDGVLKGDVKHKLLLEGGGHHRV
2HQK     DSFIYEIHLKGENFPPNGPVMQKKTTGWDASTERMYVRDGVLKGDVKHKLLLEGGGHHRV
mTFP*    DSFIYEIYLKGENFPPNGPVMQKKTTGWDASTERMYVRDGVLKGDVKHKLLLEGGGYYRV
         *******:*****************************************:**


mTFP1    DFKTIYRAKKAVKLPDYHFVDHRIEILNHDKDYNKVTVYESAVARNSTDGMDELYK
2HQK     DFKTIYRAKKAVKLPDYHFVDHRIEILNHDKDYNKVTVYESAVARNSTDGM-----
mTFP*    DFKTIYRAKKAVKLPDYHFVDHRIEILNYDKDYNKVTVYESAVARNSTD-------
         ***************************:*******************
```

Figure S 4 Alignment: mTFP1, PDB:2HQK and mTFP* show different amino acid constitution
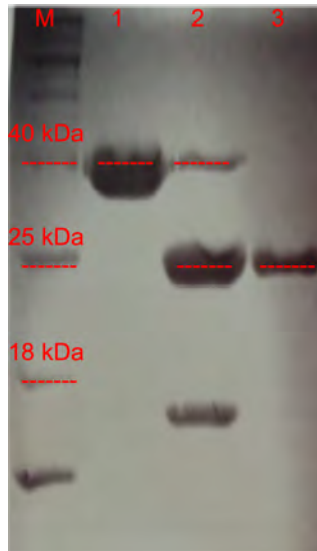
Figure S 5 SDS PAGE: Fractions of SUMO conjugated mTFP* are obtained through affinity chromatography (1), digestions (2) and further purification yields in pure fractions of mTFP* (3)

MUTANT	MUTATION	PRIMER
mbYDCHH	I197C, Y200H	5'-TGGACCACCGCATCGAGTGCCTGAACCATGACAAGGACTACAAC-3' 5'-GTTGTAGTCCTTGTCATGGTTCAGGCACTCGATGCGGTGGTCCA-3'
mbYDCHH	Y204H	5'-CTGAACTATGACAAGGACCACAACAAGGTGACCGTTT-3' 5'-AAACGGTCACCTTGTTGTGGTCCTTGTCATAGTTCAG-3'
mbYDEHH	E197	5'-TGGACCACCGCATCGAGGAGCTGAACCATGACAAGGAC-3' 5'-GTCCTTGTCATGGTTCAGCTCCTCGATGCGGTGGTCCA-3'
mbYCIHH	C55	5'-CCTGCCCTTCTCCTACTGCATTCTGACCACCGCG-3' 5'-CGCGGTGGTCAGAATGCAGTAGGAGAAGGGCAGG-3'
mbYEIHH	E55	5'-CCCTTCTCCTACGAGATTCTGACCACCGC-3' 5'-GCGGTGGTCAGAATCTCGTAGGAGAAGGG-3'
mbYHIHH	H55	5'-CTGCCCTTCTCCTACCACATTCTGACCACCG-3' 5'-CGGTGGTCAGAATGTGGTAGGAGAAGGGCAG-3'
mbYMIHH	M55	5'-CCCTGCCCTTCTCCTACATGATTCTGACCACCGCGTT-3' 5'-AACGCGGTGGTCAGAATCATGTAGGAGAAGGGCAGGG-3'
mbCYIHH	C54	5'-CCCTGCCCTTCTCCTGCGACATTCTGACC-3' 5'-GGTCAGAATGTCGCAGGAGAAGGGCAGGG-3'
mbDYIHH	D54	5'-CCCTGCCCTTCTCCGACGACATTCTGACC-3' 5'-GGTCAGAATGTCGTCGGAGAAGGGCAGGG-3'
mbHYIHH	H54	5'-CCCTGCCCTTCTCCCACGACATTCTGACC-3' 5'-GGTCAGAATGTCGTGGGAGAAGGGCAGGG-3'
mbMYIHH	M54	5'-CCCCCTGCCCTTCTCCATGGACATTCTGACCACCG-3' 5'-CGGTGGTCAGAATGTCCATGGAGAAGGGCAGGGGG-3'
mbYDIHH	I197	5'-GGACCACCGCATCGAGATCCTGAACCATGACAAG-3' 5'-CTTGTCATGGTTCAGGATCTCGATGCGGTGGTCC-3'
mbYEQHH	Q197	5'-TGGACCACCGCATCGAGCAGCTGAACCATGACAAGGAC-3' 5'-GTCCTTGTCATGGTTCAGCTGCTCGATGCGGTGGTCCA-3'
mbYDIHC	H200, C204	5'-ATCGAGATCCTGAACCACGACAAGGACTGCAACAAGGTGACCGTTT-3' 5'-AAACGGTCACCTTGTTGCAGTCCTTGTCGTGGTTCAGGATCTCGAT-3'
mbYDIMH	M200, H204	5'-CCGCATCGAGATCCTGAACATGGACAAGGACCACAACAAGG-3' 5'-CCTTGTTGTGGTCCTTGTCCATGTTCAGGATCTCGATGCGG-3'
mbYDIMC	M200, C204	5'-ACCGCATCGAGATCCTGAACATGGACAAGGACTGCAACAAGGTGAC CGTTTACG-3' 5'-CGTAAACGGTCACCTTGTTGCAGTCCTTGTCCATGTTCAGGATCTCGA TGCGGT-3'
mTFP*C164	C164	5'-GCACAAGCTGCTGCTGTGCGGCGGCGGCTATTATC-3' 5'-GATAATAGCCGCCGCCGCACAGCAGCAGCTTGTGC-3'
mTFP*C204	C204	5'-CTGAACTATGACAAGGACTGCAACAAGGTGACCGTTTAC-3' 5'-GTAAACGGTCACCTTGTTGCAGTCCTTGTCATAGTTCAG-3'
mbYDCHH[e]	A135, S137	5'-CCGTGATGCAGAAGGCGAGCACCGGCTGGGACG-3' 5'-CGTCCCAGCCGGTGCTCGCCTTCTGCATCACGG-3'
	G164, K165	5'-GCACAAGCTGCTGCTGGGGAAGGGCGGCTATTATCGCGT-3' 5'-ACGCGATAATAGCCGCCCTTCCCCAGCAGCAGCTTGTGC-3'
	Y199, K201, Y202	5'-GGACCACCGCATCGAGTGCCTGTATCATAAGTATGACCACAACAAGG TGACCGTTT-3' 5'-AAACGGTCACCTTGTTGTGGTCATACTTATGATACAGGCACTCGATGC GGTGGTCC-3'
mbXXXHH[e]	Y197, Y199, K201, Y202	5'-ATCACTTTGTGGACCACCGCATCGAGTATCTGTATCATAAGTATGACC ACAACAAGGTGACCGTTTACGAG-3' 5'-CTCGTAAACGGTCACCTTGTTGTGGTCATACTTATGATACAGATACTC GATGCGGTGGTCCACAAAGTGAT-3'

Table S 2 Oligonucleotides to establish mutants of mTFP*

2. FLUORESENCE QUENCHING STUDIES
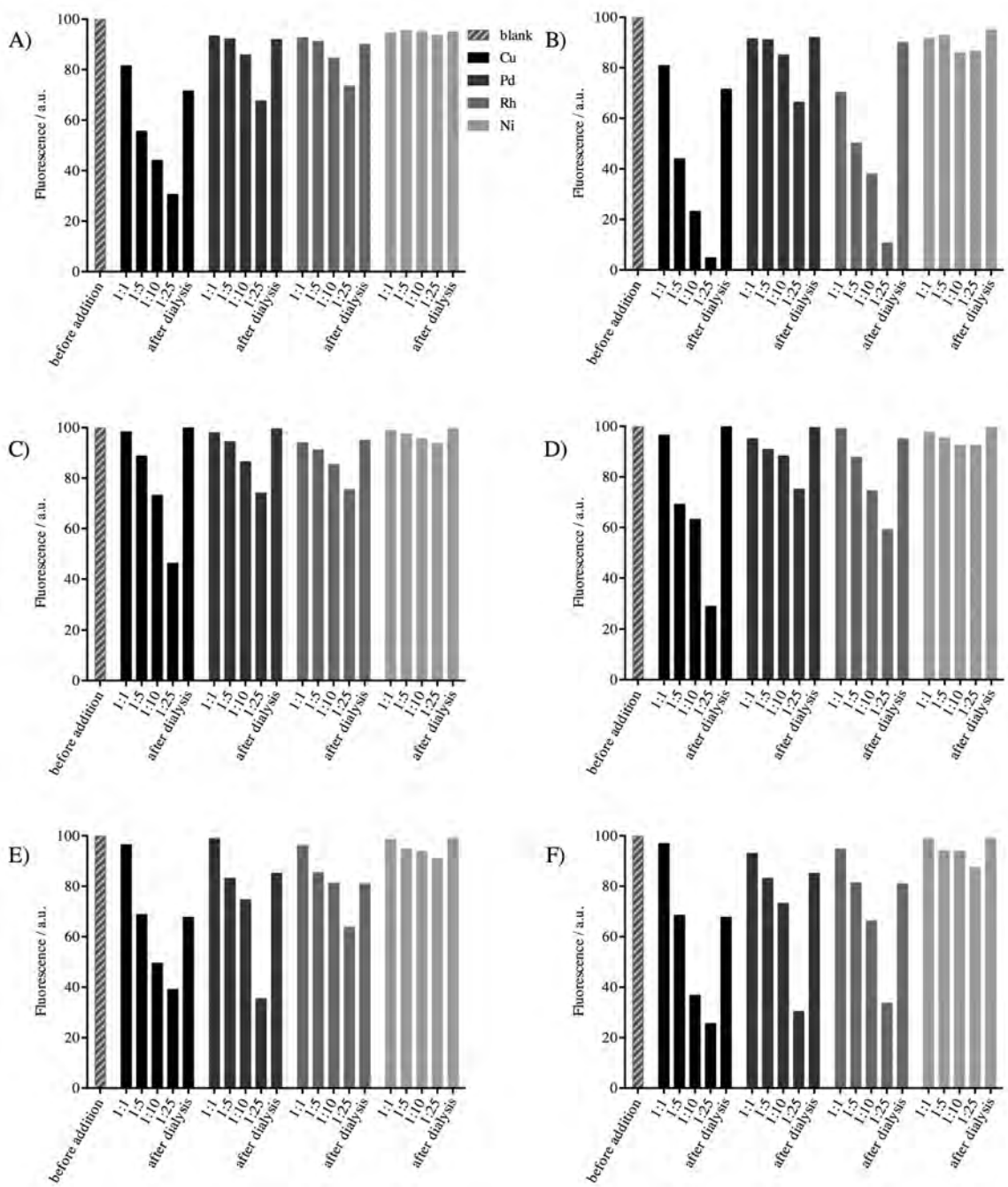
Figure S 6 Metal Affinity Screen: mTFP1 (A,B), mTFP* (C,D), mbYDCHH (E,F); Measurements A, C, D were performed immediately, B, D, F were performed 1 hour after metal addition; metal salts were added from 1M Stock solutions; concentrations varied from 1 to 25 eq. respective protein; all measurements were performed at room temperature.

3. MASS SPECTROMETRY DATA
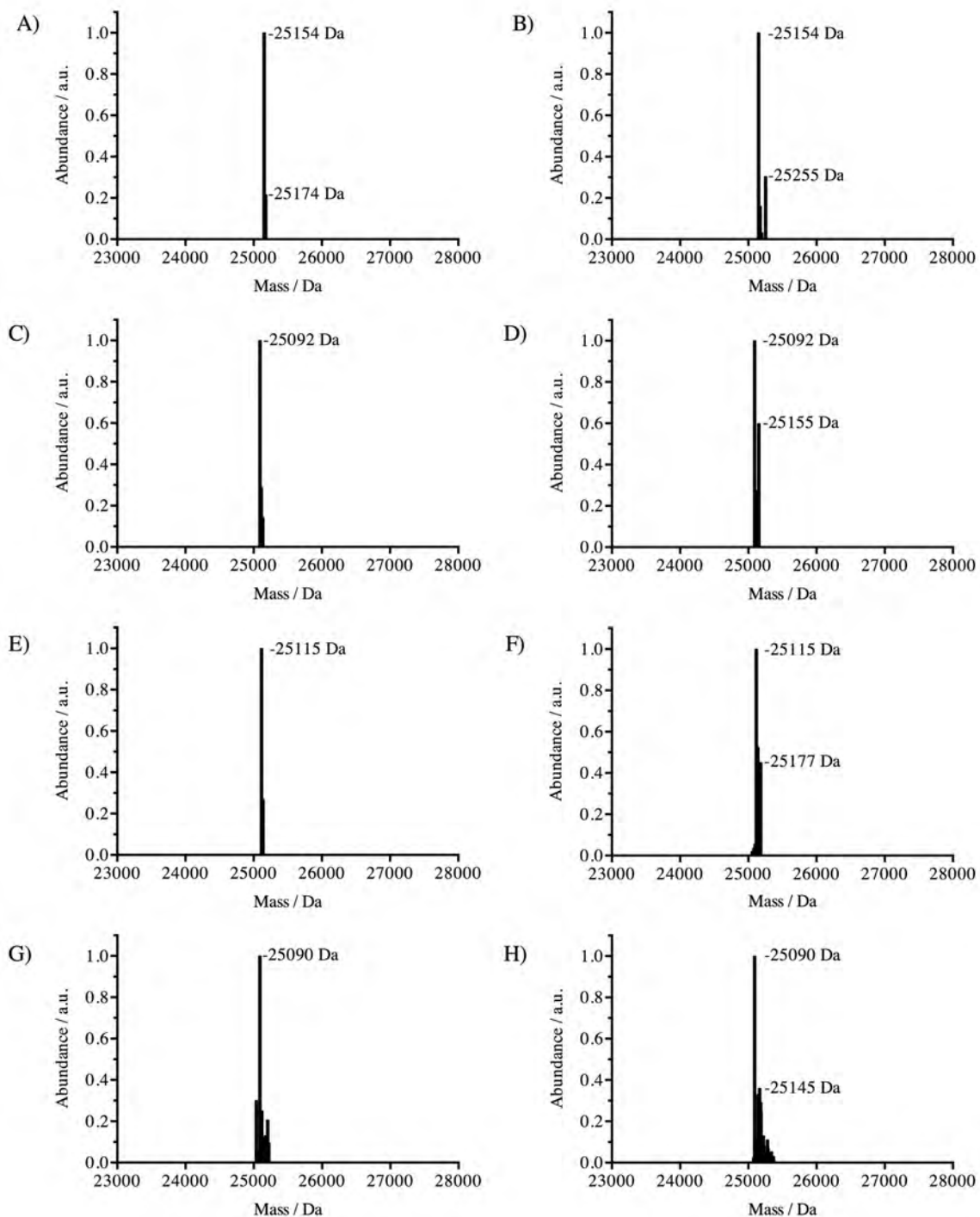
Figure S 7 ESI-TOF Mass Spectrometry Data: A) mTFP*; B) mTFP* soaked with 25eq. of PdCl$_2$, after dialyses spectra A is obtained again; C, D) mbYDCHH ± Cu(NO$_3$)$_2$, results indicate Metal conjugation; E, F) mbYDEHH ± Cu(NO$_3$)$_2$, results indicate Metal conjugation; G, H) mbYCIHH ± Cu(NO$_3$)$_2$, results indicate Metal conjugation;
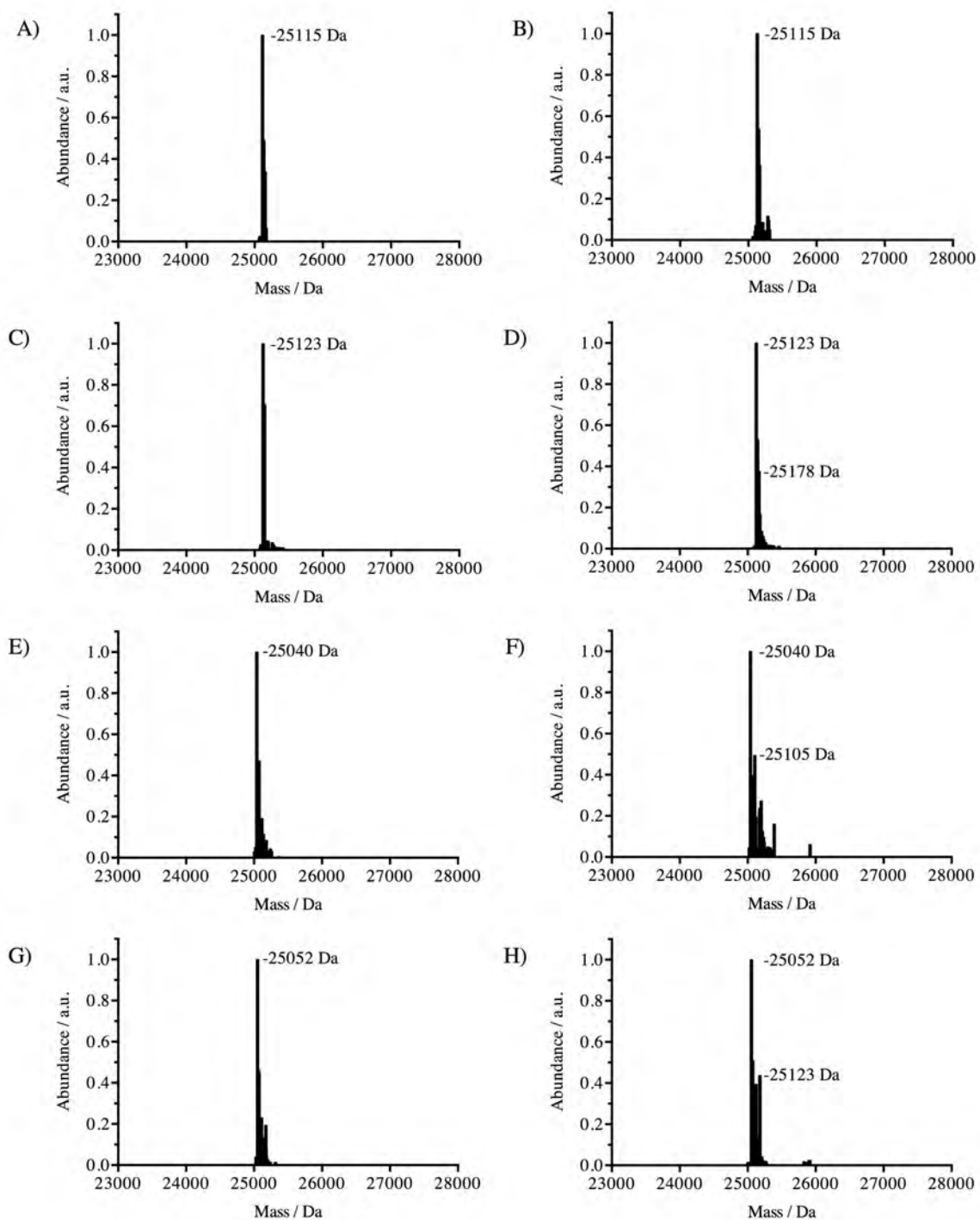
Figure S 8 ESI-TOF Mass Spectrometry Data: A, B) mbYEIHH ± Cu(NO$_3$)$_2$, results don't indicate Metal conjugation; C, D) mbYHIHH ± Cu(NO$_3$)$_2$, results indicate Metal conjugation; E, F) mbCDIHH ± Cu(NO$_3$)$_2$, results indicate Metal conjugation; G, H) mbDDIHH ± Cu(NO$_3$)$_2$, results indicate Metal conjugation;
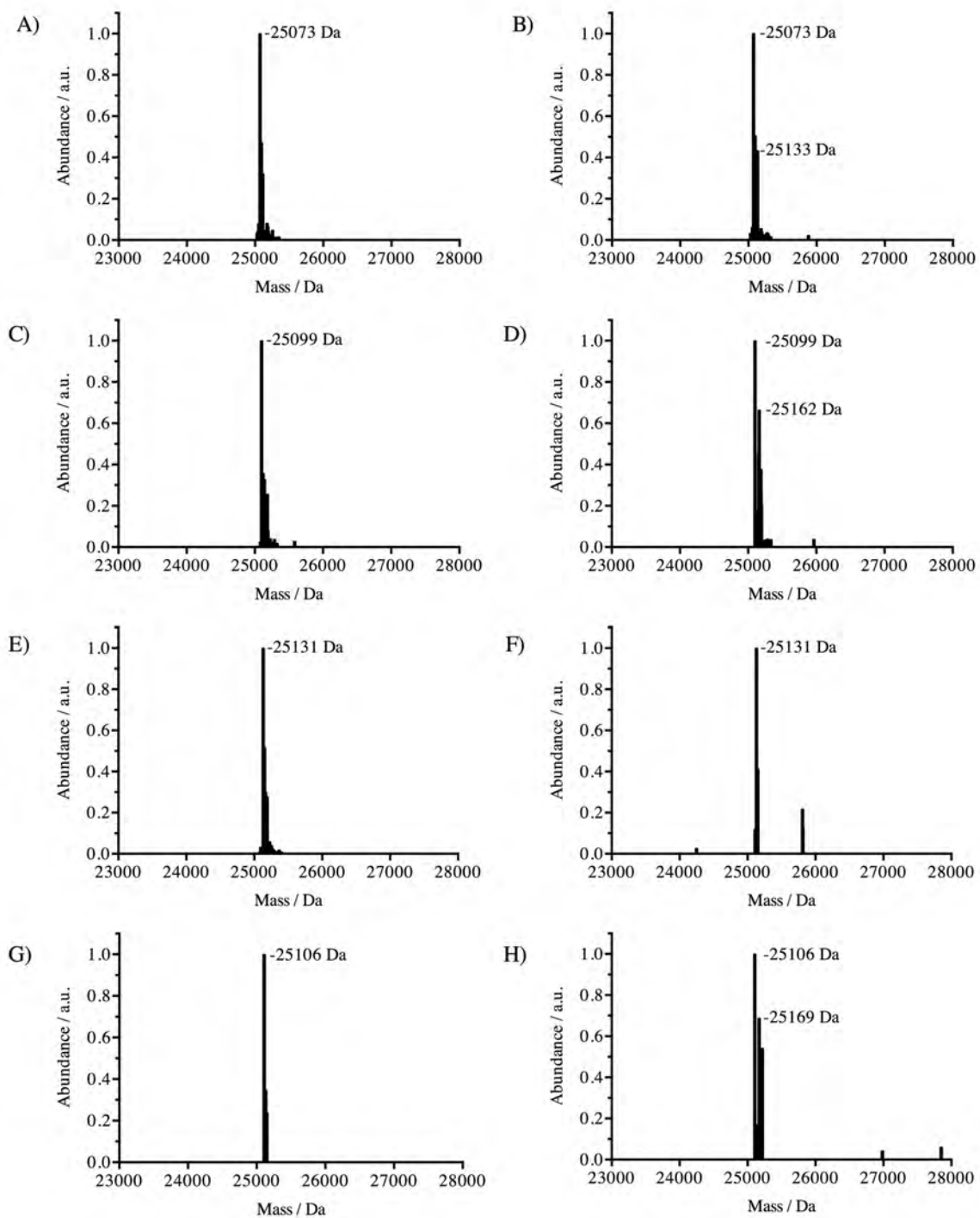
Figure S 9 ESI-TOF Mass Spectrometry Data: A, B) mbHDIHH ± Cu(NO$_3$)$_2$, results indicate Metal conjugation; C, D) mbYDIHH ± Cu(NO$_3$)$_2$, results indicate Metal conjugation; E, F) mbYEQHH ± Cu(NO$_3$)$_2$, results don't indicate Metal conjugation; G, H) mbYECHH ± Cu(NO$_3$)$_2$, results indicate Metal conjugation;
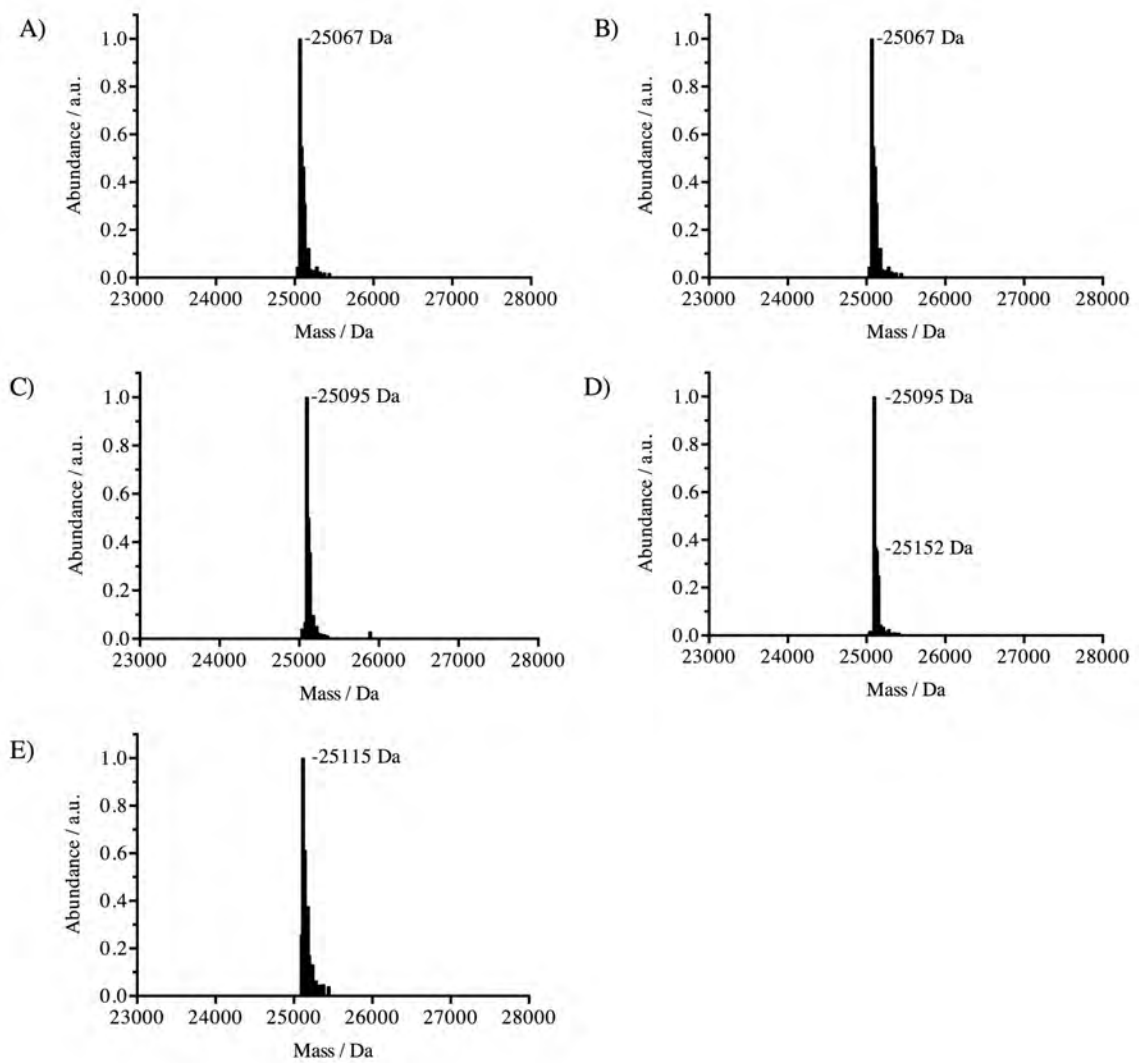
Figure S 10 ESI-TOF Mass Spectrometry Data: A, B) mbYDIHC ± Cu(NO$_3$)$_2$, results don't indicate Metal conjugation; C, D) mbYDIMH ± Cu(NO$_3$)$_2$, results indicate Metal conjugation; E) mbYDCHH^e
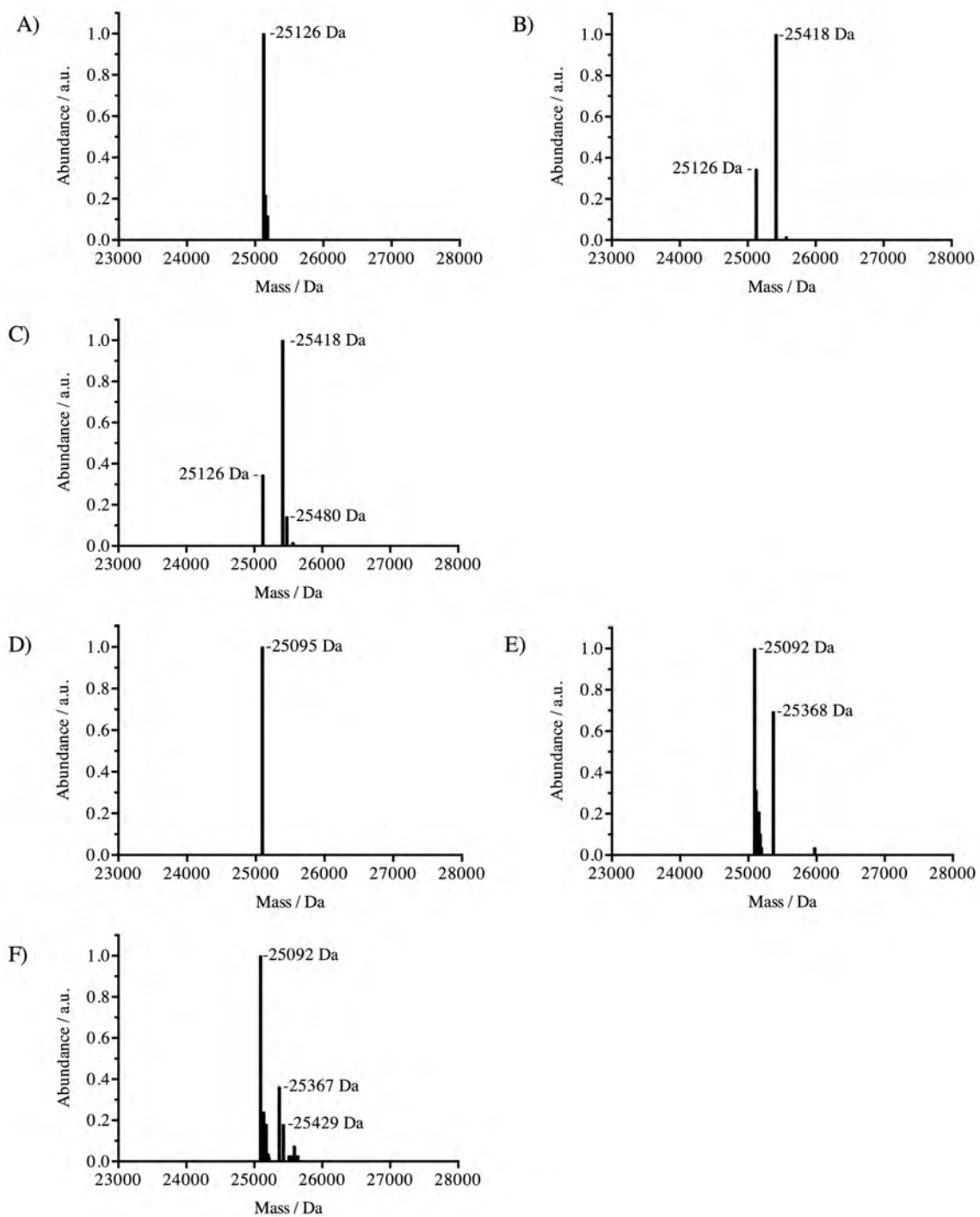
Figure S 11 ESI-TOF Mass Spectrometry Data: A) mTFP*C164; B) mTFP*C164_phenthroline; C)mTFP*C164_phenthroline_Cu – A, B, C indicate successful conjugation with phenthroline and Copper. D) mTFP*C204; E) mTFP*C204_phenthroline; F) mTFP*C204_phenthroline_Cu – D, E, F indicate successful conjugation with phenthroline and Copper.

4. SPECTROSCOPY
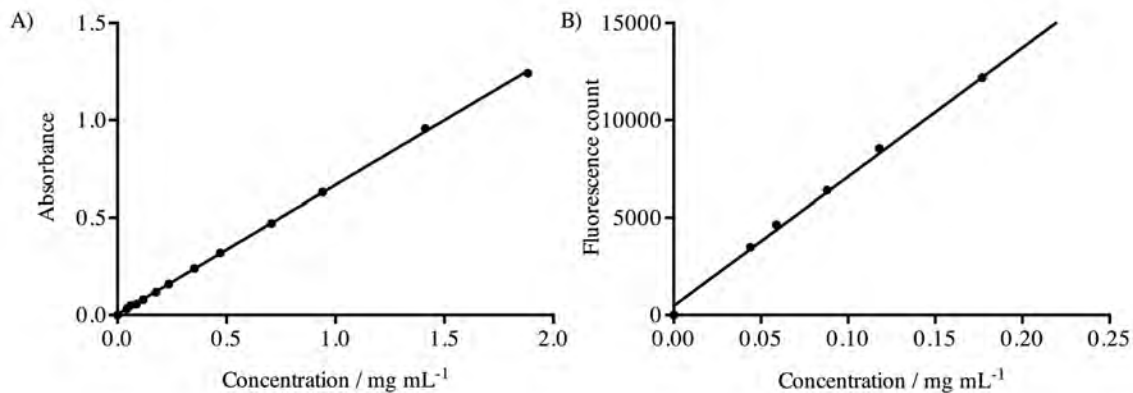
Figure S 12 Absorbance and Fluorescence of mTFP*: Absorbance at 468 nm and Fluorescence emission at 495 nm are suitable to determine concentrations of mTFP*
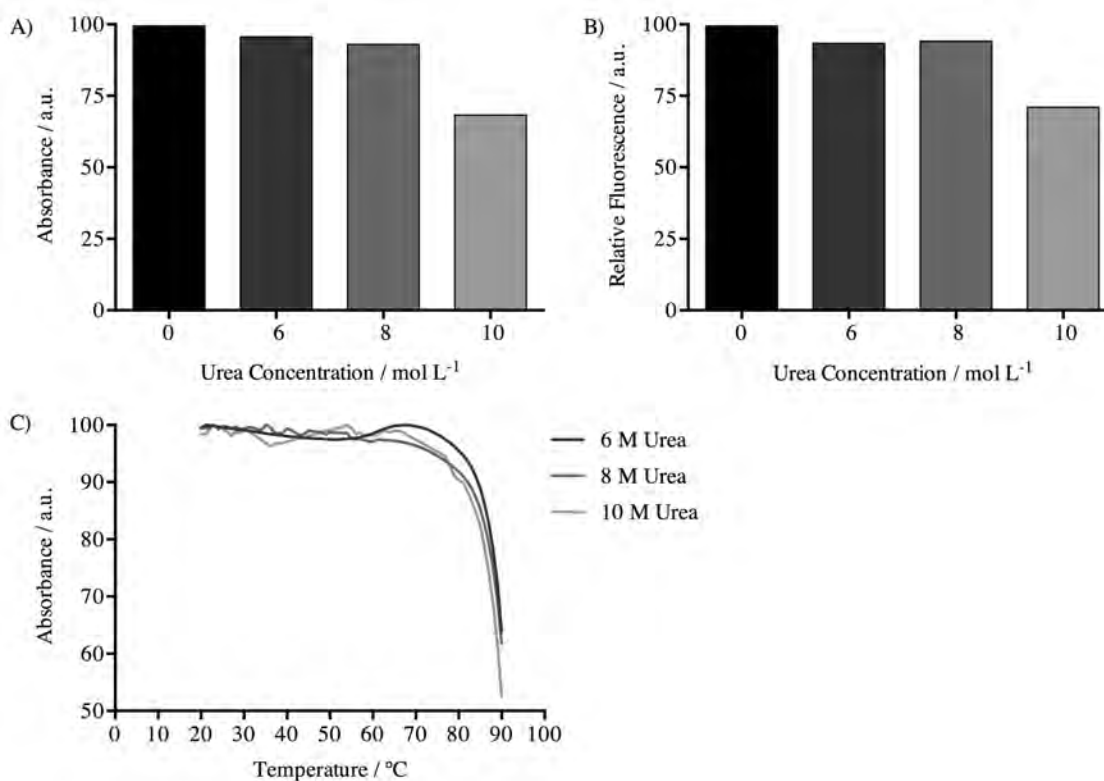
Figure S 13 Salt Stability: 0.04 mM mTFP* dissolved in 50 mM Tris/HCl pH 7.4 are supplemented with 6, 8 and 10 M UREA. No significant signal change for absorption und fluorescence measurements indicate structural perturbation until 80 °C
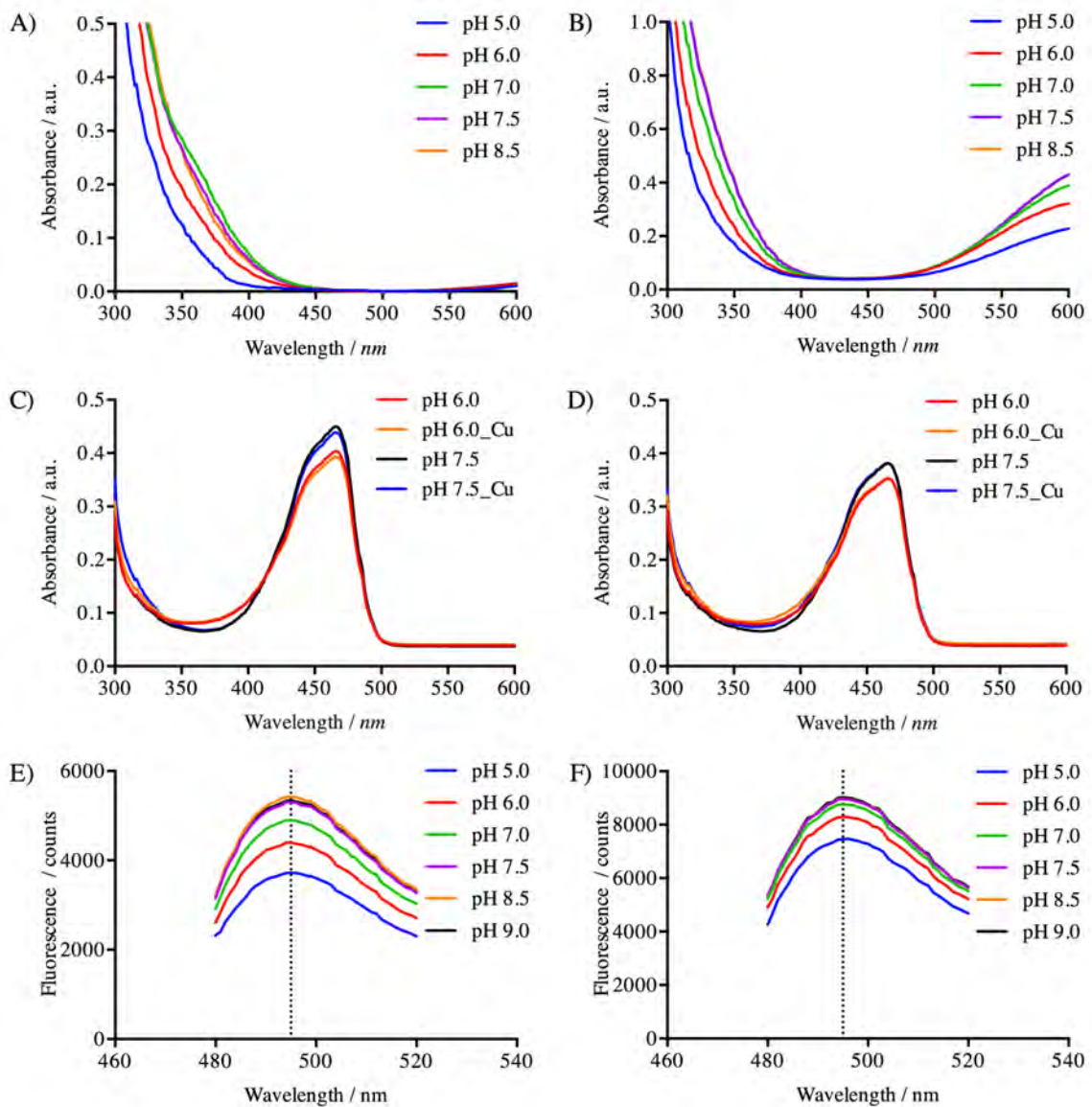
Figure S 14 Absorbance and Fluorescence Analysis: A) pH dependent Copper absorbance (50 μM Copper(II)Nitrate); B) pH dependent absorbance of Copper(II)Nitrate and 2 eq. Histidine; C) pH dependent absorbance of mTFP* ± 4 eq. Copper(II)Nitrate; D) pH dependent absorbance of mbYDCHH ± 4 eq. Copper(II)Nitrate; E) pH dependent fluorescence of mTFP*; D) pH dependent fluorescence of mbYDCHH; data indicates no significant influence of pH on Copper(II)Nitrate interaction with mTFP* derived host proteins.
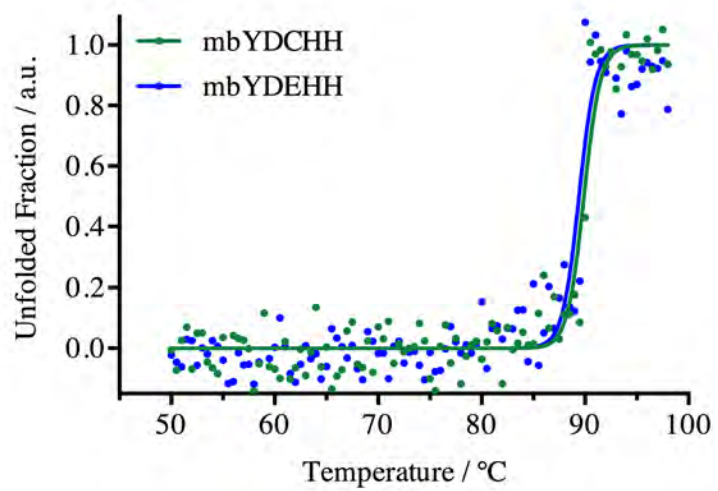
Figure S 15 Temperature Stability: Circular Dichroism indicates similar stability of mbYDCHH and mbYDEHH

5. TRANSITION METAL FRET DATA
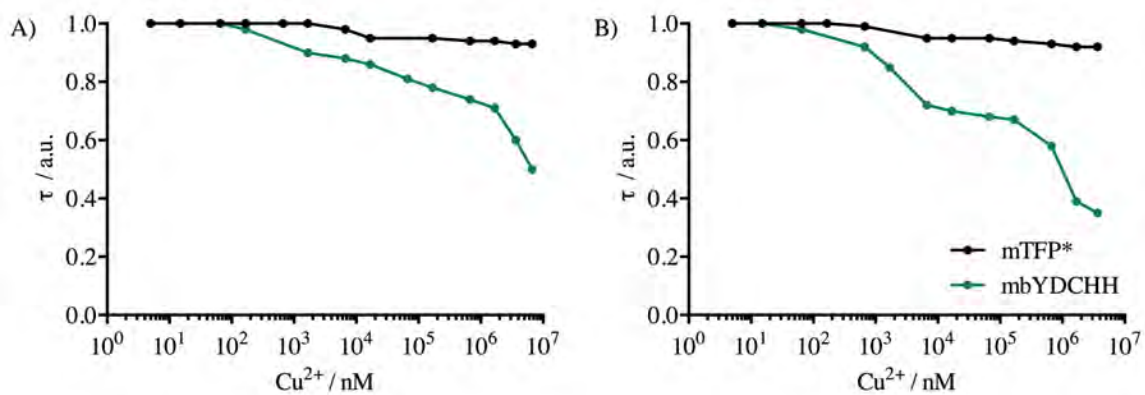
Figure S 16 Fluorescent Lifetimes: mTFP* and mbYDCHH at pH 6.0 (A) and pH 7.5 (B)

Mutant	Metal	pH	K_dStat (mM)	K_dDyn (μM)	E	R (nm)	R_0 (nm)
mTFP1	Cu	6.0	8.46	324 / 0.01	-	-	-
		7.5	0.89	269 / 2.14	-	-	-
mTFP*	Cu	6.0	8.46	-	-	-	-
		7.5	0.89	-	-	-	-
mbYDCHH	Cu	6.0	8.46	1.18	0.56	1.39	1.34
		7.5	0.89	0.97	0.19	1.17	1.48
mbYDCHH	Zn	6.0	8.46	4.04	0.56	1.39	1.34
		7.5	0.89	128.34	0.19	1.17	1.48
mbYDEHH	Cu	6.0	8.46	8.86	0.25	1.11	1.33
		7.5	0.89	5.22	0.33	1.18	1.33
mTFP*C204_phen	Cu	6.0	8.46	5.28	0.27	2.08	2.45
		7.5	0.89	2.52	0.25	2.04	2.45

Table S 3 tmFRET Data Overview
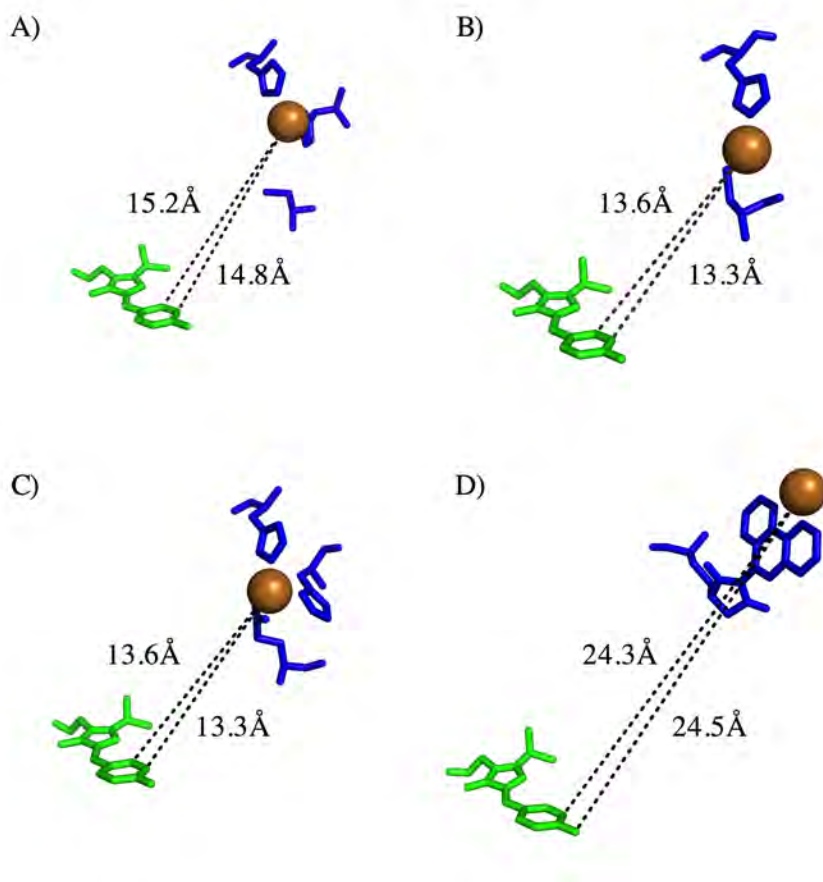
Figure S 17 Förster Radius Estimations: A) mbYDCHH_Cu; B) mbYDCHH_open_Cu; C) mbYDEHH_Cu; D) mTFP*C204_phen_Cu; Closest distances between transition metal and chromophore are indicated. Förster Radii are approximated accordingly. Distances in A derived from crystal structure; Distances in B-D derived from Model.

6. X-RAY DATA
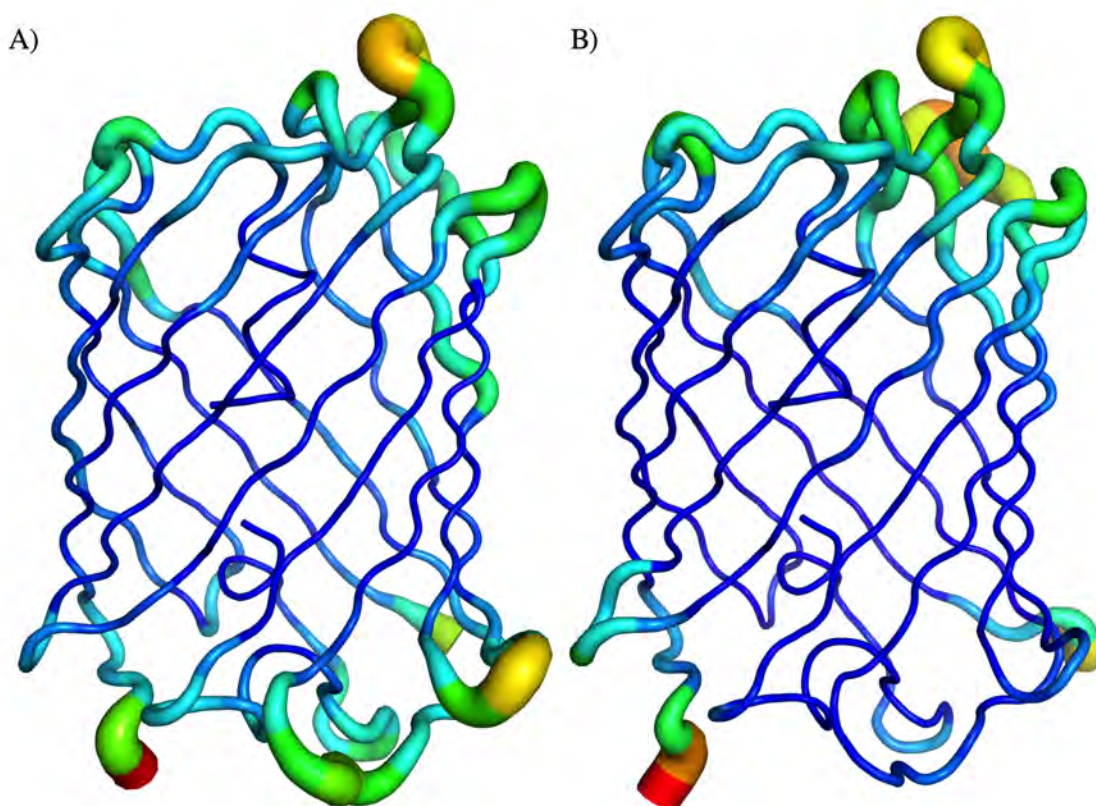
Figure S 18 B-Factor Plot: mTFP1 (PDB:2HQK) (A) and mTFP* (B) shows similarity of thermal movement

Pd	Ligand Constitution			
Pd901	K121	K102	E123	
Pd902	D7	K32	Cl913	
Pd903	E43	K45	-	
Pd904	K104$^{\Phi}$	K135	E164	
Pd905	E15	K13	E117	K202$^{\Phi}$
Pd906	E28	K154$^{\Phi}$		
Pd907	K11$^{\Phi}$	D150	Cl914	

Table S 4 Palladium Coordination Motifs PDB: 4Q9X ($^{\Phi}$denotes residues from pairing molecule)
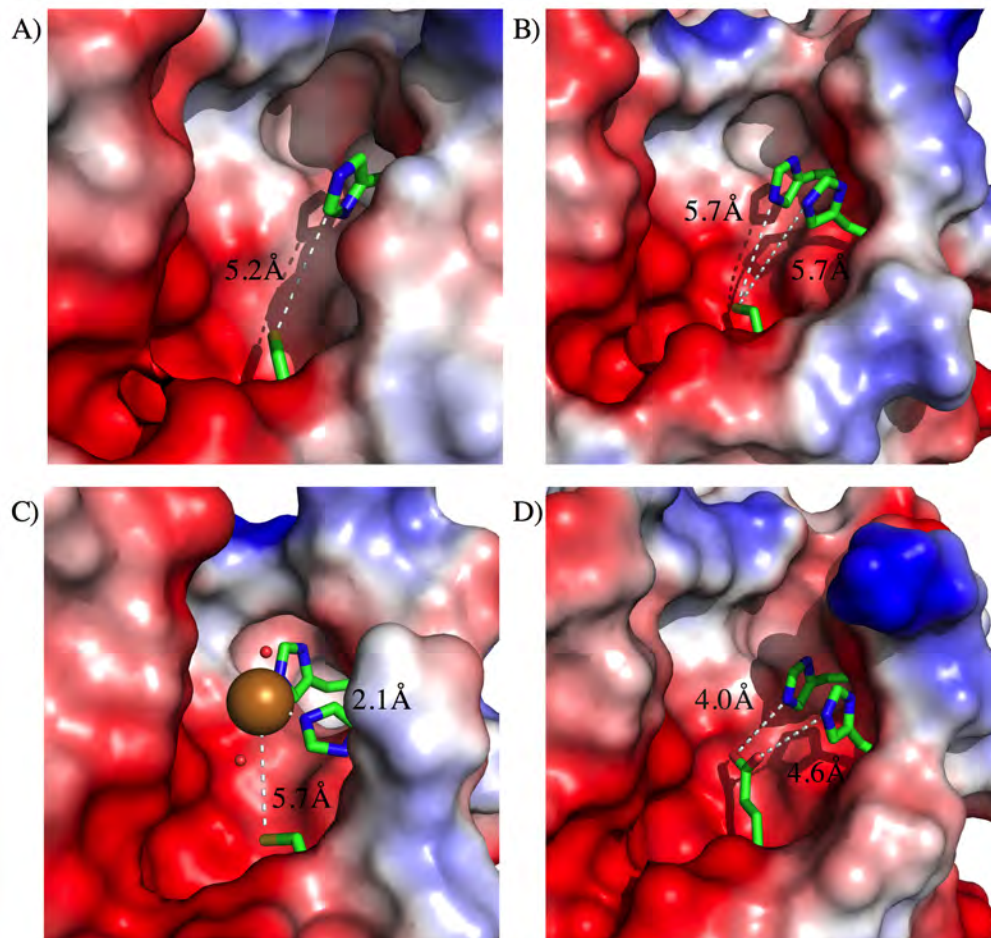
Figure S 19 Distance Mapping of Coordinating Motifs: A) mbYDCHH (open); B) mbYDCHH (closed); C) mbYDCHH_Cu; D) mbYDEHH; Data derived from crystal structure (Table S 5)
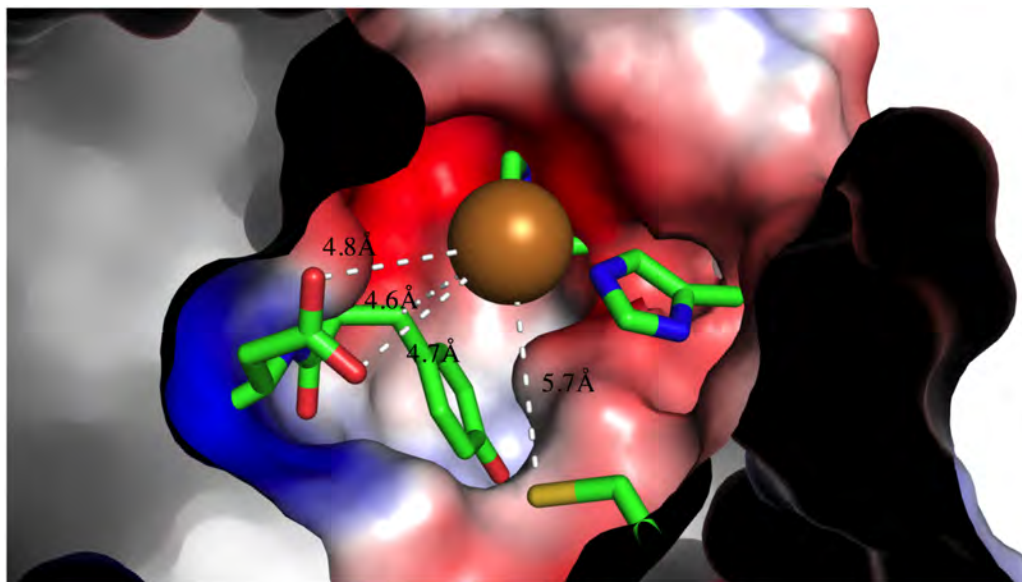
Figure S 20 Coordination sphere dimension: mbYDCHH_Cu

	mTFP*	mTFP*Pd	mTFP*Cu	mbYDCHH_open	mbYDCHH_closed	mbYDCHH_Cu	mbYDEHH
Crystal parameters							
Space group	P2$_1$	P2$_1$	P2$_1$	P2$_1$2$_1$2$_1$	P2$_1$2$_1$2$_1$	P2$_1$2$_1$2$_1$	P2$_1$2$_1$2$_1$
Cell constants (Å)	a=38.5, b=85.2, c=63.1	a=34.5, b=83.6, c=37.8	a=34.3, b=85.0, c=38.2	a=36.9, b=70.1, c=75.0	a=36.8, b=69.9, c=75.2	a=38.2, b=67.7, c=84.3	a=34.8, b=84.9, c=38.5
Molecules in asym. unit	2	1	1	1	1	1	1
Disordered regions	-	1, 218-220	-	-	-	-	
Data collection							
X-ray source	SLS, X06SA	SLS, X06SA	SLS, X06SA	CuKα	CuKα	CuKα	CuKα
Wavelength (Å)	1.0	1.0	1.0	1.55	1.55	1.55	1.55
Resolution range (Å)[a]	10-1.0 (1.1-1.1)	20-1.9 (2.0-1.9)	10-1.2	51.4-1.6	10.0-1.6	70-1.5	42.5-1.8
No. observations	548622	45858	61598	24258	26107	32546	19110
No. unique reflections[b]	204329	15454	37556	17756	20683	25543	11621
Completeness (%)[c]	94.9 (88.1)	98.2 (98.3)	98.2	99.9	99.9	99.9 (99.8)	99.7
R$_{merge}$ (%)[a, c]	3.6 (33.5)	3.6 (58.6)	4.9	5.9	4.5	0.04 (0.4)	9.1
I/σ (I)[a]	15.6 (2.8)	16.5 (1.9)				17.0 (4.7)	
Refinement (REFMAC5)							
Resolution range (Å)	10-1.0	15-1.9	10-1.2	15.0-1.6	10-1.6	10-1.5	42.5-1.8
No. reflections working set	194111	14681	61598	23021	24905	30760	19110
No. reflections test set	10217	773	58621	17756	24905	30005	18128
No. non hydrogen (protein)	3751	1752					
No. of heteroatoms	0	17	1	0	0	2	0
No. of solvent water	761	64	209	194	275	310	163
R$_{work}$/R$_{free}$ (%)[d]	13.1/15.0	17.6/21.7	14.5/18.0	15.5/20.0	14.8/19.0	15.1/20.0	18.9/25.0
RMSD bond lengths (Å)/(°)[e]	0.010/1.67	0.005/1.27					
Average B-factor (Å^2)	12.2	41.5	24.0	20.0	21.0	19.0	26.0
Ramachandran Plot (%)[f]	98.4/1.6/0.0	98.1/1.9/0.0	99.0/1.0/0.0	98.6/1.4/0.0	97.2/2.4/0.5	98.6/1.4/0.0	98.1/1.9/0.0
PDB code	4Q9W	4Q9X				4R6D	

[a] The values in parentheses of resolution range, completeness, R$_{merge}$ and I/σ (I) correspond to the last resolution shell.
[b] Friedel pairs were treated as identical reflections.
[c] R$_{merge}$(I) = Σ$_{hkl}$Σ$_j$ |[I(*hkl*)$_j$ - I(*hkl*)]|/Σ$_{hkl}$ I$_{hkl}$, where I(hkl)$_j$ is the jth measurement of the intensity of reflection hkl and <I(hkl)> is the average intensity.
[d] R = Σ$_{hkl}$ ||F$_{obs}$| - |F$_{calc}$||/Σ$_{hkl}$ |F$_{obs}$|, where R$_{free}$ is calculated without a sigma cut off for a randomly chosen 5 % of reflections, which were not used for structure refinement, and R$_{work}$ is calculated for the remaining reflections.
[e] Deviations from ideal bond lengths/angles.
[f] Number of residues in favored region/allowed region/outlier region.

Table S 5 Data Collection and Refinement Statistics

7. CATALYSIS

| Copper(II)Salt | Conversion | Endo | Exo | Solubility | | | | | | |
				DCM	THF	Acetone	ACN	MeOH	TFE	H2O
Cu(OAc)$_2$	98	87	13	+/o	+/o	+/o	+	+	o	+
Cu(OTf)$_2$	99	80	20	+	+	+	+	+	+	+
Cu(NO$_3$)$_2$	99	86	14	o	+	+	+	+	o	+
CuCl$_2$	99	88	12	o	+/o	+	+	+	+	+
Cu(SO)4	99	88	12	o	o	o	o	o	o	+

Table S 6 Overview of Copper(II)Salts: Catalytic Activity and Solubility in Solvents; Conversions and ratios are percentages (%)
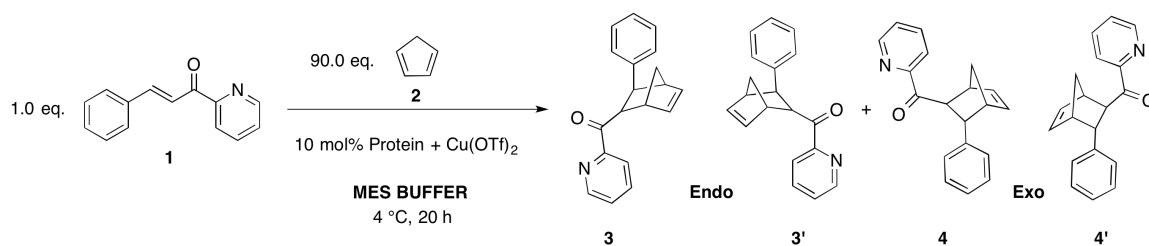
Figure S 21 Diels-Alder Screen: Substrates 1) Azachalcone 2) Cyclopentadiene; Products 3, 3') Endoproduct, 4, 4') Exoproduct
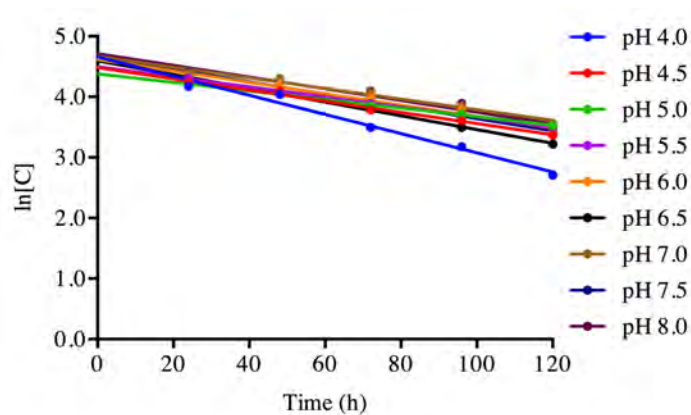
Figure S 22 Evaluation of Background Reaction: Data indicates rate constants of first order ranging from 4.39 s^{-1} to 2.68 s^{-1}, respective pH 4.0 to 8.0
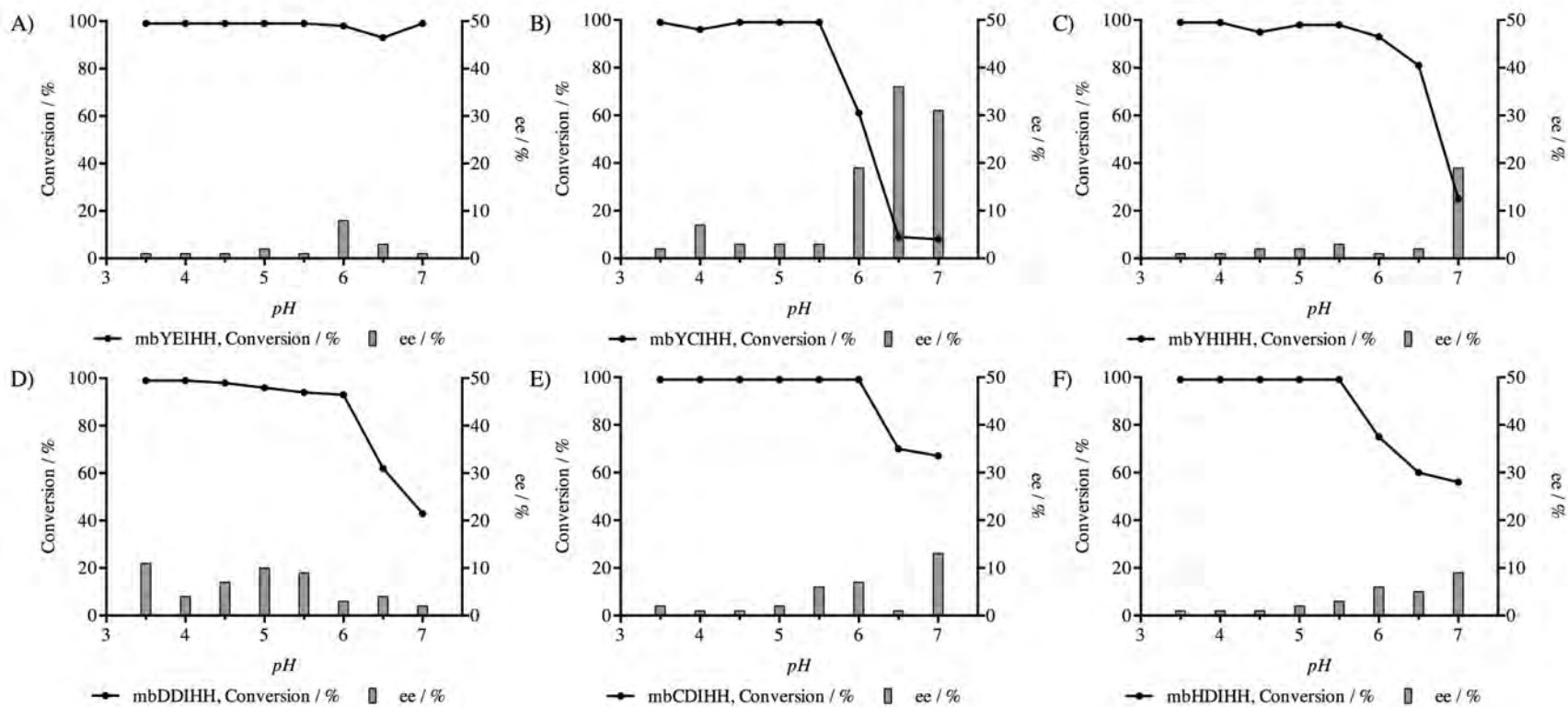
Figure S 23 Diels-Alder Screen: A – C) Mutants mbYEIHH, mbYCIHH, mbYHIHH (permutations of D55); D – F) Mutants mbDDIHH, mbCDIHH, mbHDIHH (permutations of Y54)
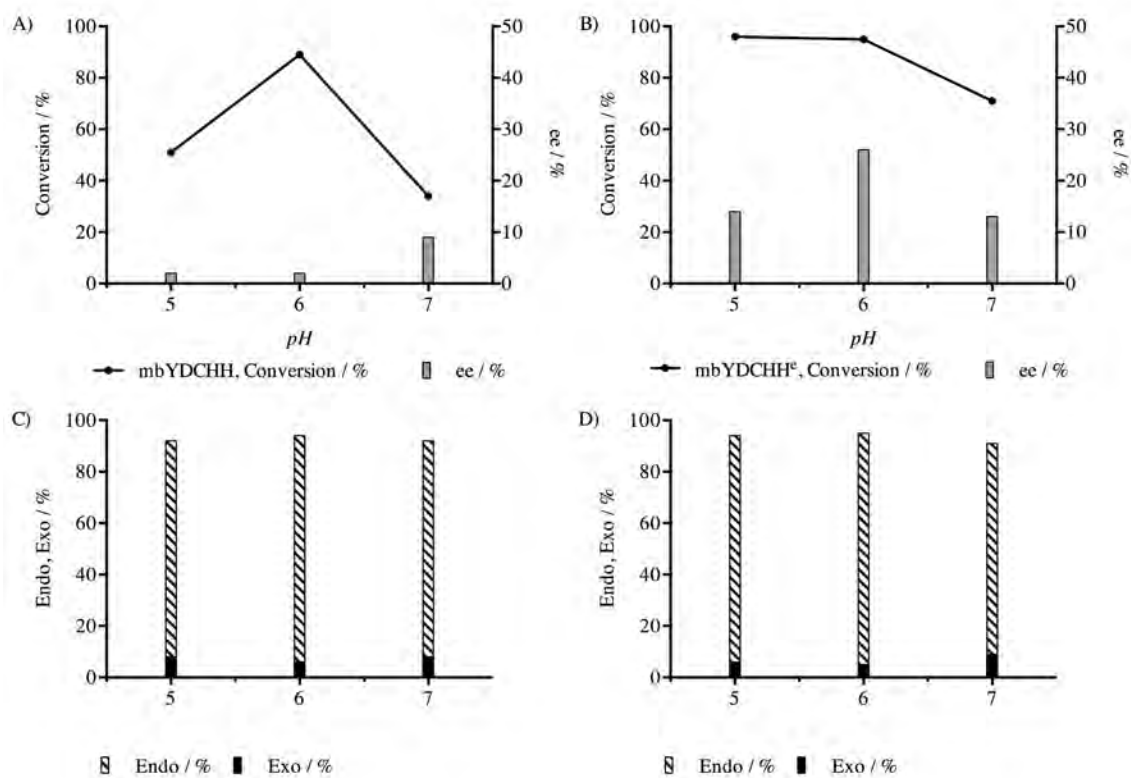
Figure S 24 Diels-Alder Results: A, C) mbYDCHH; B, D) mbYDCHHᵉ; introduced mutations show increased conversion and enantiomeric excess. Overall diastereomeric bias is not influenced by alternated second coordination sphere.
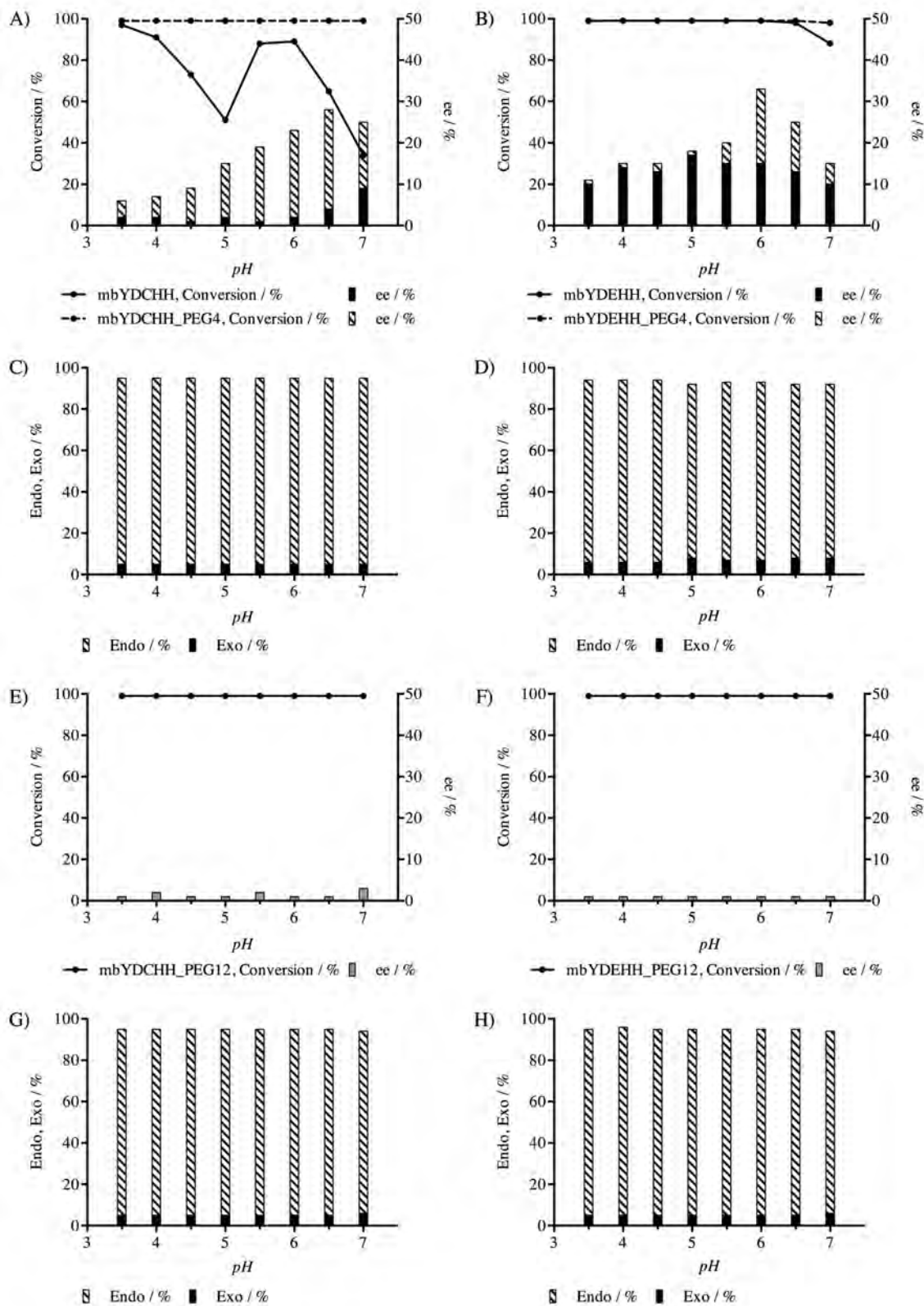
Figure S 25 Diels Alder Screen: A, C) mbYDCHH/_PEG4; B, D) mbYDEHH/_PEG4; E, G) mbYDCHH_PEG12; F, H) mbYDEHH_PEG12

PUBLICATIONS

Manuscripts

<u>Johannes Fischer</u>, Felix Quitterer, Arwa Makki, Anand Radhakrishnan, Meina Liu, S. Abdul Rajjak, Michael Groll, Jörg Eppinger, Development of a robust and versatile Host Protein for Design and Evaluation of Artificial Metal Centers, *Nature Chemistry*, **2015**, (to be submitted)

Conference Contributions

<u>Johannes Fischer</u>, Felix Quitterer, Meina Liu, Michael Groll, Jörg Eppinger, Biotrans2015, Vienna, Austria, July 27th, **2015**, Poster: Design of a potent host for artificial metal centers in asymmetric Diels-Alder Reactions

<u>Johannes Fischer</u>, Felix Quitterer, Michael Groll, Jörg Eppinger, 50th Winterseminar, Nobel Laureate Meeting, Klosters, Switzerland, January 10th, **2015**, Poster: mTFP*: a potent host for artificial metal centers

<u>Johannes Fischer</u>, Arwa Makki, Anna Zernickel, Jörg Eppinger, ICCC-41, Singapore, Singapore, July 21st, **2014**, Poster: mTFP* - A robust host for artificial metal centres for asymmetric Diels-Alder reactions